REOVIRUS CHAPERONE INTERACTION AND APOPTOSIS REGULATION

A Dissertation

Presented to the Faculty of the Graduate School

of Cornell University

In Partial Fulfillment of the Requirements for the Degree of

Doctor of Philosophy

by

Susanne Kaufer

May 2011

REOVIRUS CHAPERONE INTERACTION AND APOPTOSIS REGULATION

Susanne Kaufer, Ph.D.

Cornell University 2011

Many viruses require chaperones during viral replication. I investigated the involvement of HSP70 family chaperones in reovirus replication and assembly. Assembly and replication occurs in the cytosol of reovirus-infected cells within structures called viral factories (VFs). The nonstructural protein μNS forms the matrix of VFs. The eight structural proteins that assemble the inner core of the double-layered virion are recruited to VFs by specific interactions with μNS. However, it is unknown how the outer capsid proteins μ1 and σ3 are recruited to VFs. Using biochemical and cell biological approaches I found that recruitment of μ1 to VFs requires assembly with its partner protein σ3. In addition, I found that the μ1:σ3 complex and μ1 alone, interact with the cellular chaperone Hsc70. Moreover, the subcellular distribution of Hsc70 correlated with that of μ1 in reovirus infected cells and Hsc70 also co-localized with ectopically expressed μNS. The Hsc70-μNS interaction did not require the chaperone ATPase function, suggesting that μNS is not a substrate for Hsc70. The formation of viral factory-like structures by μNS was not affected after siRNA-mediated knockdown of Hsc70. These findings suggest that Hsc70 facilitates assembly of μ1:σ3 complexes and is likely involved in their subsequent recruitment to VFs. The specific interaction of Hsc70 with μNS may be involved in assembly of viral particles, but as in other viruses could also be involved in other replicative processes.

The last part of my thesis focused on reovirus-induced apoptosis. Apoptosis is induced by μ1 and occurs late in infection, but the regulatory mechanisms that prevent premature apoptosis induction by μ1 are poorly understood. I found that μ1 was cleaved by caspases upon μ1-induced apoptosis. This represents a negative feedback

loop where μ1-induced apoptosis leads to degradation of μ1 by caspase cleavage. I also found that μ1 was ubiquitinated, suggesting proteasomal degradation as another means to regulate μ1-induced apoptosis. Interestingly, the extent of μ1 ubiquitination was influenced by caspase activity, indicating a link between the two phenotypes. These findings suggest caspase cleavage and ubiquitination of μ1 as mechanisms to regulate μ1-induced apoptosis, and they reveal a link between these so far unrelated events.

BIOGRAPHICAL SKETCH

Susanne Kaufer, née Möβmer, was born in Freising, Bavaria, Germany on May 20th 1980. She attended high school at the Josef-Hofmiller Gymnasium in Freising, graduating in 1999. In 1997 Susanne had started a part-time job at the biotechnology company EpiLogic & EpiGene GmbH working on resistance development of plant pathogens to fungicides. A research paper she wrote as part of her high school diploma about the results of her work at EpiLogic was awarded the 3rd prize of the "Carl-Friedrich-Philipp-von-Martius Umweltpreis" which is sponsored by the GSF-National Research Centre for Environment and Health, Munich, Germany.

Susanne attended the Technical University Munich (TUM) and graduated in 2005 with a Diploma in Biology. During her studies, Susanne was an active member of several committees of the student council (Fachschaft) and also continued her job at EpiLogic where she met her future husband Benedikt, whom she married in October 2009. As part of her practical training for her Biology degree Susanne did an internship in the Osterrieder lab at Cornell University in the spring of 2003. Susanne's Diploma thesis with Dr. Ruth Brack-Werner at the GSF-National Research Centre for Environment and Health, Munich, Germany described the development of a stable cell line for an inducible fluorescence-based screening system for HIV-1 tat and rev inhibitors.

In September 2005 Susanne moved to Ithaca, NY with her future husband and worked as a visiting scientist in Dr. Marci Scidmore's lab at Cornell University on intracellular development and host-pathogen interactions of Chlamydia. Simultaneously, Susanne applied for the Ph.D. program in the Field of Comparative Biomedical Science and was accepted to start her studies in the fall of 2006. After her

rotations, Susanne started work in March 2007 in the lab of Dr. John Parker at the Baker Institute for Animal Health. Susanne was a member of the Graduate Advisory Council, organized the virology journal club and the LabOlympics and participated every year in student recruitment and orientation activities. Upon completion of her Ph.D., Susanne will move to Berlin, Germany to be reunited with her husband Benedikt.

Dedicated to my husband Benedikt,

My parents Elisabeth & Erich, my sister Barbara

And my friend Caroline

ACKNOWLEDGMENTS

After almost 6 years at Cornell I have a long list of people who I wish to thank and acknowledge for their support and help during these years. Firstly, I thank my advisor Dr. John Parker whose enthusiasm for science kept me going and who taught me so much about research. I sincerely apologize for being such a bad student at pitch & putt. Secondly, I would like to express my gratitude to Drs. Volker Vogt, Cindy Leifer and Edward Dubovi for serving as members of my special committee. A special thank you goes to Dr. Terry Dermody and all members of his lab, especially Dr. Karl Boehme and Mine Ikizler for teaching me the reovirus reverse genetic system and for taking such great care of me during my visit in Nashville. I would also like to thank the members of the Virology Journal Club, especially Drs. Volker Vogt, Colin Parrish, John Parker and Gary Blissard for many inspiring discussions. My gratitude also goes to Drs. Klaus Osterrieder and Marci Scidmore; to Klaus for giving me the chance of an internship when he had no clue if I knew the business end of a pipette and to Marci for giving me my first real job and for supporting my PhD application. A big thank you goes to Casey Moore and Janna Lamey for their great efforts in student recruitment and orientation and their constant support of all us grad students.

I am dedicating my thesis to my dear friend Dr. Caroline Coffey. She shared her bench with me in the beginning, showed me the ropes in the lab, gave me advice on how to handle the boss, pep talked my through my A-exam and was a great friend to hang out with and have fun. I miss her very much!

I would like to thank everyone at Baker for making this more than just the place where I worked. The family feeling that Baker has is wonderful; the baked goods that so often satisfied my sugar/chocolate addiction; the celebrations where most people show up because they care and not just for the free food; Sue's cheerful

good morning greeting every day; the collegiality and helpfulness amongst everybody and of course the beer-30 breaks. My special gratitude goes to all past and present members of the Parker Lab: lab-mom Lynne for knowing everything, Brenda for kicking our lazy behinds and organizing the lab to the point of no return, Jae-Won for brightening the lab with his quirks (The chase of the turkeys.), Oz for his no-nonsense attitude and his dark humor, Meagan for weekly captivating discussions about J2, Brian for his great support over the last year and Alex for balancing out the chattiness in the lab. I also would like to thank Wendy Weichert, because if lab-mom Lynne really didn't know something, lab-auntie Wendy would. A big thank you to Carole for being such a great friend! I'll always cherish the DDR and Rock Band evenings with the gang, Karla, Jess, Michael, and Swaantje you guys rock!

I would like to thank my family from the bottom of my heart. My parents have been a constant support throughout my life and by encouraging and challenging me have helped me to get where I am today. My little big sister Barbara always treated me like an equal and was my role model in my teenage years. The rational scientist in me will always admire your social intelligence and creativity. I would also like to thank my family in-law for welcoming me and my sometimes difficult personality with open hearts into their family. Finally, I would like to thank my husband Benedikt for his love and support, his optimism, for making me laugh when I'm down, for being my soul mate. Being separated for the last ten months wasn't easy, and I can't wait to be reunited with you.

TABLE OF CONTENTS

LIST OF FIGURES

CHAPTER ONE

Introduction

Reoviridae

The *Reoviridae* comprise a number of viruses that share as their core characteristic a double-stranded RNA (dsRNA) genome (86, 89). Members of this family infect many of different species including mammals, birds, reptiles, fish, molluscs, arthropods, but also fungi and plants. A total of 15 genera are recognized and have been so far grouped into turreted and nonturreted viruses based on the presence of a turret-like protrusion at the five-fold axis of symmetry of the virus capsid. Recently the formation of two subfamilies, named *Sedoreovirinae* (sedo, smooth : Latin) and *Spinareovirinae* (spina, spike : Latin) reflecting this informal grouping has been ratified (15). The mammalian orthoreoviruses, the prototype members of the *Reoviridae*, which will be the subject of this thesis, belong to the genus *Orthoreovirus*. These are the initially identified "reoviruses" that were isolated from patients with mild upper respiratory infections or gastroenteritis. Due to the fact that these viruses could not be linked as causative agents to these illnesses the name reovirus was proposed as an acronym for "**r**espiratory **e**nteric **o**rphan virus". Subsequently identified other members of the *Reoviridae*, on the other hand, are well established pathogens, like rotaviruses and Bluetongue virus of the genus *Rotavirus* and *Orbivirus*, respectively. The hallmark feature of the *Reoviridae* is their dsRNA genome which is segmented into 9-12 pieces depending on the genus. The segments are grouped into three categories, L (large), M (medium) and S (small) based on their length (89). Each segment encodes one to three, but mostly only one, protein on the positive sense RNA strand of one dsRNA. The genome is enclosed in non-enveloped capsids consisting of two or three concentric protein layers with icosahedral symmetry

(52, 68, 81). The average diameter of 60 to 85 nm does not include a fiber protein that extends from the surface of some family members. The newly discovered genus *Dinovernavirus* has only one protein shell and is therefore smaller with a diameter of about 50 nm (3).

The mammalian orthoreoviruses

As mammalian orthoreoviruses (from now on named reoviruses) are the prototype members of the family *Reoviridae* and as the subject of this thesis, will be discussed in more detail. The mature reovirus virion consists of 8 structural proteins that are arranged in two concentric protein shells (Figure 1.1). 120 copies of λ1 form the inner layer or core, which exhibits T=1 symmetry (also termed T=2 as the asymmetric unit is comprised of a parallel, asymmetric λ1 dimer) (42). On top of the λ1 shell sit two core proteins, σ2 and λ2. σ2 decorates the λ1 shell and is thought to function as a stabilizing clamp (81). λ2 occurs as pentamers at the five-fold axis of symmetry and forms the turrets that are present in the *Spinareovirinae*. Inside the core, slightly offset from each of the five-fold axis of symmetry, is thought to sit one λ3 protein, which is the RNA-dependent RNA polymerase (RdRp) (96, 99). λ3 is likely associated with the protein μ2, which is proposed to act as a cofactor for the RdRp (53). The exact location and quantity of μ2 within core particles is not known for certain. In between the λ2 turrets and atop the λ1 – σ2 core sits the outer capsid. This second protein shell has T=13 symmetry and is mainly composed of μ1 and σ3 (59). These two proteins form a heterohexamer with three intertwined μ1 monomers at the base and three σ3 monomers binding in between two μ1 proteins at the top of the complex (Figure 1.2). 600 copies of each μ1 and σ3 make up 200 heterohexamers that decorate the underlying core (67, 68). The vacant spaces due to the missing 180 subunits that would be expected in a T=13 symmetry (13 x 60 = 780) are occupied by

the pentameric λ2 turrets, which extend from the core, through and beyond the outer capsid layer. The center of these turrets anchors the attachment protein σ1, which consequently occurs at the five-fold axis of symmetry and is present as a homotrimer. The σ1 encoding genome segment S1 is the serotype-determining gene and shows the least sequence conservation (26% to 49%) compared to all other reoviral genes (70.6% to 97.8%) (29, 74). Based on their S1 sequence, reovirus isolates are separated into three serotypes whose prototype representatives are type 1 Lang (T1L), type 2 Jones (T2J) and type 3 Dearing (T3D).

A

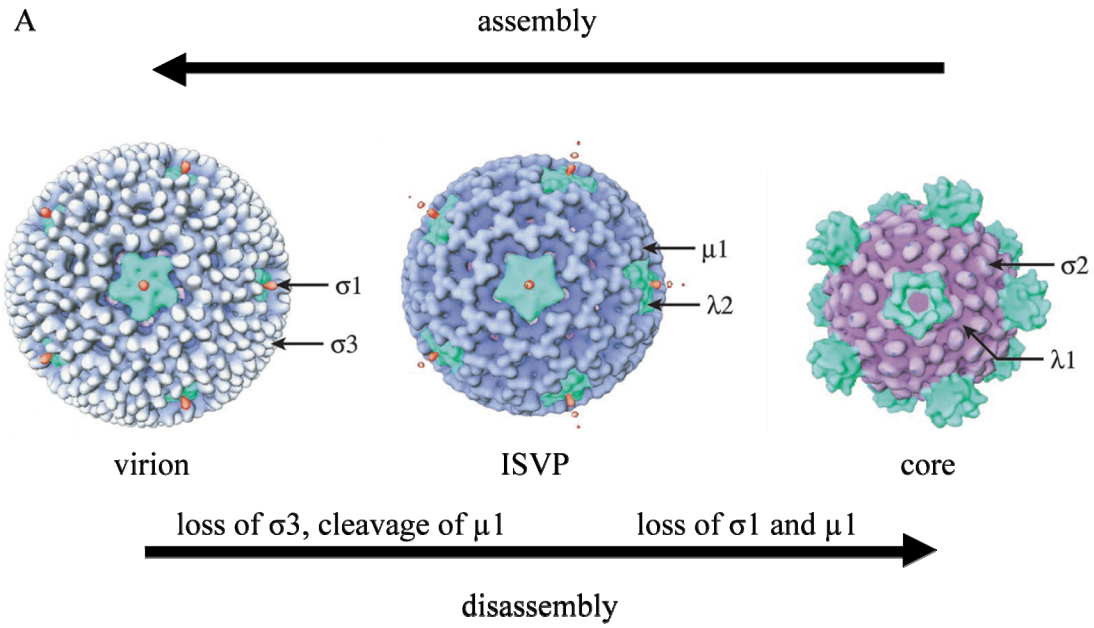

B

virion	ISVP	core
core proteins	core proteins	λ1
μ1:σ3 heterohexamer	cleaved μ1	μ2
σ1	σ1	λ2
		λ3
		σ2

Figure 1.1: Structure and composition of different reovirus particles (30). A) Illustrations of virion, ISVP and core particles were created from cryo-EM and image reconstruction. Each particle is oriented with the five fold axis of symmetry at the center of the image. B) List of proteins that make up the different reovirus particles.

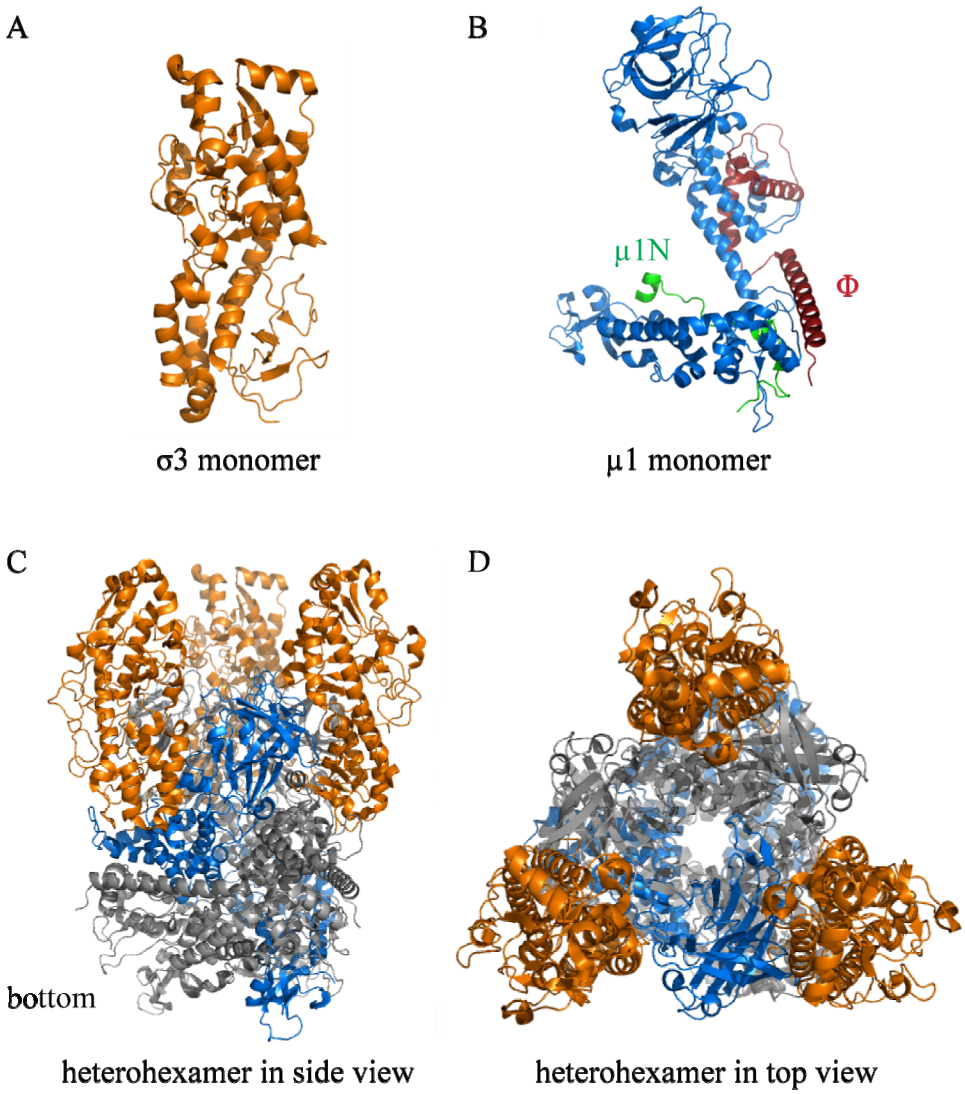

Figure 1.2: Structures of outer capsid proteins σ3 and μ1. A) σ3 monomer, B) μ1 monomer with fragments μ1N in green, δ in blue and Φ in red. C) heterohexamer in side view; One μ1 monomer colored in blue, others in grey to illustrate twisting of the three subunits. D) heterohexamer in top view. The monomeric representations of μ1 and σ3 were taken from the heterohexamer structure (PDB 1JMU) (59). Originally, σ3 was crystallized as a dimer (77).

Reovirus lifecycle

Reoviruses are ubiquitous and are frequently isolated from fresh and waste waters. Epidemiologic studies found that most individuals test positive for antibodies against all three serotypes by the end of childhood (55, 88). One study showed that more than 70% of children over three years old had anti-reovirus antibodies (57).

The reovirus lifecycle begins with the attachment of σ1 to its receptors sialic acid and junctional adhesion molecule A (JAM-A) on the surface of a host cell (see Figure 1.3 for simplified reovirus lifecycle) (13, 86). Following attachment, virions are endocytosed, a process that possibly is mediated by interactions of the λ2 turret with β1 integrin. Within endosomes partial proteolysis of the outer capsid occurs. This is mediated by cathepsins that are activated by the acidic pH within endosomes (32, 62, 63, 94). Proteolysis of the virion can also take place in the extracellular environment of the gut or lungs bypassing endocytic uptake and allowing for direct infection from the plasma membrane. Proteolytic processing of virions is necessary in order to activate the outer capsid protein μ1 for membrane penetration. To penetrate membranes, μ1 undergoes proteolytic cleavage and conformational changes. In virions, μ1 is shielded by a coat of σ3 which prevents the untimely implementation of these processes. As a result of the proteolytic digestion, σ3 is released from the virion, which is now called an intermediate/infectious subviral particle (ISVP) (30). Due to the loss of its protector protein σ3, μ1 undergoes distinct conformational changes. An apparently autocatalytic cleavage of μ1 occurs at amino acid (aa) N42 generating the N-terminal fragment, μ1N, and the remaining part called μ1C (75, 76). A second cleavage event at aa Y581 or R584 is catalyzed by chymotrypsin or trypsin *in vitro*, respectively and yields the central δ fragment and the C-terminal Φ fragment (17). Both the myristoylated μ1N and the Φ fragment are released from the ISVP and have been associated with membrane penetration although the exact mechanism remains to

be elucidated. The loss of the σ1 attachment protein and the release of the δ fragment of μ1 lead to the deposition of the core in the cytoplasm of the infected cell (18).

These cores are transcriptionally active and produce viral mRNAs, which exit the core through radial channels in the λ2 turrets at the five-fold axis of symmetry. These channels are open only in core particles, but not in virions or ISVPs. λ2 undergoes a conformational change during the ISVP-to-core particle transition which leads to the opening of the turret by an up- and outward rotation of λ2 domains (30). As they pass through the λ2 turret the non-polyadenylated mRNAs acquire a 5′ cap structure that enhances their translation by the cellular machinery (22, 60, 61).

One of the translated proteins is μNS, a non-structural protein that forms the matrix of the viral factories which are thought to be the location of ongoing viral replication and assembly (82). The primary mRNA transcripts are detectable by 2 h after infection, peak after 6 – 8 h, and are undetectable by 12 h post infection (hpi) if overall protein synthesis is inhibited with cycloheximide. Inhibition of protein synthesis prevents the formation of new core particles which contribute to mRNA transcription. The vast majority of viral mRNAs (95%) are secondary transcripts and stem from transcriptase particles. These are newly assembled core particles that are coated with μNS and seem to be hindered in their acquisition of the outer capsid (72). The secondary transcripts appear 4 – 6 hpi and decrease after reaching a maximum at 12 hpi. After assembly progeny virions they are released following cell death and disintegration.

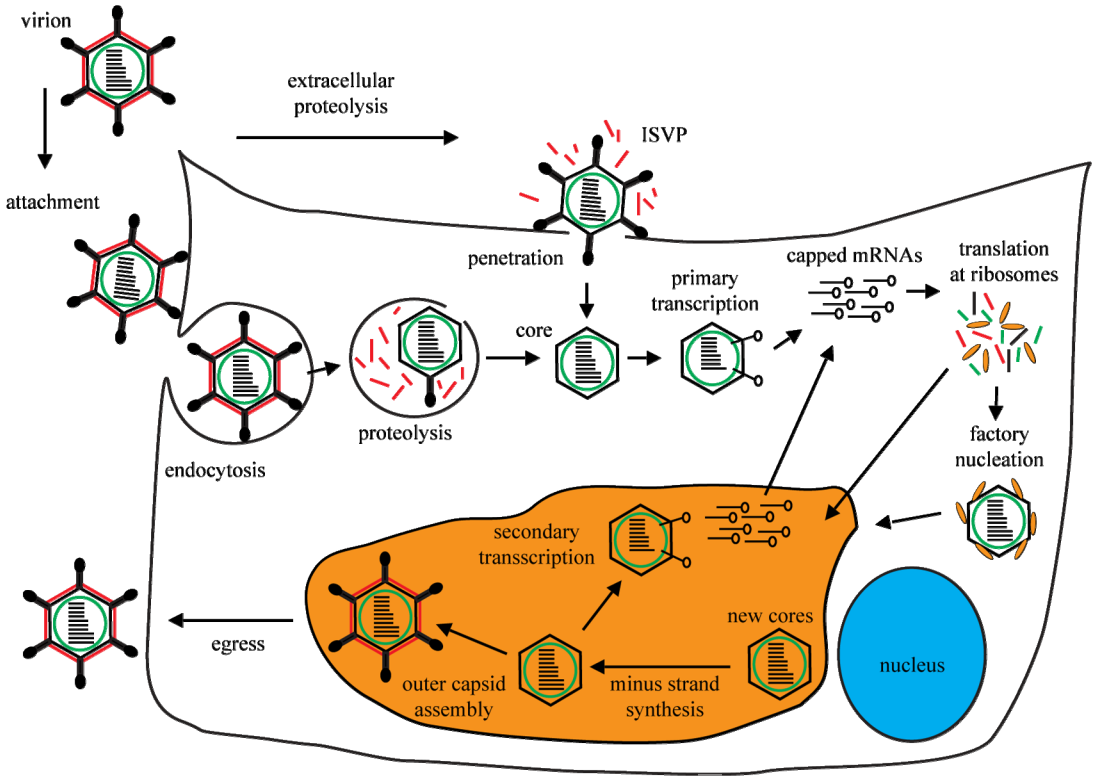

Figure 1.3: Reovirus lifecycle. Entry of virions occurs either by receptor-mediated endocytosis and endosomal proteolysis or after extracellular proteolysis generating an ISVP. After endosomal or plasma membrane penetration the transcriptionally active core arrives in the cytosol and primary, capped mRNAs are deposited in the cytosol. Viral proteins are translated and recruited to viral factories nucleated by μNS-bound cores. Newly assembled cores engage in negative sense RNA strand synthesis and continue on to secondary transcription or assemble into full virions after acquiring the outer capsid.

Generation of reovirus progeny virions

The replication and assembly of reovirus progeny virions is thought to occur in viral factories (VFs) (82). These inclusion-like structures start out as small pin points very early in infection and expand throughout the infection. Individual VFs can fuse together and eventually the cytoplasm of the infected cell will be almost filled up with large viral factories (Parker, unpublished observation). VFs are not membrane-bound and consist of a matrix of the 80 kDa nonstructural protein μNS (10). VFs can be of filamentous or globular nature depending on the virus strain. T1L and $T3D^{CD}$ show a filamentous VF morphology, while $T3D^{N}$ exhibits globular VFs. This phenotypic difference in $T3D^{N}$ is due to a point mutation in the μNS-interacting protein μ2 which abrogates the association of μ2 with microtubules (78). If μNS is expressed by itself it will form viral factory-like structures (VFLs) that resemble VFs in infected cells (10). How μNS forms viral factories remains to be elucidated. By thin section electron microscopy the matrix of VFs appears to consist of fibrils that have a distinct kink, but as an atomic resolution structure of μNS is not available, the exact mechanism remains subject to speculation (26, 27, 90). It is thought that μNS forms oligomers that represent the building block of the viral factory matrix, but the nature of such oligomers is unknown. It has been shown that μNS can bind cores *in vitro* without negatively affecting their transcription or capping activity (9). μNS-bound cores might actually have a slightly enhanced capping activity (9). Furthermore, Broering et al. expressed μNS in cells allowing the formation of VFLs before inhibiting further protein synthesis with cycloheximide and infecting the cells with ISVPs. They found that the entering core particles were recruited to the pre-formed VFLs (8). These findings support the hypothesis that newly synthesized μNS binds to the infecting core particles and utilizes them as a nucleation factor for factory formation. In these

factories the following processes have to take place in order for new progeny virions to arise (order of listing does not imply chronology): i) assembly of λ1 and σ2 into the core shell, ii) incorporation of the λ3 polymerase and of μ2 into this shell, iii) packaging of one of each of the viral genes in form of [+]-RNA and synthesis of the negative sense RNA strand, iv) addition of the pentameric λ2 turrets onto the core shell, v) formation of the outer capsid consisting of μ1:σ3 heterohexamers and the attachment protein σ1 and vi) egress of virions.

Recent findings put μNS at the center stage of virion assembly. Miller et al showed that μNS interacts with the structural proteins λ1, σ2, μ2, λ3 and λ2 as well as the nonstructural protein σNS via non-overlapping domains (Figure 1.4) (69). This means that all proteins that comprise the core particle are recruited to the viral factories. σNS has been found to bind to ssRNA and is implicated in the sorting and/or packaging of viral [+]-RNAs together with μNS and σ3 (2, 5, 40). All three proteins have been identified along with viral [+]-RNA in small nucleoprotein complexes, although the exact order of association is unclear. After a new core particle is assembled and the negative sense RNA strand has been synthesized it has two choices: a) remain as a transcriptase particle and keep producing [+]-RNAs that get translated into proteins and form new cores, or b) acquire the outer capsid thus shutting off transcription and mature into a full virion. μNS seems to play a role in this decision. Transcriptase particles isolated from infected cells show an association with μNS (72, 102). Furthermore, *in vitro* experiments revealed that μNS-bound cores can still produce capped [+]-RNAs, but unlike non-μNS bound cores do not associate with outer capsid proteins to form virions (9, 72). Reovirus has to have evolved a mechanism that regulates the switch from transcription to assembly. If all cores remained associated with μNS in the viral factories, no fully assembled virions would be generated. On the other hand if all cores were to immediately be coated with the

outer capsid, the infection would be terminated prematurely as full virions are not transcriptionally active. To date no such mechanism has been elucidated, but I will propose a hypothesis in the final summary of this thesis based on my findings presented in chapter 2.

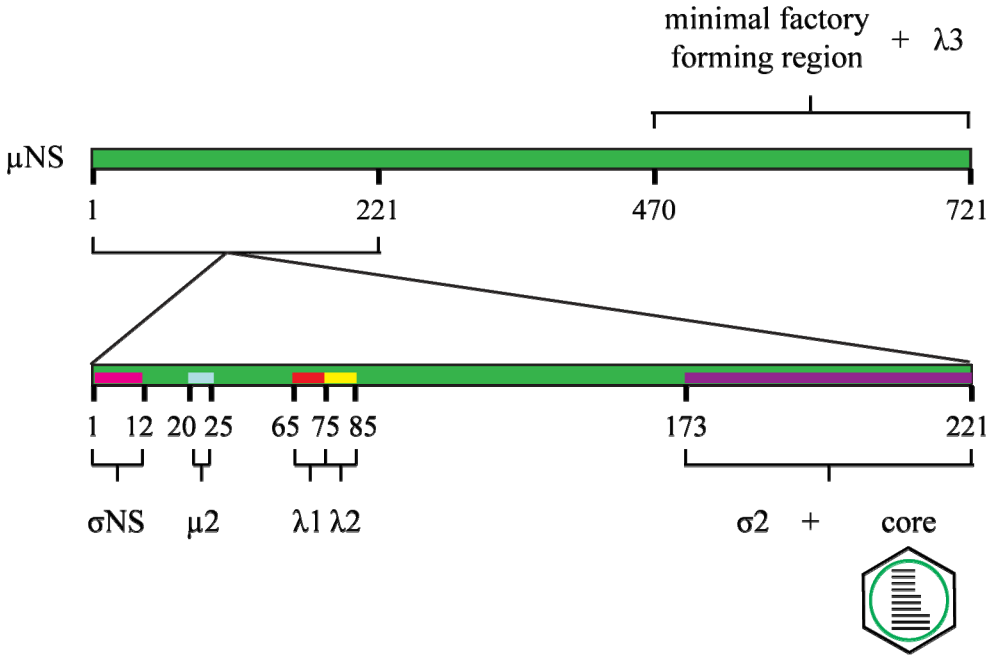

Figure 1.4: Schematic representation of μNS and its binding sites for σNS, μ2, λ1, λ2, σ2, λ3 and reoviral cores.

The recruitment of the major outer capsid proteins μ1 and σ3 to VFs is poorly understood. In a fully assembled virion the two proteins are associated into a heterohexamer with three intertwined μ1 monomers at the base and three σ3 monomers decorating the spaces in between two μ1 subunits (59). This complex forms in the absence of other viral proteins in insect cells infected with recombinant baculovirus carrying the μ1- and σ3-encoding gene segments. The atomic structure of the μ1:σ3 complex has been solved and studied extensively (30, 59). However, where and when the μ1:σ3 heterohexamer assembles in an infected cell and how these proteins are recruited to viral factories is not clear. μ1 localizes to the endoplasmic

reticulum, mitochondria, lipid droplets and in infected cells also to viral factories (24). The localization to membranes and VFs is observed more frequently late in infection while at early time points μ1 is predominantly diffuse in the cytosol (24). This time-dependent change in localization could suggest a mechanism by which μ1 is only recruited to VFs towards the end of the infectious cycle in order to prevent premature outer capsid assembly onto transcriptase particles. Experiments with a temperature sensitive mutant of σ3 (tsG453) have shown an accumulation of core-like particles in cells infected at the restrictive temperature (71).This finding indicates that μ1 and σ3 are pre-assembled into heterohexamers before this complex is assembled onto the core; otherwise one would expect cores with some sort of coat of μ1. Chapter 3 will address some of the questions concerning the trafficking and assembly of μ1 and σ3.

Chaperones

The cytosol is a very crowded place. Assuming all proteins were distributed evenly, their concentration would be around 300 mg/ml (101), but considering that ribosomes can arrange into polysomes, local protein concentrations at the site of protein synthesis are likely to be even higher. This molecular crowding leads to an increased tendency of nascent proteins to engage in nonspecific protein interactions. But irregardless of the molecular crowding, the folding of a newly translated protein is not a trivial process. Most proteins contain more than one domain or folding unit which is approximately 100 – 200 amino acids long and has to be translated completely before folding can occur (43). This means that a significant portion of the polypeptide chain will remain unfolded and exposed to the crammed cytosol until the full domain has been translated. But also after an individual protein has successfully reached its native state, it might be destined to oligomerize and still display unburied hydrophobic regions which increases the risk of aggregation. Chaperones are

ubiquitous cellular proteins that help nascent polypeptides to fold properly as well as prevent protein subunits from aggregating by aiding the assembly of protein complexes, and even dissaggregating protein aggregates (11, 43, 87). Chaperones are also involved in the translocation of proteins across organellar membranes, signal transduction and the regulation of the cell cycle and apoptosis (6, 44, 73, 84).

There are two major chaperone systems in the eukaryotic cell, the heat shock protein 70 (HSP70) and the chaperonin system (33, 36, 45, 83). Both of these systems are dependent on an ATP/ADP exchange cycle. In the ATP-bound state the substrate on/off rate of the chaperone is fast, while the rates are slow in the ADP-bound conformation (12). Chaperonins are barrel shaped protein complexes that facilitate protein folding inside their central cavity and thus are limited to substrates smaller than 60 kDa (65). Two groups can be distinguished depending on their association with a co-chaperone that serves as a lid on the barrel after substrate binding. Group I chaperonins like Hsp60 in eukaryotes and GroEL in *E. coli* interact with their "lids" Hsp10 and GroES, respectively, while group II chaperonins (for example TRiC/CCT in eukaryotes, thermosome in archaea) have a built-in lid.

Members of the HSP70 chaperone system are proteins of approximately 70 – 100 kDa. They consist of a nucleotide-binding domain (NBD) joined by a flexible linker to a substrate-binding domain (SBD) (34, 97, 100). HSP70 chaperones are not limited in their substrate size like the chaperonins as they bind relatively short, extended, hydrophobic segments of proteins. The major members of this family are the heat shock cognate protein 70 (Hsc70) in eukaryotes and its bacterial homologue DnaK in *E. coli*. These proteins are modulated in their activity by co-chaperones which also belong to the HSP70 chaperone system. Co-chaperones often display a modular composition containing a chaperone-interaction domain together with other motifs that can target them to a specific cellular compartment or enable them to recruit

other proteins besides chaperones. Thereby, co-chaperones can direct cytosolic chaperones to distinct locations and influence their local activity. In the following paragraph Hsc70 and its regulation by different co-chaperones will be discussed in more detail.

Heat shock cognate protein 70

The heat shock cognate protein 70 (Hsc70) is one of the most abundant cellular chaperones. It is constitutively expressed, but also has an inducible form, heat shock protein 70 (Hsp70) whose expression is upregulated under conditions of cellular stress such as starvation or heat shock, but also during bacterial and viral infections. Hsc70 is structurally divided into two domains, the ~44 kDa nucleotide-binding domain (NBD, aa 1-383) or ATPase domain and the ~30 kDa substrate-binding domain (SBD, 395-650) (Figure 1.5). Both domains are connected via a short, exposed linker (aa 384-394) (50). The NBD consists of two lobes divided by a deep cleft at whose bottom the nucleotide binds (34). The SBD can be further divided into two subdomains, the 18 kDa minimal substrate-binding site and the 10 kDa C-terminal tail. The substrate-binding site is composed of two β sheets, each containing four β strands. The two β sheets are twisted and create a U-shaped groove which is the site of substrate binding (100). The 10 kDa C-terminal tail assumes an α-helical fold and acts in part as a lid over the substrate binding pocket by interacting with the upwards protruding loops connecting the β strands (65). The extreme C-terminus of Hsc70 has not been crystallized so far as this region seems to be highly flexible. These last 30-40 amino acids are highly conserved among eukaryotic Hsc70 and contain several GGXP repeats and an EEVD motif (20, 100). These motifs serve as co-chaperone binding sites.

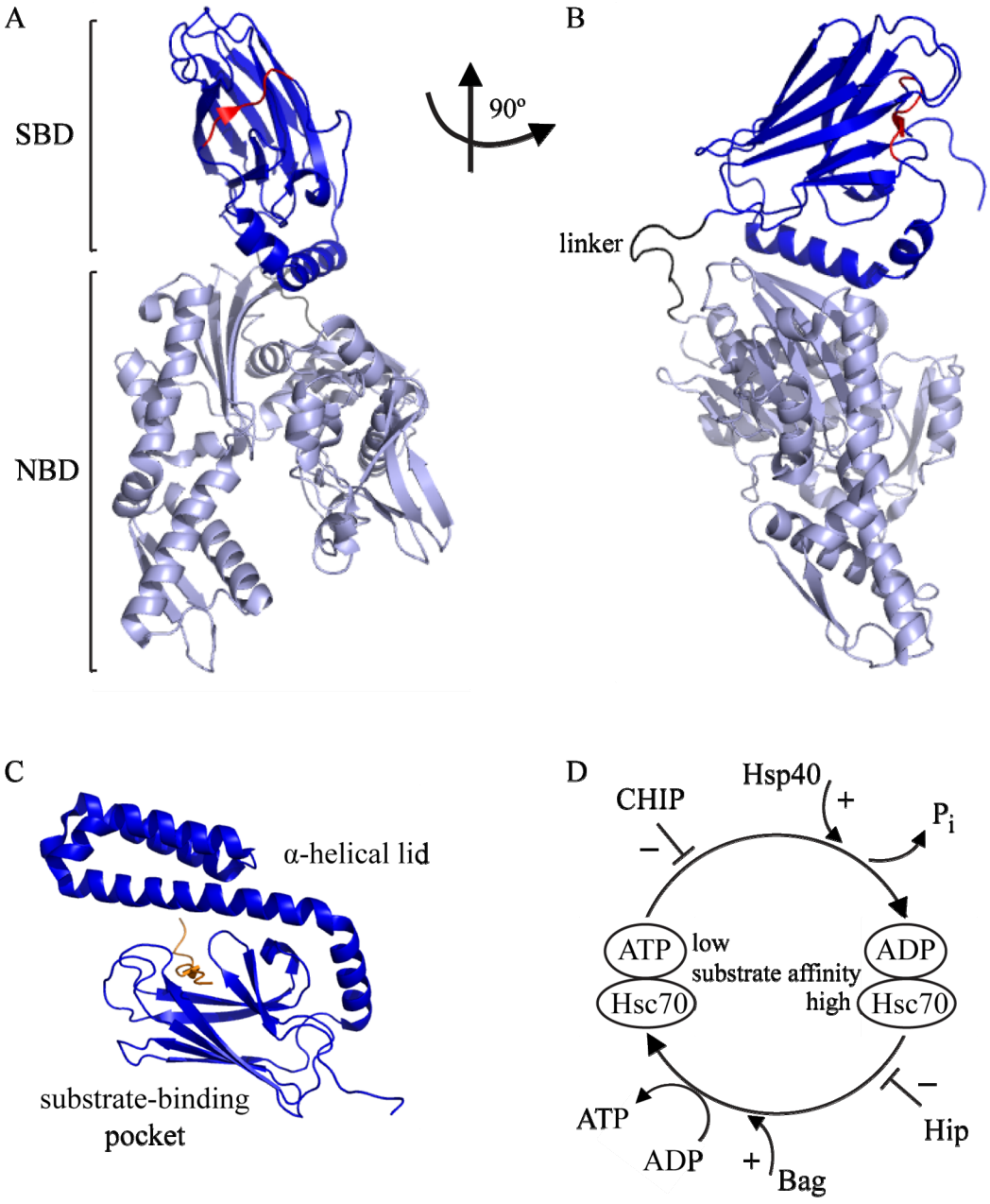

Figure 1.5: Structures of bovine Hsc70 (PDB 1YUW) and *E. coli* DnaK substrate-binding domain (PDB 3DPP) (50, 58). A) Front and B) side view of ribbon structure of bovine Hsc70 (aa 1-554, E213A/D214A) lacking the 10 kDa C-terminal tail. Nucleotide-binding domain (NBD) in light grey, linker in black (only visible in B), substrate-binding domain (SBD) in blue with residues 539-544 (red) occupying the substrate-binding pocket. C) Ribbon structure of the substrate-binding domain of DnaK bound to a synthetic peptide (orange). The α-helical 10 kDa tail forms a lid over the substrate-binding pocket. D) Model of the Hsc70 ADP/ATP cycle and its regulation by co-chaperones CHIP, Hsp40, Hip and nucleotide exchange factor Bag.

The three most studied families of co-chaperones are the J-domain family, the Bag domain family and tetratricopeptide repeat (TPR) domain containing proteins (80, 98). The prototype member of the J-domain family is Hsp40 (DnaJ in *E. coli*) whichinteracts with HSP70 proteins via a conserved J-domain and stimulates the otherwise low ATPase activity of HSP70s (70). Hsp40 thus promotes the more stable binding of substrates in the ADP-bound form. The J-domain is characterized by a His-Pro-Asp tripeptide which is critical for the co-chaperone's activity (14). The major binding site for J-domains seems to be the ATPase domain of HSP70s (54). There is also evidence, though, that the C-terminus of Hsc70 is also involved in Hsp40 binding and activity (38). A mutant of Hsc70 lacking only the C-terminal EEVD motif no longer interacts with Hsp40 in an *in vitro* binding assay, but another mutant devoid of the full 10 kDa tail still displays stimulated ATPase activity in the presence of Hsp40 (28).

Bag-1 is a member of the Bag domain family of nucleotide exchange factor co-chaperones and also interacts with the ATPase domain of HSP70s. Bag-1 binding to HSP70 chaperones facilitates the ADP-ATP exchange and thus the release of bound substrate and recycling of HSP70 proteins (46). Hop, Hip and CHIP are members of the TPR domain-containing co-chaperone family. Hop or Hsp70/Hsp90-organizing protein binds both Hsp70 and Hsp90 and coordinates them during progesterone receptor complex assembly (19). The Hsc70-interacting protein Hip can in itself function as an ATP-independent chaperone, but as the name says, also interacts with Hsc70. This interaction is enhanced in the event of Hsp40-stimulated ATP hydrolysis by Hsc70. Hip binds the nucleotide-binding domain of Hsc70 and stabilizes the ADP-bound conformation, thus prolonging the interaction of Hsc70 with its substrate and favoring the substrates proper folding (47). CHIP stands for C-terminus of Hsc70-interacting protein and is another member of the TPR domain containing co-

chaperones. CHIP interacts with the C-terminal 110 amino acids of Hsc70 and has been found to counteract the ATPase stimulating effect of Hsp40 (4). Thereby, this co-chaperone actually prevents the formation of stable chaperone-substrate complexes and hinders protein folding. CHIP is a unique co-chaperone as it also contains a U-box with E3 ubiquitin ligase activity and thus constitutes a link between the chaperone and the proteasome system (66).

Chaperones in viral lifecycles

Many viruses use chaperones in different stages of their lifecycle, such as entry, translocation of viral proteins to certain cellular compartments, genome replication or assembly of progeny virions (reviewed in reference (64). Hepadnavirus, for example, requires heat shock protein 90 (Hsp90) and its partner p23 for reverse transcription and RNA packaging (48, 92). The minor capsid protein L2 of papillomaviruses is dependent on Hsc70 for its nuclear translocation (35). Other viruses choose to encode their own chaperone proteins. African Swine Fever Virus produces the chaperone-like CAP80 protein that is necessary for capsid protein folding and assembly (23). Similarly, closterovirus encodes a heat shock protein 70 homologue (Hsp70h) and p61 protein that are essential for efficient virion assembly (85).

SV40, the prototype of the *Polyomaviridea* family engages chaperones in capsid assembly as well as cell transformation. In *in vitro* assays the capsid proteins VP1 and VP3 of SV40 forms capsids that are similar to empty virus particles derived from infected cells if the proteins are incubated with Hsc70 and the large T antigen (TAg) (21). In vivo, assembly of capsids occurs only in the nucleus, and VP1 and Hsc70 have been found to co-localize in the nucleus late in infection (25). Given the fact that the large TAg binds the polyomavirus genome and possesses a co-chaperone

specific J-domain, the following scenario seems possible (79, 91). Hsc70-bound VP1 translocates into the nucleus where it is recruited through the interaction of Hsc70 with the J-domain of the large TAg to the TAg-bound viral genome. One of the mechanisms of cell transformation by the large TAg involves the liberation of cell cycle regulatory transcription factor E2F, a process that has also been found to involve the association of TAg with Hsc70 via its J-domain (95).

Chaperones in the reovirus lifecycle

Chaperones have already been found to be involved in some parts of the reovirus life cycle. After attachment of the virion to the cell and endocytic uptake, the outer capsid protein σ3 is proteolytically removed, leaving behind the ISVP (7, 51). In ISVPs, μ1 is cleaved into three μ1 fragments, μ1N and the δ and Φ fragments (17, 76). The smaller μ1N and Φ fragments are released from the ISVP during membrane penetration, but the δ portion of μ1 remains associated with the ISVP (1, 16, 76). Ivanovic et al. showed that the release of the δ fragment from ISVPs is aided by the cellular chaperone Hsc70 (49).

Another role for chaperones in the reovirus life cycle has been described for the folding of the σ1 attachment protein. σ1 resembles a long fiber consisting of a tail and head domain (31, 37). In the mature virion one σ1 trimer is located at each of the fivefold axis of symmetry (39, 93). The trimerization of σ1 occurs in two distinct steps. The N-terminal tail trimerizes cotranslationally and without the aid of chaperones (56). However, the C-terminal head domain depends on ATP, Hsp70 and Hsp90 in order to post-translationally achieve the proper folding (41, 56).

So far no other roles of chaperones in the reovirus life cycle have been described.

In this thesis I present the results of my studies on the interaction of different reoviral proteins with the cellular chaperone, heat shock cognate protein 70 (Hsc70). Chapter 2, shows how the nonstructural protein μNS of reovirus interacts with Hsc70 independently of its chaperoning function. Chapter 3 discusses the association of Hsc70 with the outer capsid protein μ1, the influence of the chaperone on the trafficking of another outer capsid protein, σ3, and the possible implications for μ1:σ3 complex formation. Chapter 4 explores other potential ways how the functions of μ1 are regulated during infection and investigates ubiquitination and caspase cleavage of μ1. Specific background information pertinent to each chapter will be reviewed in each chapter's introduction.

Reference List

1. **Agosto, M. A., T. Ivanovic, and M. L. Nibert**. 2006. Mammalian reovirus, a nonfusogenic nonenveloped virus, forms size-selective pores in a model membrane. Proc. Natl. Acad. Sci. U. S. A **103**:16496-16501.

2. **Antczak, J. B. and W. K. Joklik**. 1992. Reovirus genome segment assortment into progeny genomes studied by the use of monoclonal antibodies directed against reovirus proteins. Virology **187**:760-776.

3. **Attoui, H., J. F. Mohd, M. Belhouchet, P. Biagini, J. F. Cantaloube, M. P. de, and L. de, X**. 2005. Expansion of family *Reoviridae* to include nine-segmented dsRNA viruses: isolation and characterization of a new virus designated Aedes pseudoscutellaris reovirus assigned to a proposed genus (Dinovernavirus). Virology **343**:212-223.

4. **Ballinger, C. A., P. Connell, Y. Wu, Z. Hu, L. J. Thompson, L. Y. Yin, and C. Patterson**. 1999. Identification of CHIP, a novel tetratricopeptide repeat-containing protein that interacts with heat shock proteins and negatively regulates chaperone functions. Mol. Cell Biol. **19**:4535-4545.

5. **Becker, M. M., M. I. Goral, P. R. Hazelton, G. S. Baer, S. E. Rodgers, E. G. Brown, K. M. Coombs, and T. S. Dermody**. 2001. Reovirus σNS protein is required for nucleation of viral assembly complexes and formation of viral inclusions. J Virol **75**:1459-1475.

6. **Beere, H. M. and D. R. Green**. 2001. Stress management - heat shock protein-70 and the regulation of apoptosis. Trends Cell Biol. **11**:6-10.

7. **Borsa, J., T. P. Copps, M. D. Sargent, D. G. Long, and J. D. Chapman**. 1973. New intermediate subviral particles in the in vitro uncoating of reovirus virions by chymotrypsin. J Virol **11**:552-564.

8. **Broering, T. J., J. Kim, C. L. Miller, C. D. Piggott, J. B. Dinoso, M. L. Nibert, and J. S. Parker**. 2004. Reovirus nonstructural protein μNS recruits viral core surface proteins and entering core particles to factory-like inclusions. J. Virol. **78**:1882-1892.

9. **Broering, T. J., A. M. McCutcheon, V. E. Centonze, and M. L. Nibert**. 2000. Reovirus nonstructural protein μNS binds to core particles but does not inhibit their transcription and capping activities. J Virol **74**:5516-5524.

10. **Broering, T. J., J. S. Parker, P. L. Joyce, J. Kim, and M. L. Nibert**. 2002. Mammalian reovirus nonstructural protein μNS forms large inclusions and colocalizes with reovirus microtubule-associated protein μ2 in transfected cells. J Virol **76**:8285-8297.

11. **Bukau, B., E. Deuerling, C. Pfund, and E. A. Craig**. 2000. Getting newly synthesized proteins into shape. Cell **101**:119-122.

12. **Bukau, B. and A. L. Horwich**. 1998. The Hsp70 and Hsp60 chaperone machines. Cell **92**:351-366.

13. **Campbell, J. A., P. Schelling, J. D. Wetzel, E. M. Johnson, J. C. Forrest, G. A. Wilson, M. urrand-Lions, B. A. Imhof, T. Stehle, and T. S. Dermody**. 2005. Junctional adhesion molecule a serves as a receptor for prototype and field-isolate strains of mammalian reovirus. J Virol **79**:7967-7978.

14. **Caplan, A. J., D. M. Cyr, and M. G. Douglas**. 1993. Eukaryotic homologues of *Escherichia coli* dnaJ: a diverse protein family that functions with hsp70 stress proteins. Mol. Biol. Cell **4**:555-563.

15. **Carstens, E. B.** 2010. Ratification vote on taxonomic proposals to the International Committee on Taxonomy of Viruses (2009). Arch. Virol **155**:133-146.

16. **Chandran, K., D. L. Farsetta, and M. L. Nibert**. 2002. Strategy for nonenveloped virus entry: a hydrophobic conformer of the reovirus membrane penetration protein μ1 mediates membrane disruption. J Virol **76**:9920-9933.

17. **Chandran, K. and M. L. Nibert**. 1998. Protease cleavage of reovirus capsid protein μ1/μ1C is blocked by alkyl sulfate detergents, yielding a new type of infectious subvirion particle. J Virol **72**:467-475.

18. **Chandran, K., J. S. Parker, M. Ehrlich, T. Kirchhausen, and M. L. Nibert**. 2003. The δ region of outer-capsid protein μ1 undergoes conformational change and release from reovirus particles during cell entry. J Virol **77**:13361-13375.

19. **Chen, S., V. Prapapanich, R. A. Rimerman, B. Honore, and D. F. Smith**. 1996. Interactions of p60, a mediator of progesterone receptor assembly, with heat shock proteins hsp90 and hsp70. Mol. Endocrinol. **10**:682-693.

20. **Chou, C. C., F. Forouhar, Y. H. Yeh, H. L. Shr, C. Wang, and C. D. Hsiao**. 2003. Crystal structure of the C-terminal 10-kDa subdomain of Hsc70. J Biol. Chem. **278**:30311-30316.

21. **Chromy, L. R., J. M. Pipas, and R. L. Garcea**. 2003. Chaperone-mediated in vitro assembly of Polyomavirus capsids. Proc. Natl. Acad. Sci. U. S. A **100**:10477-10482.

22. **Cleveland, D. R., H. Zarbl, and S. Millward**. 1986. Reovirus guanylyltransferase is L2 gene product λ2. J Virol **60**:307-311.

23. **Cobbold, C., M. Windsor, and T. Wileman**. 2001. A virally encoded chaperone specialized for folding of the major capsid protein of African swine fever virus. J Virol **75**:7221-7229.

24. **Coffey, C. M., A. Sheh, I. S. Kim, K. Chandran, M. L. Nibert, and J. S. Parker**. 2006. Reovirus outer capsid protein μ1 induces apoptosis and associates with lipid droplets, endoplasmic reticulum, and mitochondria. J Virol **80**:8422-8438.

25. **Cripe, T. P., S. E. Delos, P. A. Estes, and R. L. Garcea**. 1995. In vivo and in vitro association of hsc70 with polyomavirus capsid proteins. J Virol **69**:7807-7813.

26. **Dales, S.** 1963. Association between the spindle apparatus and reovirus. Proc. Natl. Acad. Sci. U. S. A **50**:268-275.

27. **Dales, S., P. J. Gomatos, and K. C. Hsu**. 1965. The uptake and development of reovirus in strain L cells followed with labeled viral ribonucleic acid and ferritin-antibody conjugates. Virology **25**:193-211.

28. **Demand, J., J. Luders, and J. Hohfeld**. 1998. The carboxy-terminal domain of Hsc70 provides binding sites for a distinct set of chaperone cofactors. Mol. Cell Biol. **18**:2023-2028.

29. **Dermody, T. S., M. L. Nibert, R. Bassel-Duby, and B. N. Fields**. 1990. Sequence diversity in S1 genes and S1 translation products of 11 serotype 3 reovirus strains. J Virol **64**:4842-4850.

30. **Dryden, K. A., G. Wang, M. Yeager, M. L. Nibert, K. M. Coombs, D. B. Furlong, B. N. Fields, and T. S. Baker**. 1993. Early steps in reovirus infection are associated with dramatic changes in supramolecular structure and protein conformation: analysis of virions and subviral particles by cryoelectron microscopy and image reconstruction. J Cell Biol. **122**:1023-1041.

31. **Duncan, R., D. Horne, J. E. Strong, G. Leone, R. T. Pon, M. C. Yeung, and P. W. Lee**. 1991. Conformational and functional analysis of the C-terminal globular head of the reovirus cell attachment protein. Virology **182**:810-819.

32. **Ebert, D. H., J. Deussing, C. Peters, and T. S. Dermody**. 2002. Cathepsin L and cathepsin B mediate reovirus disassembly in murine fibroblast cells. J Biol. Chem. **277**:24609-24617.

33. **Ellis, J.** 1987. Proteins as molecular chaperones. Nature **328**:378-379.

34. **Flaherty, K. M., C. Luca-Flaherty, and D. B. McKay**. 1990. Three-dimensional structure of the ATPase fragment of a 70K heat-shock cognate protein. Nature **346**:623-628.

35. **Florin, L., K. A. Becker, C. Sapp, C. Lambert, H. Sirma, M. Muller, R. E. Streeck, and M. Sapp**. 2004. Nuclear translocation of papillomavirus minor capsid protein L2 requires Hsc70. J Virol **78**:5546-5553.

36. **Flynn, G. C., T. G. Chappell, and J. E. Rothman**. 1989. Peptide binding and release by proteins implicated as catalysts of protein assembly. Science **245**:385-390.

37. **Fraser, R. D., D. B. Furlong, B. L. Trus, M. L. Nibert, B. N. Fields, and A. C. Steven**. 1990. Molecular structure of the cell-attachment protein of reovirus: correlation of computer-processed electron micrographs with sequence-based predictions. J Virol **64**:2990-3000.

38. **Freeman, B. C., M. P. Myers, R. Schumacher, and R. I. Morimoto**. 1995. Identification of a regulatory motif in Hsp70 that affects ATPase activity, substrate binding and interaction with HDJ-1. EMBO J **14**:2281-2292.

39. **Furlong, D. B., M. L. Nibert, and B. N. Fields**. 1988. σ1 protein of mammalian reoviruses extends from the surfaces of viral particles. J Virol **62**:246-256.

40. **Gillian, A. L., S. C. Schmechel, J. Livny, L. A. Schiff, and M. L. Nibert**. 2000. Reovirus protein σNS binds in multiple copies to single-stranded RNA and shares properties with single-stranded DNA binding proteins. J Virol **74**:5939-5948.

41. **Gilmore, R., M. C. Coffey, and P. W. Lee**. 1998. Active participation of Hsp90 in the biogenesis of the trimeric reovirus cell attachment protein σ1. J Biol. Chem. **273**:15227-15233.

42. **Grimes, J. M., J. N. Burroughs, P. Gouet, J. M. Diprose, R. Malby, S. Zientara, P. P. Mertens, and D. I. Stuart**. 1998. The atomic structure of the bluetongue virus core. Nature **395**:470-478.

43. **Hartl, F. U.** 1996. Molecular chaperones in cellular protein folding. Nature **381**:571-580.

44. **Helmbrecht, K. and L. Rensing**. 1999. Different constitutive heat shock protein 70 expression during proliferation and differentiation of rat C6 glioma cells. Neurochem. Res. **24**:1293-1299.

45. **Hemmingsen, S. M., C. Woolford, d. van, V, K. Tilly, D. T. Dennis, C. P. Georgopoulos, R. W. Hendrix, and R. J. Ellis**. 1988. Homologous plant and bacterial proteins chaperone oligomeric protein assembly. Nature **333**:330-334.

46. **Hohfeld, J. and S. Jentsch**. 1997. GrpE-like regulation of the hsc70 chaperone by the anti-apoptotic protein BAG-1. EMBO J **16**:6209-6216.

47. **Hohfeld, J., Y. Minami, and F. U. Hartl**. 1995. Hip, a novel cochaperone involved in the eukaryotic Hsc70/Hsp40 reaction cycle. Cell **83**:589-598.

48. **Hu, J., D. O. Toft, and C. Seeger**. 1997. Hepadnavirus assembly and reverse transcription require a multi-component chaperone complex which is incorporated into nucleocapsids. EMBO J **16**:59-68.

49. **Ivanovic, T., M. A. Agosto, K. Chandran, and M. L. Nibert**. 2007. A role for molecular chaperone Hsc70 in reovirus outer capsid disassembly. J. Biol. Chem. **282**:12210-12219.

50. **Jiang, J., K. Prasad, E. M. Lafer, and R. Sousa**. 2005. Structural basis of interdomain communication in the Hsc70 chaperone. Mol. Cell **20**:513-524.

51. **Joklik, W. K.** 1972. Studies on the effect of chymotrypsin on reovirions. Virology **49**:700-715.

52. **Joklik, W. K.** 1980. The structure and function of the reovirus genome. Ann. N. Y. Acad. Sci. **354**:107-124.

53. **Kim, J., J. S. Parker, K. E. Murray, and M. L. Nibert**. 2004. Nucleoside and RNA triphosphatase activities of orthoreovirus transcriptase cofactor μ2. J Biol. Chem. **279**:4394-4403.

54. **Landry, S. J.** 2003. Structure and energetics of an allele-specific genetic interaction between dnaJ and dnaK: correlation of nuclear magnetic resonance chemical shift perturbations in the J-domain of Hsp40/DnaJ with binding affinity for the ATPase domain of Hsp70/DnaK. Biochemistry **42**:4926-4936.

55. **Leers, W. D. and K. R. Rozee**. 1966. A survey of reovirus antibodies in sera of urban children. Can. Med. Assoc. J **94**:1040-1042.

56. **Leone, G., M. C. Coffey, R. Gilmore, R. Duncan, L. Maybaum, and P. W. Lee**. 1996. C-terminal trimerization, but not N-terminal trimerization, of the reovirus cell attachment protein is a posttranslational and Hsp70/ATP-dependent process. J Biol. Chem. **271**:8466-8471.

57. **Lerner, A. M., J. D. Cherry, J. O. Klein, and M. Finland**. 1962. Infections with reoviruses. N. Engl. J Med. **267**:947-952.

58. **Liebscher, M. and A. Roujeinikova**. 2009. Allosteric coupling between the lid and interdomain linker in DnaK revealed by inhibitor binding studies. J Bacteriol. **191**:1456-1462.

59. **Liemann, S., K. Chandran, T. S. Baker, M. L. Nibert, and S. C. Harrison**. 2002. Structure of the reovirus membrane-penetration protein, μ1, in a complex with is protector protein, σ3. Cell **108**:283-295.

60. **Luongo, C. L., C. M. Contreras, D. L. Farsetta, and M. L. Nibert**. 1998. Binding site for S-adenosyl-L-methionine in a central region of mammalian reovirus λ2 protein. Evidence for activities in mRNA cap methylation. J Biol. Chem. **273**:23773-23780.

61. **Luongo, C. L., K. M. Reinisch, S. C. Harrison, and M. L. Nibert**. 2000. Identification of the guanylyltransferase region and active site in reovirus mRNA capping protein λ2. J Biol. Chem. **275**:2804-2810.

62. **Maginnis, M. S., J. C. Forrest, S. A. Kopecky-Bromberg, S. K. Dickeson, S. A. Santoro, M. M. Zutter, G. R. Nemerow, J. M. Bergelson, and T. S. Dermody**. 2006. β1 integrin mediates internalization of mammalian reovirus. J Virol **80**:2760-2770.

63. **Maginnis, M. S., B. A. Mainou, A. Derdowski, E. M. Johnson, R. Zent, and T. S. Dermody**. 2008. NPXY Motifs in the β1 Integrin Cytoplasmic Tail Are Required for Functional Reovirus Entry. J Virol **82**:3181-3191.

64. **Mayer, M. P.** 2005. Recruitment of Hsp70 chaperones: a crucial part of viral survival strategies. Rev. Physiol Biochem. Pharmacol. **153**:1-46.

65. **Mayer, M. P.** 2010. Gymnastics of molecular chaperones. Mol. Cell **39**:321-331.

66. **McDonough, H. and C. Patterson**. 2003. CHIP: a link between the chaperone and proteasome systems. Cell Stress. Chaperones. **8**:303-308.

67. **Metcalf, P.** 1982. The symmetry of the reovirus outer shell. J Ultrastruct. Res. **78**:292-301.

68. **Metcalf, P., M. Cyrklaff, and M. Adrian**. 1991. The three-dimensional structure of reovirus obtained by cryo-electron microscopy. EMBO J. **10**:3129-3136.

69. **Miller, C. L., M. M. Arnold, T. J. Broering, C. E. Hastings, and M. L. Nibert**. 2010. Localization of mammalian orthoreovirus proteins to cytoplasmic factory-like structures via nonoverlapping regions of μNS. J Virol **84**:867-882.

70. **Minami, Y., J. Hohfeld, K. Ohtsuka, and F. U. Hartl**. 1996. Regulation of the heat-shock protein 70 reaction cycle by the mammalian DnaJ homolog, Hsp40. J Biol. Chem. **271**:19617-19624.

71. **Morgan, E. M. and H. J. Zweerink**. 1974. Reovirus morphogenesis. Corelike particles in cells infected at 39 degrees with wild-type reovirus and temperature-sensitive mutants of groups B and G. Virology **59**:556-565.

72. **Morgan, E. M. and H. J. Zweerink**. 1975. Characterization of transcriptase and replicase particles isolated from reovirus-infected cells. Virology **68**:455-466.

73. **Neupert, W. and M. Brunner**. 2002. The protein import motor of mitochondria. Nat. Rev. Mol. Cell Biol. **3**:555-565.

74. **Nibert, M. L., T. S. Dermody, and B. N. Fields**. 1990. Structure of the reovirus cell-attachment protein: a model for the domain organization of sigma 1. J Virol **64**:2976-2989.

75. **Nibert, M. L., A. L. Odegard, M. A. Agosto, K. Chandran, and L. A. Schiff**. 2005. Putative autocleavage of reovirus μ1 protein in concert with outer-capsid disassembly and activation for membrane permeabilization. J. Mol. Biol. **345**:461-474.

76. **Odegard, A. L., K. Chandran, X. Zhang, J. S. Parker, T. S. Baker, and M. L. Nibert**. 2004. Putative autocleavage of outer capsid protein μ1, allowing release of myristoylated peptide μ1N during particle uncoating, is critical for cell entry by reovirus. J Virol **78**:8732-8745.

77. **Olland, A. M., J. Jane-Valbuena, L. A. Schiff, M. L. Nibert, and S. C. Harrison**. 2001. Structure of the reovirus outer capsid and dsRNA-binding protein σ3 at 1.8 Å resolution. EMBO J. **20**:979-989.

78. **Parker, J. S., T. J. Broering, J. Kim, D. E. Higgins, and M. L. Nibert**. 2002. Reovirus core protein μ2 determines the filamentous morphology of viral inclusion bodies by interacting with and stabilizing microtubules. J Virol **76**:4483-4496.

79. **Peng, Y. C. and N. H. Acheson**. 1998. Polyomavirus large T antigen binds cooperatively to its multiple binding sites in the viral origin of DNA replication. J Virol **72**:7330-7340.

80. **Qiu, X. B., Y. M. Shao, S. Miao, and L. Wang**. 2006. The diversity of the DnaJ/Hsp40 family, the crucial partners for Hsp70 chaperones. Cell Mol. Life Sci. **63**:2560-2570.

81. **Reinisch, K. M., M. L. Nibert, and S. C. Harrison**. 2000. Structure of the reovirus core at 3.6 Å resolution. Nature **404**:960-967.

82. **Rhim, J. S., L. E. Jordan, and H. D. Mayor**. 1962. Cytochemical, fluorescent-antibody and electron microscopic studies on the growth of reovirus (ECHO 10) in tissue culture. Virology **17**:342-355.

83. **Rothman, J. E.** 1989. Polypeptide chain binding proteins: catalysts of protein folding and related processes in cells. Cell **59**:591-601.

84. **Ryan, M. T. and N. Pfanner**. 2001. Hsp70 proteins in protein translocation. Adv. Protein Chem. **59**:223-242.

85. **Satyanarayana, T., S. Gowda, M. Mawassi, M. R. biach-Marti, M. A. Ayllon, C. Robertson, S. M. Garnsey, and W. O. Dawson**. 2000. Closterovirus encoded HSP70 homolog and p61 in addition to both coat proteins function in efficient virion assembly. Virology **278**:253-265.

86. **Schiff, L. A., M. L. Nibert, and K. L. Tyler**. 2006. Orthoreoviruses and Their Replication *In* D. M. Knipe, P. M. Howley, and D. E. Griffin (eds.), Fields Virology. Wolters Kluwer, Lippincott Williams & Wilkins, Philadelphia, PA.

87. **Schlieker, C., B. Bukau, and A. Mogk**. 2002. Prevention and reversion of protein aggregation by molecular chaperones in the *E. coli* cytosol: implications for their applicability in biotechnology. J Biotechnol. **96**:13-21.

88. **Selb, B. and B. Weber**. 1994. A study of human reovirus IgG and IgA antibodies by ELISA and western blot. J Virol Methods **47**:15-25.

89. **Shatkin, A. J., J. D. Sipe, and P. Loh**. 1968. Separation of ten reovirus genome segments by polyacrylamide gel electrophoresis. J Virol **2**:986-991.

90. **Spendlove, R. S., E. H. Lennette, and A. C. John**. 1963. The role of the mitotic apparatus in the intracellular location of reovirus antigen. J Immunol. **90**:554-560.

91. **Srinivasan, A., A. J. McClellan, J. Vartikar, I. Marks, P. Cantalupo, Y. Li, P. Whyte, K. Rundell, J. L. Brodsky, and J. M. Pipas**. 1997. The amino-terminal transforming region of simian virus 40 large T and small t antigens functions as a J domain. Mol. Cell Biol. **17**:4761-4773.

92. **Stahl, M., J. Beck, and M. Nassal**. 2007. Chaperones activate hepadnavirus reverse transcriptase by transiently exposing a C-proximal region in the terminal protein domain that contributes to epsilon RNA binding. J Virol **81**:13354-13364.

93. **Strong, J. E., G. Leone, R. Duncan, R. K. Sharma, and P. W. Lee**. 1991. Biochemical and biophysical characterization of the reovirus cell attachment protein σ1: evidence that it is a homotrimer. Virology **184**:23-32.

94. **Sturzenbecker, L. J., M. Nibert, D. Furlong, and B. N. Fields**. 1987. Intracellular digestion of reovirus particles requires a low pH and is an essential step in the viral infectious cycle. J Virol **61**:2351-2361.

95. **Sullivan, C. S. and J. M. Pipas**. 2002. T antigens of simian virus 40: molecular chaperones for viral replication and tumorigenesis. Microbiol. Mol. Biol. Rev. **66**:179-202.

96. **Tao, Y., D. L. Farsetta, M. L. Nibert, and S. C. Harrison**. 2002. RNA synthesis in a cage--structural studies of reovirus polymerase λ3. Cell **111**:733-745.

97. **Wang, H., A. V. Kurochkin, Y. Pang, W. Hu, G. C. Flynn, and E. R. Zuiderweg**. 1998. NMR solution structure of the 21 kDa chaperone protein DnaK substrate binding domain: a preview of chaperone-protein interaction. Biochemistry **37**:7929-7940.

98. **Young, J. C., J. M. Barral, and F. Ulrich Hartl**. 2003. More than folding: localized functions of cytosolic chaperones. Trends in Biochemical Sciences **28**:541-547.

99. **Zhang, X., S. B. Walker, P. R. Chipman, M. L. Nibert, and T. S. Baker**. 2003. Reovirus polymerase λ3 localized by cryo-electron microscopy of virions at a resolution of 7.6 Å. Nat. Struct. Biol. **10**:1011-1018.

100. **Zhu, X., X. Zhao, W. F. Burkholder, A. Gragerov, C. M. Ogata, M. E. Gottesman, and W. A. Hendrickson**. 1996. Structural analysis of substrate binding by the molecular chaperone DnaK. Science **272**:1606-1614.

101. **Zimmerman, S. B. and S. O. Trach**. 1991. Estimation of macromolecule concentrations and excluded volume effects for the cytoplasm of Escherichia coli. J Mol. Biol. **222**:599-620.

102. **Zweerink, H. J., E. M. Morgan, and J. S. Skyler**. 1976. Reovirus morphogenesis: characterization of subviral particles in infected cells. Virology **73**:442-453.

CHAPTER TWO

The cellular chaperone Hsc70 is specifically recruited to reovirus viral factories independently of its chaperone function*

***Susanne Kaufer, Caroline M. Coffey and John S.L. Parker**, Journal of Virology, In Revision.

Abstract

Mammalian orthoreoviruses replicate and assemble in the cytosol of infected cells. A viral nonstructural protein, μNS, forms large inclusion-like structures called viral factories (VFs) in which assembling viral particles can be identified. Here we examined the localization of the cellular chaperone Hsc70 and found that it co-localizes with VFs in infected cells and also with viral factory-like structures (VFLs) formed by ectopically expressed μNS. SiRNA-mediated knockdown of Hsc70 did not affect the formation or maintenance of VFLs. We further showed that dominant negative mutants of Hsc70 were also recruited to VFLs, indicating that Hsc70 recruitment to VFLs was independent of chaperoning function. In support of this finding μNS was immunoprecipitated with wild type Hsc70, with a dominant negative mutant of Hsc70, and with the minimal substrate-binding site of Hsc70 (amino acids 395-540). We identified the minimal region of μNS sufficient to interact with Hsc70 between amino acids 222-271, a region of μNS that has not been ascribed any function to date. However, point mutants in this region or the complete deletion of this domain did not abrogate μNS-Hsc70 interaction, indicating that a second portion of μNS also interacts with Hsc70. Taken together these findings suggest a specific chaperone function for Hsc70 within viral factories, the sites of reovirus replication and assembly in cells.

Introduction

Mammalian orthoreoviruses have a genome of ten double-stranded RNA (dsRNA) segments that are encased in a double-layered nonenveloped capsid. Replication and assembly of reoviruses are thought to take place in distinct cytoplasmic inclusion bodies called viral factories (VFs) (32). The matrix of these structures is formed by the nonstructural viral protein μNS (5). The factories are not static elements, but can fuse with other viral factories in the same infected cell (Parker, unpublished findings). During the course of infection other viral proteins are recruited to the viral factories at distinct times (2, 8, 27). By thin section electron microscopy the matrix of viral factories appears to consist of fibrils that have a distinct kink (9, 10, 34). However, an atomic resolution structure of μNS is not available. If expressed alone without other viral proteins, the 80 kDa μNS protein forms viral factory-like (VFL) structures that resemble VFs in infected cells (5). The carboxyl-terminal (C-terminal) third of μNS comprising amino acids (aa) 471-721 is sufficient for VFL formation (2). This minimal factory-forming region has two predicted coiled-coil domains linked by a putative zinc hook and followed by a short C-terminal tail (25). The first third of μNS (aa 1-221) has been identified as a scaffold for the recruitment of the viral proteins λ1, λ2, μ2, σ2, and σNS; in contrast the RNA-dependent RNA polymerase (RdRp), λ3, interacts with the C-terminal minimal factory-forming region (5, 26, 27). So far no function has been elucidated for the middle portion of μNS (aa 222-470).

Many viruses are dependent upon or at least aided during their lifecycle by either cellular or virally encoded chaperones (22). Cellular chaperones are involved in folding and refolding of proteins, disaggregation of protein aggregates, translocation of proteins across membranes and the assembly and disassembly of oligomeric protein complexes [reviewed in (38)]. One of the most abundant chaperones in eukaryotic

cells is the heat shock cognate protein 70 (Hsc70). In addition, a closely related protein, heat shock protein 70 (Hsp70) is induced during cellular stress. Chaperones are involved in entry/disassembly of virions, translocation of the viral genome to the site of replication, replication itself, packaging of the genome, folding of capsid proteins and assembly of capsids (reviewed in (22)). During reovirus entry the outer shell of the double-layered particle is first proteolytically processed to remove the outer capsid protein σ3. The remaining outer capsid protein μ1 then undergoes autoproteolysis and conformational change that allows the particle to penetrate into the cytosol. Following entry of this subviral particle into the cytosol of cells the δ fragment of μ1 remains associated with the viral core particle (reviewed in (11)). This δ fragment of μ1 is removed from core particles in a process dependent upon Hsc70 (18). Furthermore, folding of the σ1 attachment protein is dependent on Hsp70 and Hsp90 (16, 20).

Here we show that the cellular chaperone Hsc70 specifically interacts with the VF matrix protein μNS.

Materials and Methods

Cells and viruses. CV-1 cells were grown at 37°C in 5% CO_2 in Eagles Minimum Essential Medium (MEM) (CellGro) supplemented with 10% fetal bovine serum (HyClone), 100 U ml^{-1} of penicillin, 100 μg ml^{-1} streptomycin, 250 ng ml^{-1} amphotericin B, 50 μg ml^{-1} gentamycin, 125 ng ml^{-1} amphotericin B (antibiotic-antimycotic solution, Cellgro) and non-essential amino acids (CellGro). 293F (human embryonic kidney cells) cells were grown on a shaker (125 rpm) at 37°C in 8% CO_2 in FreeStyle™ 293 Expression Medium (Gibco) supplemented with 50 U ml^{-1} penicillin, 50 μg ml^{-1} streptomycin and 125 ng ml^{-1} amphotericin B (antibiotic-antimycotic solution, Cellgro). Reoviruses T1L and T3D were laboratory stocks of the isolates previously identified as T1/human/Ohio/Lang/1953 and T3/human/Ohio/Dearing/1955, respectively (17). The superscript N in $T3D^N$ differentiates a laboratory stock obtained from the Nibert laboratory from a T3D clone obtained from L. W. Cashdollar (Medical College of Wisconsin), denoted $T3D^{CD}$. The $T3D^{CD}$ clone differs from the $T3D^N$ clone in viral factory morphology and in the nucleotide sequence of its M1 genome segment (31). Viruses were plaque-purified and amplified in murine L929 cells in Joklik's modified minimal essential medium (Gibco) supplemented with 4% fetal bovine serum (HyClone), 2 mM glutamine (Cellgro), 100 U ml^{-1} penicillin, 100 μg ml^{-1} streptomycin, 250 ng ml^{-1} amphotericin B (antibiotic-antimycotic solution, Cellgro) and 50 μg ml^{-1} gentamycin (Cellgro).

Antibodies and reagents. Rabbit polyclonal antiserum against μNS has been described previously (4, 35, 36). Rat monoclonal antibody (mAb) against Hsc70 (1B5; not cross-reactive with Hsp70) immunoglobulin G (IgG) isotype 2a (IgG_{2a}) was purchased from Stressgen and rat mAB anti-HA (3F10) IgG_1 antibody was obtained from Roche Diagnostics (Mannheim, Germany). A rat mAb IgG_{2a} against Trichinella spiralis 18H1.1 (Tsp) was a kind gift from Dr. Judith Appleton. Mouse mAb against α-

tubulin (DM1A) was purchased from Sigma Aldrich. Rabbit pAb against the HaloTag7 was purchased from Promega. Secondary antibodies for immunofluorescence (IF) microscopy were goat anti-mouse IgG, goat anti-rabbit IgG, and goat anti-rat IgG conjugated to Alexa 488 or Alexa 594 (Invitrogen). Secondary antibodies for immunoblot detection were donkey anti-rabbit IgG, donkey anti-mouse IgG, and rabbit anti-rat IgG conjugated to horseradish peroxidase (HRP) (Jackson ImmunoResearch). Secondary antibodies used with the Odyssey Infrared Scanner (LI-COR) were IRDye 800CW goat anti-mouse IgG and IRDye 680 goat anti-rat IgG (LI-COR). All antibodies were titrated to optimize signal to noise ratios.

Plasmid construction. Plasmid pCI-M3(T1L) has been described previously (4). The gene encoding bovine Hsc70 was PCR-amplified using pEGFP-Hsc70 (courtesy of S. Schmid) as template. The PCR product was purified and cut with *XhoI* and *NheI* restriction enzymes (NEB Biolabs) then ligated into pCI-neo cut with the same enzymes. Dominant negative mutants K71M, D199S and T204V of Hsc70 were cloned similarly from their pEGFP background into pCI-neo. Wild type and mutant Hsc70 were tagged at the C-terminus with an HA-tag by Phusion PCR. pFN21A-HaloTag7-Flexi and HaloTag control vectors were purchased from Promega. Various truncation and/or point mutants of pCI-Hsc70-HA, pCI-M3(T1L) and pFN21A-HaloTag7-M3(T1L) were constructed using standard mutagenesis. The following twenty point mutants of μNS were prepared: H223A, G229A, D232A, E234A, Y236A, N237A, R240A, M242A, F243A, Q245A, H246A, P248A, L249A, Q253A, Y255A, D262A, Y263A, F264A, P268A, and D271A. Cloning details and primers available upon request.

Infections and transfections. CV-1 cells were seeded the day before transfection or infection at a density of 5×10^4 in twelve-well plates containing 18-mm-diameter round glass cover slips. Infections were begun by adsorbing virus stocks

to cells at an MOI of 5 PFU/cell or as indicated, for 1 h at room temperature in phosphate-buffered saline (PBS) (137 mM NaCl, 3 mM KCl, 8 mM Na_2HPO_4, 1 mM KH_2PO_4 [pH 7.5]). Cells were then overlaid with growth medium and incubated at 37°C for 24 h or as indicated. CV-1 cells were transfected using FuGene HD transfection reagent (Roche) according to the manufacturer's instructions. A 7:2 ratio of FuGene HD reagent to DNA was used. Transfected cells were incubated at 37°C for 24 h or as indicated. 293F cells were transfected using 293fectin (Invitrogen) according to the manufacturer's instructions. The day before transfection 293F cells were set up at a density of 5-7 × 10^5 per ml in 14 or 28 ml of antibiotic-free FreeStyle™ 293 Expression Medium. A 2:1 ratio of 293fectin to DNA was used.

siRNA treatment. For IF studies CV-1 cells were seeded the day before transfection at a density of 1.5 × 10^4 in twelve- well plates containing 18-mm-diameter round cover slips. Cells were transfected with 100 nM siRNA J-017609-08 (Dharmacon) using Dharmafect 1 transfection reagent (Dharmacon) according to the manufacturer's instructions. The complexes were incubated for 20 min then added to cells and incubated at 37°C for the indicated amount of time.

To evaluate the knockdown efficiency, CV-1 cells were seeded the day before transfection at a density of 5 × 10^4 in six-well plates and transfected as above with either Hsc70 siRNA or non-specific control siRNA. Cells were harvested 48, 72 and 96 h after transfection by trypsinization. Pellets were lysed in 30 µl of 10% SDS and 31.2 mM Tris-HCl pH 7.4 then sonicated with a microtip (power 2, duty cycle 20%, 2 × 10 times on ice). Total protein concentration of the lysates was determined (DC Protein Assay; BioRad) and equal amounts were analyzed by SDS-PAGE and immunoblotting. Simultaneous detection of Hsc70 and α-tubulin was performed with the Odyssey Infrared Scanner (LI-COR) utilizing primary antibodies rat anti-Hsc70 and mouse anti-α-tubulin followed by secondary antibodies IRDye 680 goat anti-rat

IgG and IRDye 800CW goat anti-mouse IgG. The integrated intensity of the selected Hsc70 and α-tubulin bands was measured by the Odyssey program and the relative amount of Hsc70 was normalized to the amount of α-tubulin. Data from three independent experiments were collected and differences in the means were evaluated by a paired one-tailed Student's t-test.

Immunofluorescence (IF) microscopy. Cells on glass cover slips were fixed for 10 min at room temperature in 2% paraformaldehyde in PBS, washed 3 times in PBS, then permeabilized for 15 min in PBS containing 1% bovine serum albumin (BSA), 0.1% Triton X-100 and 0.05% sodium azide (PBSA-T). Where indicated, cells were fixed with 100% methanol for 20 seconds at -20°C and then rehydrated by washing 3 × 5 min in PBSA-T. All antibody incubations were carried out for 30 min at room temperature in PBSA-T. Cover slips were washed 3 times in PBS between primary and secondary antibody incubations. Cover slips were mounted on glass slides with ProLong Gold + DAPI reagent (Molecular Probes). Fluorescence and phase images were obtained with a Nikon TE2000 inverted microscope equipped with fluorescence and phase optics through a 60 × 1.4 NA oil objective with 1.5 × optical zoom. Images were collected digitally with a Coolsnap HQ CCD camera (Roper) and Openlab software (Improvision) then were prepared for publication using Photoshop and Illustrator software (Adobe Systems).

Immunoprecipitation (IP) and immunoblotting. 293F cells were harvested by centrifuging the cell suspension for 5 min at 500 × g and 4°C. Cells were washed twice with cold PBS and lysed in 1 ml lysis buffer (50 mM Tris-HCl pH 7.4, 100 mM NaCl, 1% Tween-20, 1 mM phenylmethylsulfonylfluoride) on ice for 30 min. Lysates were cleared by centrifuging for 15 min at 16,060 × g and 4°C. For each sample 2.5 µg of anti-Trichinella spiralis (anti-Tsp) or anti-Hsc70 antibody was bound to 30 µl of recombinant protein G agarose (Invitrogen) by rotating for 1 h at room temperature in

500 µl PBS with 0.5 µl of 10% Triton X-100. Afterwards the antibody-bound agarose was washed 3 times in 1 ml of TBST (Tris buffered saline Tween-20) and incubated 30 min or overnight at 4°C with the pre-cleared cell lysate. Anti-HA 3F10 antibody (and anti-Tsp control antibody) were added unbound together with 30 µl of recombinant protein G agarose to the pre-cleared cell lysate at a concentration of 0.25 µg per sample and incubated as above. Samples were washed 4-6 × 5 min with 1 ml of wash buffer (50 mM Tris-HCl pH 7.4, 100 mM NaCl, 2% Tween-20) on ice. After a final wash with 1 ml PBS, 5 µl of 5 × sodium dodecyl sulfate (SDS) sample buffer was added to each sample and boiled for 5 min at 95°C. Bound proteins were separated by SDS polyacrylamide gel electrophoresis (PAGE). Proteins were transferred from gels to nitrocellulose membranes and blocked for 30 min at room temperature in 1 × PBS (pH 7.4) containing 0.1% Tween-20, 100 U ml^{-1} penicillin, 100 µg ml^{-1} streptomycin and 5% powdered milk. Precipitated proteins were detected with rabbit anti-µNS antiserum, rat anti-Hsc70 and rat anti-HA 3F10 antibodies in blocking buffer for 1 h at RT or overnight at 4°C. Membranes were washed 3 × 5 min in 1 × TBST before incubation with secondary antibodies for 1 h at RT and final washes of 6 × 5 min in 1 × TBST. Secondary antibodies used were donkey anti-rabbit, donkey anti-mouse and rabbit anti-rat IgG conjugated to horseradish peroxidase (HRP) and were detected with SuperSignal West Pico Chemiluminescent Substrate (Pierce) and fluorography. For consecutive probing with different antibodies, immunoblots were stripped with 10% SDS, 6.25 mM Tris, 143 mM β-mercaptoethanol, heated to 65°C for 15 min at room temperature, followed by 3 × 5 min washes in 1 × TBST.

Results

Hsc70 localizes to VFs in infected cells and co-localizes with ectopically-expressed μNS in VFLs. During immunofluorescence experiments to identify cellular proteins that interact with the reovirus outer capsid protein μ1, we noted that the constitutively expressed cellular chaperone Hsc70, in addition to localizing with μ1 on membranous structures, localized to viral factories (Figure 2.1A; see arrowheads). To confirm this observation, we co-stained infected cells with antibodies for Hsc70 and μNS. In mock-infected CV-1 cells Hsc70 was distributed diffusely in the cytosol and nucleus (data not shown). However, in cells infected with T1L, $T3D^{CD}$ or $T3D^{N}$ reovirus we found that Hsc70, also co-localized with μNS in viral factories (Figure 2.1B; data not shown for $T3D^{CD}$ and $T3D^{N}$). As several viral proteins localize to VFs, we tested if Hsc70 co-localized with VFLs formed by μNS alone. In CV-1 cells transfected with a plasmid encoding μNS derived from reovirus strain T1L Hsc70 co-localized with μNS VFLs (Figure 2.1C). We conclude from these results that the cellular chaperone Hsc70 co-localizes with VFs and in VFLs formed by expression of μNS.

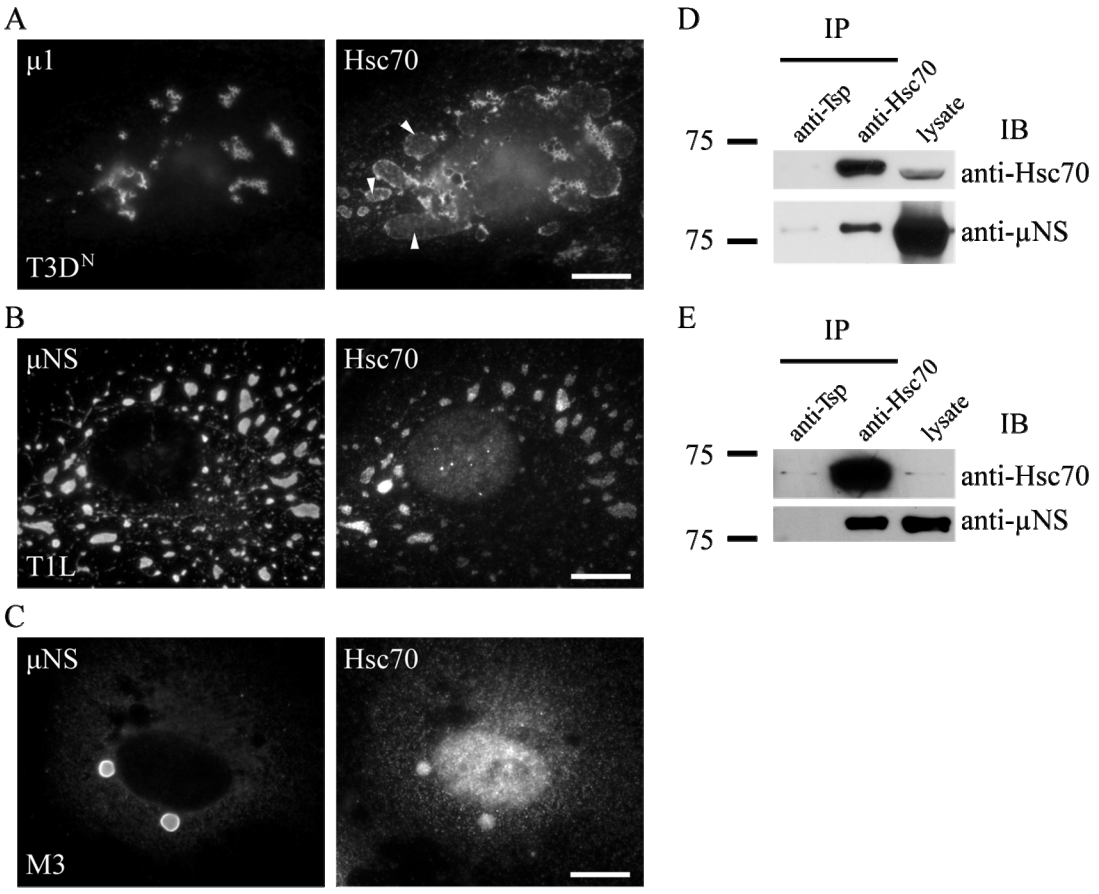

Figure 2.1: Hsc70 interacts with the VF matrix protein μNS. A) $T3D^N$- or B) T1L-infected CV-1 cells were immunostained for A) μ1 and Hsc70 or B) μNS and Hsc70. C) CV-1 cells transfected with a μNS-encoding plasmid (pCI-M3 T1L) were immunostained for μNS and Hsc70. Arrowheads in A) indicate VFs. Scale bars, 10 μm. D) IP of μNS by Hsc70 from pCI-M3(T1L)-transfected 293F cells or from E) $T3D^{CD}$-infected L929 cells (IB, immunoblot). anti-Tsp anti-Trichinella spiralis control antibody. Volume of lysate loaded corresponds to 1% of volume used in IP.

μNS co-immunoprecipitates with Hsc70 in infected cells and in cells ectopically expressing μNS. Having found that Hsc70 and μNS co-localized in VFLs, we determined if the two proteins interacted by immunoprecipitating endogenous Hsc70 from 293F cells ectopically expressing μNS. Immunoblots probed with anti-μNS antiserum revealed that μNS co-immunoprecipitated with Hsc70, while a control antibody did not precipitate μNS or Hsc70 (Figure 2.1D). To confirm that this

interaction also occurred in infected cells, we immunoprecipitated Hsc70 from $T3D^N$-infected cells and similarly found that μNS co-precipitated with anti-Hsc70 antibody, but not with control antibody (Figure 2.1E). Based on these findings we conclude that Hsc70 and μNS interact.

Formation and maintenance of VFLs is not impaired by siRNA knockdown of Hsc70. The matrix of VFs is believed to form by oligomerization of μNS, a process that might require the assistance of chaperones. Given the interaction of Hsc70 and μNS, we tested the possibility that Hsc70 was required for the formation and/or maintenance of VFLs, as Hsc70 chaperones aid in the oligomerization of some proteins (23). To test this hypothesis, we depleted Hsc70 from CV-1 cells using small interfering RNA (siRNA) and then transfected the cells with a plasmid encoding μNS. We measured the efficiency of depletion of Hsc70 by immunoblot and detection by infrared scanning and found that after treatment with Hsc70 siRNA 68%, 87%, and 96% of Hsc70 was depleted at 48, 72, and 96 h post-treatment, respectively (Figure 2.2A). To evaluate the role of Hsc70 in the initial formation of VFLs, cells were treated with Hsc70 or control siRNAs and then transfected with a μNS-encoding plasmid 24, 48 or 72 h post siRNA. In this way μNS was introduced into a cellular environment with less and less Hsc70 present. At the last transfection time point, when only 13% of Hsc70 was available, we detected VFLs that were indistinguishable from VFLs formed in control siRNA treated cells (Figure 2.2B).

Viral factories in infected cells are not static in the cytosol, but can divide or fuse with other VFs (Parker unpublished observations). Hsc70, if dispensable for the initial formation of VFs, could be important for the long term maintenance or remodeling of VFs. Therefore, we treated cells with Hsc70 siRNA as before, then transfected the cells with a plasmid encoding μNS 24 h later. We then evaluated the morphology of VFLs at 48, 72, and 96 h after siRNA (24, 48, and 72 h after μNS

transfection). We found that there was no difference in the size, shape or number of μNS VFLs between control siRNA-treated and Hsc70 siRNA-treated cells (Figure 2.2C). Taken together these results suggest depletion of Hsc70 does not affect the formation and/or maintenance of VFLs.

Figure 2.2: Depletion of endogenous Hsc70 does not affect the formation or maintenance of μNS VFLs. A) siRNA depletion of endogenous Hsc70. IF images of CV-1 cells stained for Hsc70 at 48, 72, and 96 h after treatment with control or Hsc70 siRNAs . The efficiency of Hsc70 depletion was quantified by immunoblot (a representative immunoblot is shown top right; quantitation is shown below). CV-1 cells were treated with control (-) or Hsc70 siRNA (+) for 48, 72 or 96 h. Bars show mean ± SD of three independent experiments. Statistically significant differences between control- and Hsc70 siRNA-treated cells are indicated, one-tailed Student's t-test. * $p < 0.05$, ** $p < 0.001$. B) siRNA depletion of Hsc70 does not affect the B) formation or maintenance C) of μNS VFLs. IF images of CV-1 cells treated with control (con) or Hsc70 siRNA (si) for 48, 72 or 96 h and then transfected with pCI-M3(T1L) as diagrammed in the schematics above the IF panels. Cells were fixed and immunostained for μNS and Hsc70. Scale bars, 10 μm.

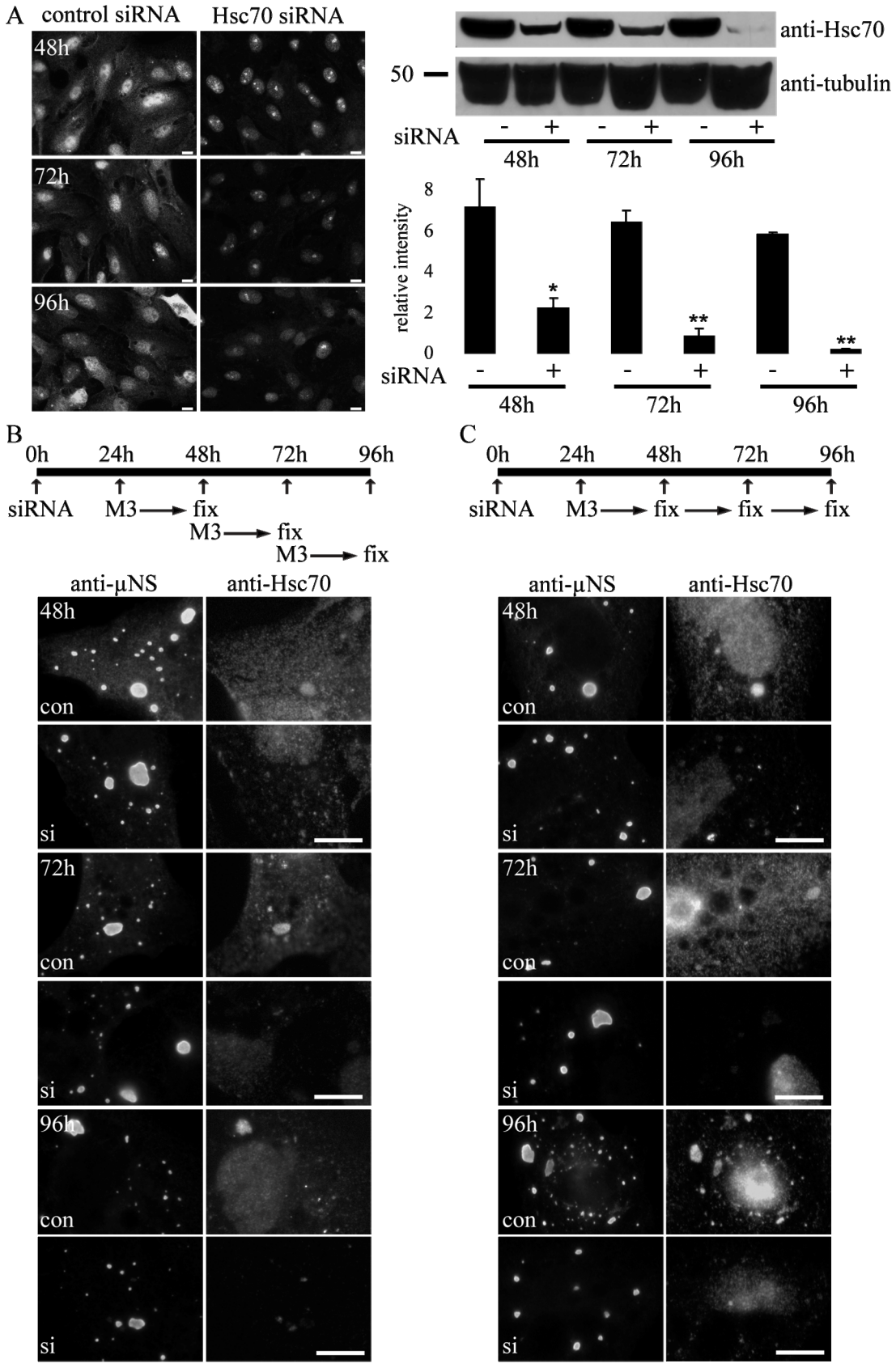
A
control siRNA
Hsc70 siRNA
48h
72h
96h
anti-Hsc70
50
anti-tubulin
siRNA
- + - + - +
48h 72h 96h
relative intensity
8
6
4
2
0
*
**
**
siRNA
- + - + - +
48h 72h 96h
B
0h 24h 48h 72h 96h
siRNA M3 fix
M3 fix
M3 fix
C
0h 24h 48h 72h 96h
siRNA M3 fix fix fix
anti-μNS
anti-Hsc70
48h
con
si
72h
con
si
96h
con
si
anti-μNS
anti-Hsc70
48h
con
si
72h
con
si
96h
con
si

Dominant negative mutants of Hsc70 still co-localize with μNS. To further investigate how Hsc70 was recruited by μNS, we examined the capacity of different dominant negative mutants of Hsc70 to be recruited to μNS VFLs. Dominant negative mutants of Hsc70 have a mutation in their nucleotide binding site that affects the ATP-ADP-cycle of the chaperone (28). The ATPase rate of Hsc70-K71M is undetectable, while it is reduced 50-fold in Hsc70-D199S. These two mutants are predominantly ATP-bound and they bind and release substrate rapidly (29, 37). A third mutant, Hsc70-T204V, has normal ATP-hydrolysis activity, but a 100-fold reduced ATP-binding activity (30). Thus, Hsc70-T204V is predominantly ADP-bound and binds and releases substrate slowly. As anti-Hsc70 antibody cannot distinguish between endogenous Hsc70 and mutant Hsc70, the dominant negative mutants were HA-tagged. When we co-expressed the dominant negative Hsc70 mutants with μNS we found that like wild type Hsc70, all the dominant negative mutants co-localized with VFLs formed by μNS (Figure 2.3). We conclude from these results that the interaction between Hsc70 and μNS likely does not require Hsc70 chaperone activity.

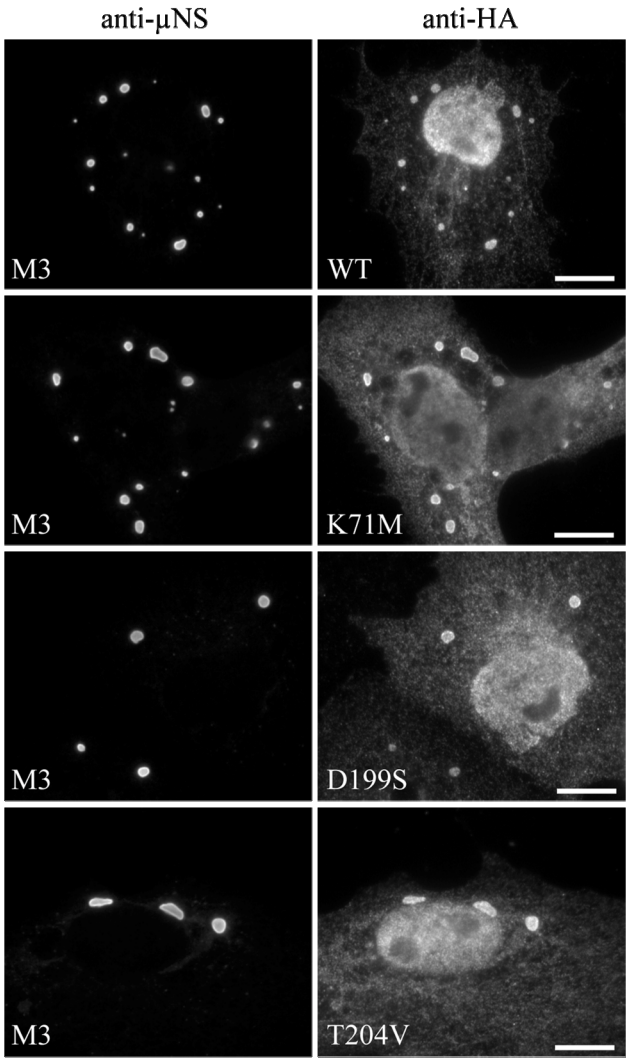

Figure 2.3: Dominant inhibitory mutants of Hsc70 co-localize with μNS VFLs. CV-1 cells were co-transfected with plasmids expressing μNS and HA-tagged WT or the indicated DN mutants of Hsc70. Cells were fixed and immunostained for μNS and the HA tag 24 h post-transfection. Scale bars, 10 μm.

Mapping of the minimal region of Hsc70 required for interaction with μNS. The co-localization of the dominant negative mutants of Hsc70 with μNS VFLs suggested that the interaction of Hsc70 with μNS was independent of Hsc70 chaperone function. Therefore, to identify the region of Hsc70 that interacted with μNS, we constructed C-terminally HA-tagged truncation mutants of Hsc70 that

comprised either the N-terminal ATPase domain (aa 1-394), including the interdomain linker (aa 384-394) or the C-terminal substrate-binding domain (SBD; aa 395-650) (19) (Figure 2.4A). As a control, we also tested an HA-tagged version of the VP1 protein of feline calicivirus, which is not known to interact with μNS. We co-expressed each of the truncated Hsc70 domains with μNS and immunoprecipitated the HA-tagged Hsc70 domains with an anti-HA antibody. Immunoblots showed that μNS co-immunoprecipitated with the SBD (aa 395-650), but not the ATPase domain of Hsc70 (Figure 2.4B). As expected μNS did not co-immunoprecipitate with the VP1-HA control protein (data not shown).

The SBD of Hsc70 can be subdivided into the substrate-binding site, which consists of β-sheets connected by loops and an α-helical 10 kDa C-terminal tail (Figure 2.4A). The C-terminal tail of Hsc70 is not involved in substrate binding but has been found to interact with different co-chaperones via distinct interaction motifs (13, 21). The EEVD motif at the very C-terminus of Hsc70 is necessary for Hsc70 interaction with Hsp40 co-chaperones (14). Another co-chaperone interaction domain is comprised of an α-helical domain and multiple degenerate repeats of the tetrapeptide GGMP (1). To define the interacting region of the SBD of Hsc70 for μNS, we created: i) a mutant of the SBD that was truncated at aa 540 and thus only contained the minimal substrate-binding site, ii) a truncation comprising aa 395-560 which includes the first α-helix of the α-helical domain, iii) a mutant that lacks the GGXP repeats and the EEVD motif (aa 395-614), and iv) the SBD without the C-terminal EEVD motif (aa 395-646) (Figure 2.4A). When these mutants were co-expressed with μNS, we found that the constructs 395-540, 395-614 and 395-646 interacted with μNS (Figure 2.4C). We confirmed that the minimal region of Hsc70 (aa 395-540) localized to VFLs by co-expressing this construct with μNS in CV-1 cells (Figure 2.4D, bottom panels). In agreement with our IP findings, the ATPase

domain of Hsc70 (aa 1-394) did not colocalize with μNS VFLs (Figure 2.4D, top panels). Although, we were unable to show that immunoprecipitation of HA-tagged Hsc70 (395-560) pulled down μNS (Figure 2.4C), this mutant co-localized with μNS VFLs (data not shown) suggesting that the interaction in vitro may be sterically hindered. Taken together, these results indicate that the GGMP tetrapeptide repeats and the EEVD motif are dispensable for interaction of Hsc70 with μNS and that μNS interacts with the minimal substrate-binding site (aa 395-540) of Hsc70.

Figure 2.4: The ATPase domain of Hsc70 is not required for its interaction with μNS. A) Diagram of Hsc70 subdomains and truncation mutants (SBD = substrate binding domain). B) 293F cells were co-transfected with the μNS-encoding plasmid and either the HA-tagged ATPase or SBD of Hsc70. HA-tagged constructs were immunoprecipitated from cell lysates with an anti-HA mAb then immunoblotted (IB) and probed for the HA tag or μNS antibody. A control antibody (anti-Tsp) did not immunoprecipitate the tagged Hsc70 or μNS. C) 293F cells were co-transfected with plasmids encoding μNS and the HA-tagged truncation mutants of Hsc70 depicted in A). Immunoprecipitates were prepared and immunoblotted as in B). Volume of lysate loaded corresponds to 1% of volume used in IP. D) IF images of cells ectopically expressing μNS and Hsc70 (1-394) (top panels) or μNS and Hsc70 (395-540) (bottom panels). Cells were fixed with 100% methanol. Scale bars, 2 μm.

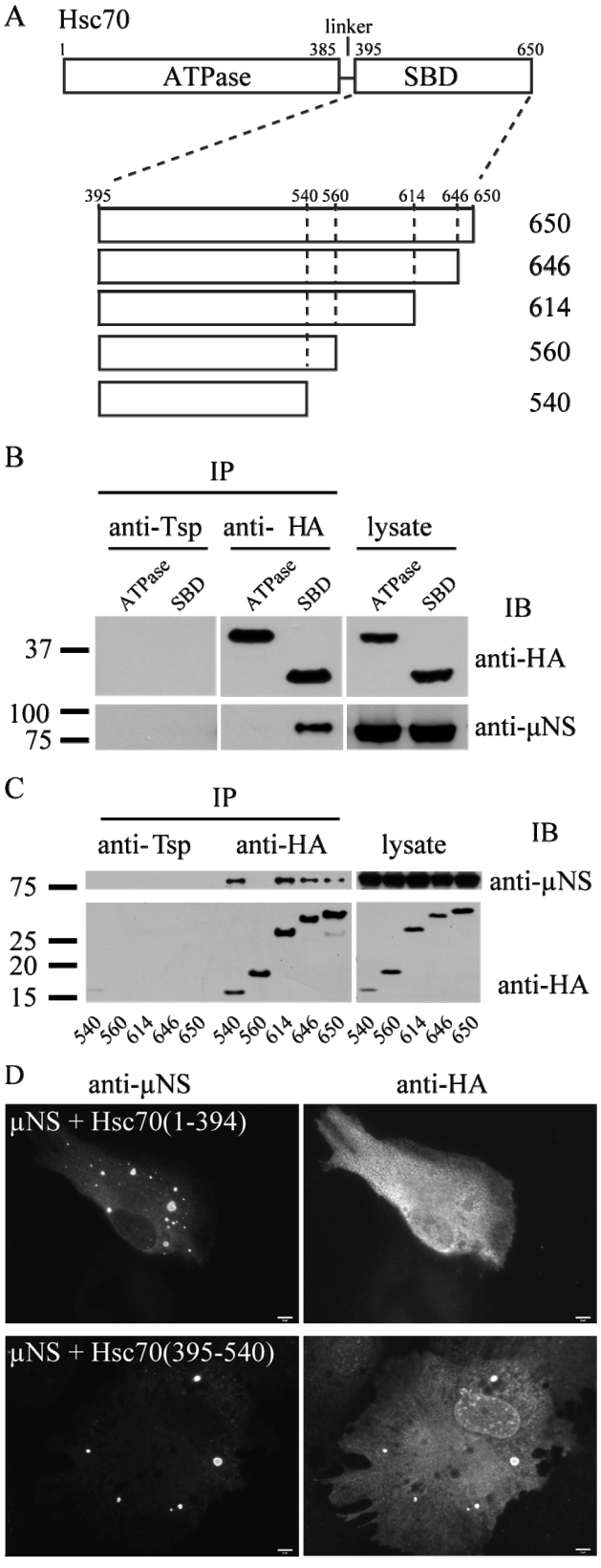
A
Hsc70
linker
1
385
395
650
ATPase
SBD
395
540
560
614
646
650
650
646
614
560
540
B
IP
anti-Tsp
anti- HA
lysate
ATPase
SBD
ATPase
SBD
ATPase
SBD
IB
37
anti-HA
100
75
anti-μNS
C
IP
anti-Tsp
anti-HA
lysate
IB
75
anti-μNS
25
20
15
anti-HA
540
560
614
646
650
540
560
614
646
650
540
560
614
646
650
D
anti-μNS
anti-HA
μNS + Hsc70(1-394)
μNS + Hsc70(395-540)

Mapping of the minimal necessary μNS interaction domain. Our knockdown experiments suggested that Hsc70 was dispensable for VFL formation. VFs are the site of viral replication and assembly. The viral structural proteins (λ1, λ2, λ3, μ1, μ2, σ2, and σ3), and nonstructural protein σNS are recruited to VFs in infected cells (3, 5, 8, 27, 33). In cells ectopically expressing μNS, the λ1, λ2, λ3, μ2, σ2 and σNS proteins are recruited to VFLs independently of each other (3, 26, 27). Therefore, it is possible that Hsc70 plays a role within VFs in preventing aggregation of partially folded viral proteins prior to their assembly. Alternatively, Hsc70 may play a role in virion assembly or replication. To identify the minimal region of μNS necessary for its interaction with Hsc70, we prepared different μNS truncation mutants and tested their capacity to co-immunoprecipitate with full-length Hsc70. In contrast to full-length μNS, the minimal region of μNS necessary to form VFLs (aa 471-721) (2) did not interact with Hsc70 (Figure 2.5A). This result supported our finding that viral factory formation occurred independently of Hsc70 and indicated that the region encompassing the N-terminal 470 amino acids of μNS interacts with Hsc70.

The first 221 aa of μNS serve as a scaffold to recruit several of the reoviral structural proteins (3, 5, 26). To determine if Hsc70 interacted with this N-terminal region of μNS, we created two truncation mutants comprising aa 1-221 and aa 1-470. We found that the longer of these truncation mutants (aa 1-470), but not the shorter (aa 1-221) co-immunoprecipitated with Hsc70 (Figure 2.5B). As Hsc70 did not interact with aa 471-721 of μNS, we inferred that the Hsc70-interacting region of μNS lies between amino acids 222-470.

Hsc70 is often recruited to protein aggregates (24). To ensure that the truncation mutants of μNS were not misfolding, we examined immunofluorescence images of the expressed proteins for co-localization with polyubiquitin. The distribution of μNS(1-470) and μNS(1-221) in transfected cells was diffuse

throughout the cytosol and we did not see aggregates that co-localized with polyubiquitin (data not shown). In addition we found that a co-expressed HA-tagged dominant negative form of Hsc70 (T204V) and the SBD of Hsc70 immunoprecipitated μNS (1-470) and WT μNS (1-721) (Figure 2.5C). A small amount of full-length μNS was non-specifically pulled down by the control antibody, but this was not a consistent finding (compare Figure 2.5B with Figure 2.5C). These results suggest that the interaction of Hsc70 with the μNS fragment was not due to misfolding of the μNS fragment and did not require functional chaperone activity.

To further narrow down the minimal domain of μNS necessary for interaction with Hsc70, we prepared additional truncation mutants of μNS, 1-271, 1-301, 1-341, 1-381, 1-396 and 1-431. To reduce the risk that the truncated proteins would misfold, the truncations were placed in predicted hydrophilic locations of the primary sequence of μNS. Although we had already established that the N-terminal 221 amino acids of μNS did not interact with Hsc70, we included this portion of the protein in the new mutants in order to maintain proper N-terminal folding. After co-IP using an anti-Hsc70 antibody, we found that all six truncation mutants were able to bind Hsc70, suggesting that the minimal region of μNS necessary to interact with Hsc70 lies between amino acids 222-271 (Figure 2.6A).

Figure 2.5: The region of μNS that interacts with Hsc70 lies between aa 222-271. A) 293F cells were transfected with a plasmid encoding full length μNS (aa 1-721) or the minimal factory-forming region of μNS (aa 471-721). Cell lysates were prepared and immunoprecipitated with control anti-Tsp or anti-Hsc70 antibodies. Immunoblots were then probed for μNS or Hsc70 as indicated. The bottom panel on the left shows a longer exposure of the area above. B) Hsc70 in lysates from 293F cells ectopically expressing full length μNS or the indicated truncations of μNS was immunoprecipitated as described above and the immunoblots were then probed for μNS and Hsc70. C) 293F cells were co-transfected with full length μNS (1-721) or μNS (1-470) together with HA-tagged SBD (aa 395-650) of Hsc70 or Hsc70 (T204V) (DN). An anti-HA mAb was used to immunoprecipitate the HA-tagged Hsc70 constructs and immunoblots were probed for co-precipitation of μNS. The blot to the right at the top shows a longer exposure of the higher molecular weight bands outlined in the dotted box in the blot probed with anti-HA. Volume of lysate loaded corresponds to 1% of volume used in IP.

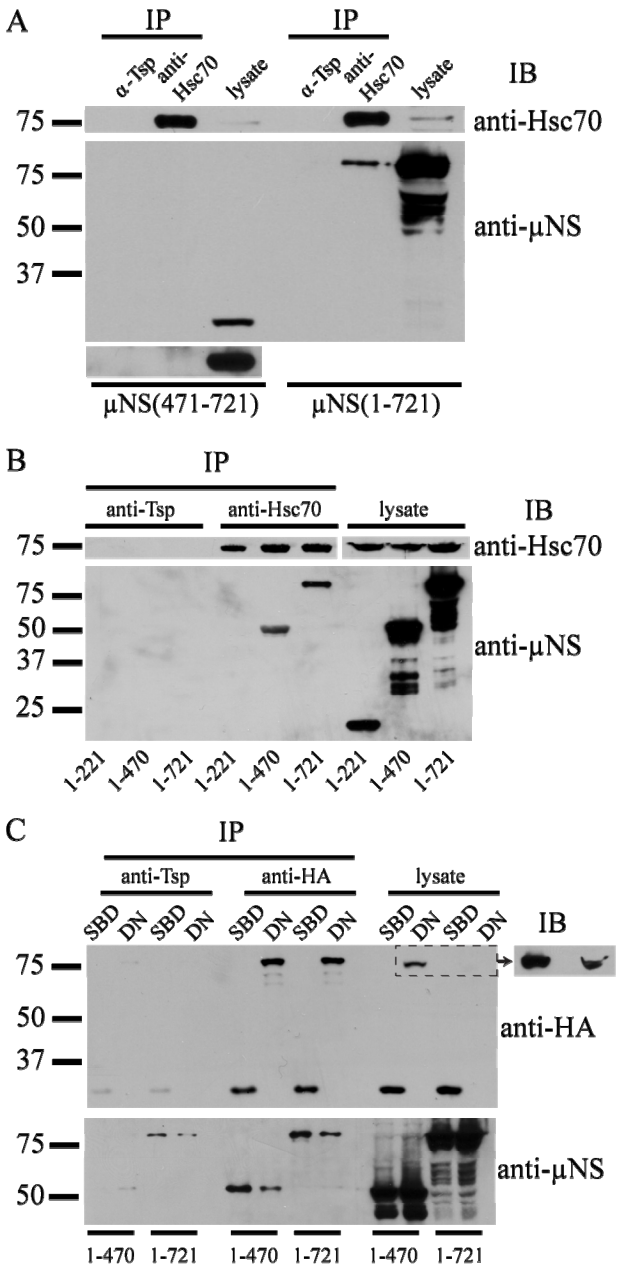
A
IP
IP
α-Tsp
anti-Hsc70
lysate
α-Tsp
anti-Hsc70
lysate
IB
75
anti-Hsc70
75
50
37
anti-μNS
μNS(471-721)
μNS(1-721)
B
IP
anti-Tsp
anti-Hsc70
lysate
IB
75
anti-Hsc70
75
50
37
25
anti-μNS
1-221
1-470
1-721
1-221
1-470
1-721
1-221
1-470
1-721
C
IP
anti-Tsp
anti-HA
lysate
SBD
DN
SBD
DN
SBD
DN
SBD
DN
SBD
DN
SBD
DN
IB
75
50
37
anti-HA
75
50
anti-μNS
1-470
1-721
1-470
1-721
1-470
1-721

Mapping of the minimal region of μNS sufficient to interact with Hsc70. To determine if aa 222-271 of μNS were sufficient to recruit Hsc70 to the viral factories, we prepared HA-tagged μNS truncation mutants that lacked the N-terminal 221 amino acids resulting in fragments starting at aa 222 and ending at aa 271, 301, 341, 381, 396 or 431. Unfortunately, none of these constructs was expressed at detectable levels (data not shown). We hypothesized that the loss of the natural N-terminus led to misfolding and rapid degradation of the μNS fragments.

Because the HA-tagged μNS fragments were not expressed, we tagged the constructs at their N-terminus with a larger soluble protein tag, HaloTag, that is derived from bacterial hydrolase in the hope that it might stabilize the μNS fragments and allow their proper folding. We prepared the truncations described above plus an additional truncation mutant comprising aa 222-470. All of the constructs bearing the N-terminal HaloTag were expressed at detectable levels. We, therefore, co-expressed the constructs with the HA-tagged SBD of Hsc70 (aa 395-650) and immunoprecipitated using an anti-HA antibody. We found that all of the tested HaloTagged μNS fragments interacted with the SBD of Hsc70. However, the HaloTag protein expressed alone did not interact with the Hsc70 SBD (Figure 2.6B). We concluded from this finding that aa 222-271 of μNS are sufficient for interaction with the SBD of Hsc70. We also tested if the minimal region of μNS that interacted with full length Hsc70 was capable of interacting with the minimal interaction domain of Hsc70. We co-expressed HaloTagged μNS (aa 222-271) or the HaloTag protein alone together with the HA-tagged substrate-binding site (aa 395-540) or SBD (aa 395-650) of Hsc70 and immunoprecipitated using an anti-HA antibody. We found that the μNS fragment was co-immunoprecipitated (Figure 2.6C) and thus deduced that the identified minimal interaction domains in μNS and Hsc70 are sufficient for interaction with each other.

Figure 2.6: Amino acids 221-271 of μNS interact with Hsc70. A) 293F cells were transfected with plasmids encoding the indicated C-terminal truncations of μNS. Cell lysates were prepared 24 h post-transfection and Hsc70 was immunoprecipitated with anti-Hsc70 antibodies. Immunoblots were then probed for μNS or Hsc70 as indicated. 1-721 denotes full length μNS. Numbers indicate the amino acids of μNS in the truncation mutant. B) 293F cells were co-transfected with plasmids encoding the HA-tagged SBD of Hsc70 (aa 395-650) together with the indicated Halo-tagged fragments of μNS. Numbers below indicate the amino acids of μNS in the construct. HA-tagged proteins were immunoprecipitated from cell lysates then immunoblotted and probed with anti-HaloTag and anti-HA antibodies. C) 293F cells were co-transfected with plasmids encoding Halo-tagged μNS(222-271) or the HaloTag Vector alone (Halo) together with HA-tagged Hsc70 (395-540) or Hsc70 (395-650; SBD). HA-tagged proteins were immunoprecipitated from cell lysates then immunoblotted and probed with anti-HaloTag and anti-HA antibodies. Volume of lysate loaded corresponds to 1% of volume used in IP.

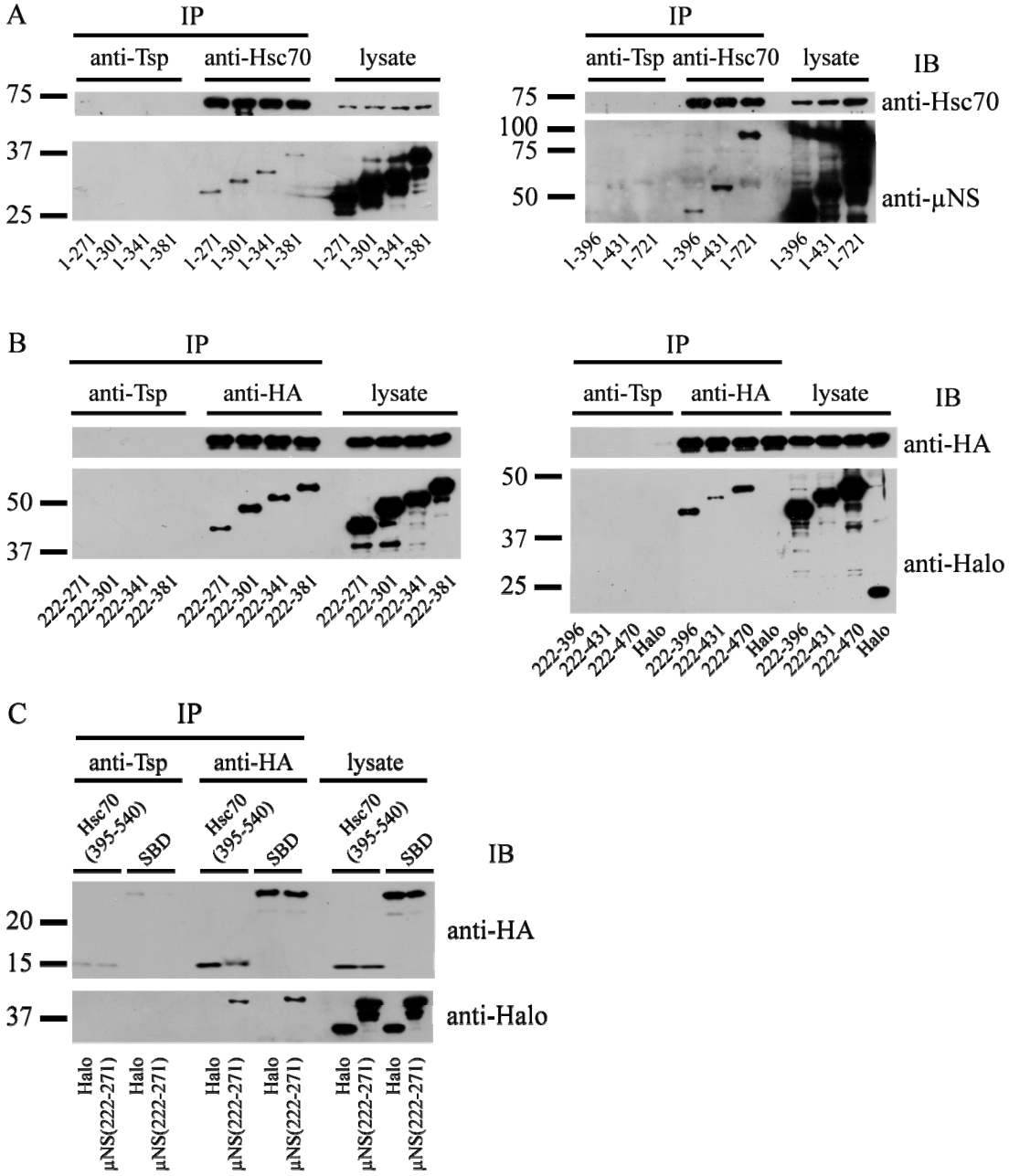
A
IP
anti-Tsp
anti-Hsc70
lysate
75
37
25
1-271
1-301
1-341
1-381
IB
anti-Hsc70
100
anti-μNS
50
1-396
1-431
1-721
B
anti-HA
222-271
222-301
222-341
222-381
anti-Halo
222-396
222-431
222-470
Halo
C
Hsc70 (395-540)
SBD
20
15
Halo μNS(222-271)

Point mutants in μNS in the region between amino acids 222-271 fail to disrupt the μNS-Hsc70 interaction. Having identified the region between amino acids 222 and 271 of μNS as sufficient for interacting with Hsc70, we prepared twenty point mutants (see Materials and Methods) within this region to identify individual residues important for the μNS-Hsc70 interaction. We chose these mutations based on the predicted secondary structure of this region of μNS (Jpred, APSSP, CFSSP, NetSurfP) and residue conservation with other homologous reovirus proteins (the Muscovy duck reovirus μC protein, Avian orthoreovirus μNS protein, and the American grass carp reovirus NS73 protein; the μNS protein is not homologous to any protein other than other reoviral proteins). We prepared several mutations within two predicted α-helices spanning aa 235-243 and aa 261-266 and analyzed the capacity of the mutants to form VFLs by immunofluorescence. Three mutants, F243A, H246A and Y263A differed from WT μNS by being unable to form large VFLs and instead forming many, very small, pinpoint-like structures in transfected cells (data not shown). Co-staining for polyubiquitin revealed that these structures co-localized with ubiquitin indicating that these three point mutants were likely misfolding and aggregating. The other mutants formed VFLs comparable to those formed by wild-type μNS and did not co-localize with ubiquitin (an example μNS(D271A) is shown in Figure 2.7A). All of the mutants co-immunoprecipitated with Hsc70 (data not shown). From these results we concluded that either single point mutants were insufficient to disrupt the μNS-Hsc70 association or that an additional Hsc70-interacting region of μNS existed.

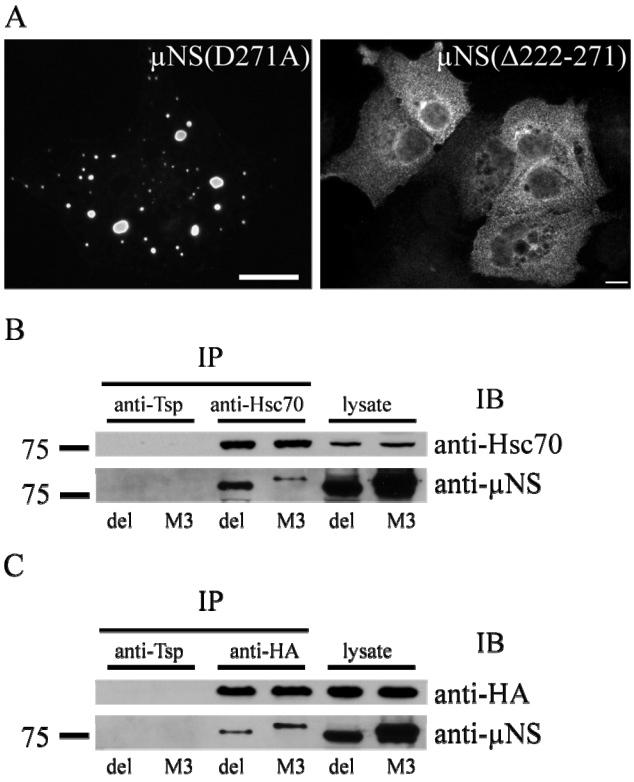

Figure 2.7: A deletion mutant of μNS lacking the minimal interaction domain (aa 222-271) still interacts with Hsc70. A) Immunofluorescence images showing the distribution of the μNS(D271A) point mutant (left) and the μNS(Δ222-271) mutant (right). CV-1 cells were fixed and immunostained for μNS at 24 h post-transfection. Scale bars, 10 μm. B) 293F cells were transfected with plasmids encoding μNS(Δ222-271) (del) or full-length μNS (M3). Hsc70 was immunoprecipitated from cell lysates and immunoblotted and probed with anti-Hsc70 and anti-μNS antibodies. C) 293F cells were co-transfected with plasmids encoding μNS(Δ222-271) (del) or full-length μNS (M3) together with the HA-tagged SBD of Hsc70 (Hsc70-395-650-HA). HA-tagged proteins were immunoprecipitated from cell lysates then immunoblotted and probed with anti-HA and anti-μNS antibodies. Volume of lysate loaded corresponds to 1% of volume used in IP.

Deletion of residues 222-271 from μNS does not abrogate its capacity to interact with Hsc70. To test the hypothesis that an additional region of μNS interacted with Hsc70 we prepared a deletion mutant of μNS lacking aa 222-271 - μNS(Δ222-271). This deletion mutant was unable to form VFLs at 24 h post-transfection. Instead it was diffusely distributed in most transfected cells, occasionally

forming aggregates (Figure 2.7A) that co-localized with polyubiquitin (data not shown). This deletion mutant co-immunoprecipitated with full length Hsc70 (Figure 2.7B). This interaction was not likely due to misfolding of the protein, as we found that it also interacted with the SBD of Hsc70 that lacks chaperoning function (Figure 2.7C). Taken together these findings suggest that the initially defined minimal interaction domain lying between aa 222-271 of μNS is not the only region of μNS that interacts with Hsc70 and that an additional region of μNS between aa 272-470 likely interacts with Hsc70.

Discussion

Chaperones are required for the efficient replication of many viruses. The *E. coli* HSP70 homolog DnaK protein was discovered as an essential bacterial factor for replication of the bacteriophage λ (15). Cellular or viral chaperones play roles in virus entry, translocation of viral proteins to different cellular compartments, genome replication or assembly and morphogenesis of progeny virions (reviewed in (22)). The cellular chaperone Hsc70 is thought to be involved in uncoating of reovirus particles during virus entry and Hsp70 is required for post-translational folding and assembly of the globular portion of the trimeric σ1 attachment protein (16, 18, 20). Our findings in this paper indicate that the constitutively expressed Hsc70 is involved in other phases of the reovirus lifecycle. Hsc70 was recruited to viral factories via interaction with the factory matrix protein μNS. Although, this interaction was mediated by the SBD of Hsc70 it likely occurs independently of Hsc70's chaperoning function as we found that μNS coimmunoprecipitated with dominant negative mutants of Hsc70, which also co-localized with VFLs. Additional support for the idea that μNS is not a substrate for Hsc70 was our finding that knockdown of Hsc70 did not influence the size or morphology of VFLs or their maintenance. Despite these findings, it remains possible that μNS is a substrate for Hsc70. Knockdown of Hsc70 was not complete and we have found that the inducible form of Hsc70, Hsp70 is also recruited to viral factories (unpublished data). Based on these findings we cannot rule out the possibility that μNS is a substrate for Hsc70; however, the co-IP of dominant negative mutants of Hsc70 strongly suggests that μNS serves as a spatial anchor to recruit Hsc70.

The N-terminal third (aa 1-221) of μNS is responsible for recruiting most of the viral core proteins (λ1,λ2, μ2, and σ2) (3, 5, 26) and nonstructural protein σNS (27), while the C-terminal third (471-721) contains the minimal factory forming region and has been shown to recruit the core and the λ3 polymerase (26). In contrast,

the middle part of μNS (aa 222-470) has no ascribed function. Our findings here indicate that a region between amino acids 222-271 within this portion of μNS serves to recruit the Hsc70 chaperone. Although our data clearly show that μNS (aa 222-271) is sufficient to recruit Hsc70, when these residues were deleted from the full length μNS protein, we still detected an association with Hsc70 that was not likely due to misfolding of this mutant suggesting that an additional region of μNS potentially between aa 272-470 also interacts with Hsc70. The presence of a second region of μNS that interacts with Hsc70 may explain our failure to identify point mutants with the region of μNS (aa 222-271) that prevented the interaction.

Why is Hsc70 recruited to μNS VFLs and VFs in infected cells? The μNS protein has been hypothesized to act as a scaffold for recruitment of viral proteins required for assembly of new viral particles and replication of the viral genome (3, 26). To this end it seems possible that chaperones are required to assemble the viral structural proteins to form virions. The reovirus virion is a double-shelled particle that comprises eight structural proteins (λ1, λ2, λ3, μ1, μ2, σ1, σ2, and σ3). The addition of the outer shell of the virion to core particles shuts off transcription and it would seem possible that this process is regulated by chaperones to prevent premature termination of viral transcription. We have found that the μ1 and σ3 heterohexameric complexes are associated with Hsc70 (Kaufer and Parker, unpublished findings). Chaperones have also been shown to be involved in genome replication for several viruses (6, 7). It is also possible that Hsc70 is involved in assortment of genome segments for packaging into assembling viral core particles.

Another possible reason for recruitment of the Hsc70 chaperone is to aid in the oligomerization or de-oligomerization of μNS itself. In vitro experiments indicate that viral cores readily associate with purified μNS; however, the presence of μNS on viral cores inhibits the assembly of outer capsid proteins. Therefore, another possible

function for Hsc70 chaperones would be to remove μNS from core particles to allow assembly of the outer-capsid proteins to form infectious virions. We found that Hsc70 is capable of interacting with a non-oligomerized form of μNS, namely a point mutant (H570Q) that does not form viral factories but is diffusely distributed in cells (unpublished findings).

A mutant of μNS in which the region between aa 222-271 was deleted formed VFLs. However, these VFLs were small in comparison to those derived from WT μNS protein. This observation suggests that the region between aa 222-271 of μNS is important for formation of larger VFLs. If and how Hsc70 binding to μNS and factory formation are connected remains to be elucidated. Our experiments with siRNA mediated knockdown of Hsc70 did not reveal any detectable effect of the absence of Hsc70 on VFL formation. However, given that there are six highly homologues isoforms of HSP70 family members found in the cytosol, one or more of these could also be recruited to VFLs and compensate for the loss of Hsc70 in these experiments (12).

In summary, we have defined a region of μNS that specifically interacts with the constitutively expressed cellular chaperone Hsc70. Future experiments will define the function of this chaperone in reovirus replication.

Acknowledgement

We thank Brian Ingel, Lynne Anguish, and Brenda Werner for excellent technical assistance. We thank Drs. Judy Appleton and Sondra Schmid for the kind gift of reagents. This research was supported by Public Health Service award R01 AI063036 (J.S.L.P.).

Reference List

1. **Ballinger, C. A., P. Connell, Y. Wu, Z. Hu, L. J. Thompson, L. Y. Yin, and C. Patterson**. 1999. Identification of CHIP, a novel tetratricopeptide repeat-containing protein that interacts with heat shock proteins and negatively regulates chaperone functions. Mol. Cell Biol. **19**:4535-4545.

2. **Broering, T. J., M. M. Arnold, C. L. Miller, J. A. Hurt, P. L. Joyce, and M. L. Nibert**. 2005. Carboxyl-proximal regions of reovirus nonstructural protein μNS necessary and sufficient for forming factory-like inclusions. J Virol **79**:6194-6206.

3. **Broering, T. J., J. Kim, C. L. Miller, C. D. Piggott, J. B. Dinoso, M. L. Nibert, and J. S. Parker**. 2004. Reovirus nonstructural protein μNS recruits viral core surface proteins and entering core particles to factory-like inclusions. J. Virol. **78**:1882-1892.

4. **Broering, T. J., A. M. McCutcheon, V. E. Centonze, and M. L. Nibert**. 2000. Reovirus nonstructural protein μNS binds to core particles but does not inhibit their transcription and capping activities. J Virol **74**:5516-5524.

5. **Broering, T. J., J. S. Parker, P. L. Joyce, J. Kim, and M. L. Nibert**. 2002. Mammalian reovirus nonstructural protein μNS forms large inclusions and colocalizes with reovirus microtubule-associated protein μ2 in transfected cells. J Virol **76**:8285-8297.

6. **Brown, G., H. W. Rixon, J. Steel, T. P. McDonald, A. R. Pitt, S. Graham, and R. J. Sugrue**. 2005. Evidence for an association between heat shock protein 70 and the respiratory syncytial virus polymerase complex within lipid-raft membranes during virus infection. Virology **338**:69-80.

7. **Chen, Y. J., Y. H. Chen, L. P. Chow, Y. H. Tsai, P. H. Chen, C. Y. Huang, W. T. Chen, and L. H. Hwang**. 2010. Heat shock protein 72 is associated with the hepatitis C virus replicase complex and enhances viral RNA replication. J Biol. Chem. **285**:28183-28190.

8. **Coffey, C. M., A. Sheh, I. S. Kim, K. Chandran, M. L. Nibert, and J. S. Parker**. 2006. Reovirus outer capsid protein μ1 induces apoptosis and associates with lipid droplets, endoplasmic reticulum, and mitochondria. J Virol **80**:8422-8438.

9. **Dales, S.** 1963. Association between the spindle apparatus and reovirus. Proc. Natl. Acad. Sci. U. S. A **50**:268-275.

10. **Dales, S., P. J. Gomatos, and K. C. Hsu**. 1965. The uptake and development of reovirus in strain L cells followed with labeled viral ribonucleic acid and ferritin-

antibody conjugates. Virology **25**:193-211.

11. **Danthi, P., K. M. Guglielmi, E. Kirchner, B. Mainou, T. Stehle, and T. S. Dermody**. 2010. From touchdown to transcription: the reovirus cell entry pathway. Curr. Top. Microbiol. Immunol. **343**:91-119.

12. **Daugaard, M., M. Rohde, and M. Jaattela**. 2007. The heat shock protein 70 family: Highly homologous proteins with overlapping and distinct functions. FEBS Lett. **581**:3702-3710.

13. **Demand, J., J. Luders, and J. Hohfeld**. 1998. The carboxy-terminal domain of Hsc70 provides binding sites for a distinct set of chaperone cofactors. Mol. Cell Biol. **18**:2023-2028.

14. **Freeman, B. C., M. P. Myers, R. Schumacher, and R. I. Morimoto**. 1995. Identification of a regulatory motif in Hsp70 that affects ATPase activity, substrate binding and interaction with HDJ-1. EMBO J **14**:2281-2292.

15. **Georgopoulos, C. P.** 1977. A new bacterial gene (groPC) which affects lambda DNA replication. Mol. Gen Genet. **151**:35-39.

16. **Gilmore, R., M. C. Coffey, G. Leone, K. McLure, and P. W. Lee**. 1996. Co-translational trimerization of the reovirus cell attachment protein. EMBO J **15**:2651-2658.

17. **Goral, M. I., M. Mochow-Grundy, and T. S. Dermody**. 1996. Sequence diversity within the reovirus S3 gene: reoviruses evolve independently of host species, geographic locale, and date of isolation. Virology **216**:265-271.

18. **Ivanovic, T., M. A. Agosto, K. Chandran, and M. L. Nibert**. 2007. A role for molecular chaperone Hsc70 in reovirus outer capsid disassembly. J. Biol. Chem. **282**:12210-12219.

19. **Jiang, J., K. Prasad, E. M. Lafer, and R. Sousa**. 2005. Structural basis of interdomain communication in the Hsc70 chaperone. Mol. Cell **20**:513-524.

20. **Leone, G., M. C. Coffey, R. Gilmore, R. Duncan, L. Maybaum, and P. W. Lee**. 1996. C-terminal trimerization, but not N-terminal trimerization, of the reovirus cell attachment protein is a posttranslational and Hsp70/ATP-dependent process. J Biol. Chem. **271**:8466-8471.

21. **Liu, F. H., S. J. Wu, S. M. Hu, C. D. Hsiao, and C. Wang**. 1999. Specific interaction of the 70-kDa heat shock cognate protein with the tetratricopeptide repeats. J Biol. Chem. **274**:34425-34432.

22. **Mayer, M. P.** 2005. Recruitment of Hsp70 chaperones: a crucial part of viral survival strategies. Rev. Physiol Biochem. Pharmacol. **153**:1-46.

23. **Mayer, M. P.** 2010. Gymnastics of molecular chaperones. Mol. Cell **39**:321-331.

24. **Mayer, M. P. and B. Bukau**. 2005. Hsp70 chaperones: cellular functions and molecular mechanism. Cell Mol. Life Sci. **62**:670-684.

25. **McCutcheon, A. M., T. J. Broering, and M. L. Nibert**. 1999. Mammalian reovirus M3 gene sequences and conservation of coiled-coil motifs near the carboxyl terminus of the μNS protein. Virology **264**:16-24.

26. **Miller, C. L., M. M. Arnold, T. J. Broering, C. E. Hastings, and M. L. Nibert**. 2010. Localization of mammalian orthoreovirus proteins to cytoplasmic factory-like structures via nonoverlapping regions of μNS. J Virol **84**:867-882.

27. **Miller, C. L., T. J. Broering, J. S. Parker, M. M. Arnold, and M. L. Nibert**. 2003. Reovirus σNS protein localizes to inclusions through an association requiring the μNS amino terminus. J Virol **77**:4566-4576.

28. **Newmyer, S. L. and S. L. Schmid**. 2001. Dominant-interfering Hsc70 mutants disrupt multiple stages of the clathrin-coated vesicle cycle in vivo. J Cell Biol. **152**:607-620.

29. **O'Brien, M. C., K. M. Flaherty, and D. B. McKay**. 1996. Lysine 71 of the chaperone protein Hsc70 is essential for ATP hydrolysis. J Biol. Chem. **271**:15874-15878.

30. **O'Brien, M. C. and D. B. McKay**. 1993. Threonine 204 of the chaperone protein Hsc70 influences the structure of the active site, but is not essential for ATP hydrolysis. J Biol. Chem. **268**:24323-24329.

31. **Parker, J. S., T. J. Broering, J. Kim, D. E. Higgins, and M. L. Nibert**. 2002. Reovirus core protein μ2 determines the filamentous morphology of viral inclusion bodies by interacting with and stabilizing microtubules. J Virol **76**:4483-4496.

32. **Rhim, J. S., L. E. Jordan, and H. D. Mayor**. 1962. Cytochemical, fluorescent-antibody and electron microscopic studies on the growth of reovirus (ECHO 10) in tissue culture. Virology **17**:342-355.

33. **Schmechel, S., M. Chute, P. Skinner, R. Anderson, and L. Schiff**. 1997. Preferential translation of reovirus mRNA by a σ3-dependent mechanism. Virology **232**:62-73.

34. **Spendlove, R. S., E. H. Lennette, and A. C. John**. 1963. The role of the mitotic apparatus in the intracellular location of reovirus antigen. J Immunol. **90**:554-560.

35. **Tyler, K. L., M. A. Mann, B. N. Fields, and H. W. Virgin**. 1993. Protective anti-reovirus monoclonal antibodies and their effects on viral pathogenesis. J Virol **67**:3446-3453.

36. **Virgin, H. W., M. A. Mann, B. N. Fields, and K. L. Tyler**. 1991. Monoclonal antibodies to reovirus reveal structure/function relationships between capsid proteins and genetics of susceptibility to antibody action. J Virol **65**:6772-6781.

37. **Wilbanks, S. M., C. Luca-Flaherty, and D. B. McKay**. 1994. Structural basis of the 70-kilodalton heat shock cognate protein ATP hydrolytic activity. I. Kinetic analyses of active site mutants. J Biol. Chem. **269**:12893-12898.

38. **Young, J. C., V. R. Agashe, K. Siegers, and F. U. Hartl**. 2004. Pathways of chaperone-mediated protein folding in the cytosol. Nat. Rev. Mol. Cell Biol. **5**:781-791.

CHAPTER THREE

Implications of the interaction of cellular chaperone Hsc70 with reovirus protein μ1 for recruitment of the μ1:σ3 heterohexamer to viral factories

Abstract

Mammalian orthoreoviruses (reoviruses) are non-enveloped viruses that replicate and assemble in the cytosol of infected cells within inclusion-like structures called viral factories (VFs). The matrix of VFs is composed of reovirus non-structural protein μNS which forms viral factory-like structures (VFLs) if expressed ectopically. Here we examined the subcellular distribution of the major outer capsid proteins μ1 and σ3 in respect to μNS. We found in transfected and infected cells that μ1 depended on σ3 for recruitment to VFLs and VFs. This finding suggested that μ1 and σ3 are recruited as a complex. We further discovered by immunoprecipitation that the cellular chaperone Hsc70 interacted with μ1 and the μ1:σ3 complex. Over-expression of Hsc70 increased the frequency of σ3 localization to VFLs. Hsc70 also co-localized with μ1 on lipid droplets. Dominant negative forms of Hsc70 did not co-localize with μ1, indicating that the μ1-Hsc70 association is dependent on Hsc70 chaperone function. siRNA-mediated knockdown of Hsc70, however, had no effect on μ1 localization to lipid droplets. Taken together these findings suggest a role for Hsc70 in outer capsid protein recruitment to viral factories and the formation of the μ1:σ3 complex.

Introduction

Mammalian orthoreoviruses (reoviruses) possess a genome of ten segments of double-stranded RNA (dsRNA) enclosed in a non-enveloped double-layered capsid. Reovirus replicates in the cytosol of infected cells. Replication is believed to occur within inclusion-like structures called viral factories (VFs) (29). The matrix of the VFs is formed by the viral non-structural protein μNS (4). If μNS is expressed ectopically, it forms viral factory-like structures (VFLs) that resemble the VFs seen in infected cells (4). μNS recruits the viral structural proteins that constitute the core particle, λ1, λ2, λ3, μ2 and σ2, as well as the non-structural protein σNS (2, 20, 21). All these proteins localize to viral factories from early time points in infection and also co-localize with VFLs if expressed individually with μNS (1, 2, 6, 19, 21). In order to generate full virions, cores need to acquire the outer capsid layer consisting mainly of μ1 and σ3. Coffey et al found that μ1 exhibits different localization patterns during the course of infection, being initially diffusely distributed in the cytosol and associating later (12 h -18 h pi) with membranous structures and viral factories (10). The σ3 protein shows no specific localization besides recruitment to VFs and is diffusely distributed in the cytosol and nucleus (33). It is unknown how μ1 and σ3 are recruited to viral factories and what mechanism governs the delayed translocation of μ1 to VFs.

μ1 and σ3 form a complex consisting of three copies of each of the two proteins. This heterohexamer is the building block for the outer capsid (18). Preformed μ1:σ3 heterohexamers are able to recoat cores *in vitro* (8). This finding suggests that μ1 and σ3 might be recruited to viral factories in a pre-assembled form. Indeed, co-expression of μ1, σ3 and μNS revealed that while σ3 can co-localize with μNS on its own, μ1 is recruited to VFLs only in the presence of σ3 (9). Similarly, a temperature sensitive mutant of σ3 which does not expresses viable σ3 at the restrictive temperature shows no μ1 association with viral factories (9) and an accumulation of

core-like particles in infected cells (23). When and where the μ1:σ3 heterohexamer forms in infected cells is unclear. The heterohexamer consists of a base of an intertwined μ1 trimer and three σ3 monomers that decorate that trimer and sit in between two adjacent μ1 proteins (Figure 1.2) (18). It seems likely that μ1 exists as monomers and trimers, and I speculate that μ1 trimerization might occur on membranes. σ3 has been crystallized as a dimer, but given the structure of the heterohexamer, must monomerize in order to associate with μ1 (27). Because of the extensive conformational rearrangements necessary to assemble the μ1:σ3 heterohexamer, I hypothesize that cellular chaperones might be needed to facilitate these rearrangements. Chaperones are proteins that help other proteins to fold properly; they aid in the assembly of multi-subunit complexes and prevent subunit aggregation (5, 13, 32). Chaperones bind exposed hydrophobic regions until these are buried through folding of the protein or association with a binding partner. Two very important cellular chaperones are the heat shock cognate protein 70 (Hsc70) and its inducible form, heat shock protein 70 (Hsp70). It is already known that these two chaperones are involved in the reovirus lifecycle. Folding of the globular head domain of the trimeric σ1 attachment protein is dependent on Hsp70 and Hsp90 (16). Additionally, complete removal of the δ fragment of the μ1 outer capsid protein from infecting virions is aided by Hsc70 (14). Preliminary data also suggest a role for Hsc70 in the recruitment of σ3 to VFLs (9). My other work (chapter 2) shows an interaction between Hsc70 and μNS. However, the recruitment of Hsc70 to VFLs does not seem to be due to a role of Hsc70 in VFL formation (15). So far the role of chaperones in assembly of reovirus has not been fully investigated.

Here I show that the chaperone Hsc70 interacts with μ1 as well as the μ1:σ3 heterohexamer and that the co-localization of Hsc70 and μ1 is dependent on chaperoning function.

Materials and Methods

Cells and viruses. CV-1 cells were grown at 37°C in 5% CO_2 in Eagles Minimum Essential Medium (MEM) (CellGro) supplemented with 10% fetal bovine serum (HyClone), 100 U ml^{-1} of penicillin, 100 μg ml^{-1} streptomycin, 250 ng ml^{-1} amphotericin B, 50 μg ml^{-1} gentamycin, 125 ng ml^{-1} amphotericin B (antibiotic-antimycotic solution, Cellgro) and non-essential amino acids (CellGro). 293F cells were grown on a shaker at 125 rotations per minute (rpm) at 37°C in 8% CO_2 in FreeStyle™ 293 Expression Medium (Gibco) supplemented with 50 U ml^{-1} penicillin, 50 μg ml^{-1} streptomycin and 125 ng ml^{-1} amphotericin B (antibiotic-antimycotic solution, Cellgro). Reoviruses T1L and T3D were laboratory stocks of the isolates previously identified as T1/human/Ohio/Lang/1953 and T3/human/Ohio/Dearing/1955, respectively (12). The superscript N in $T3D^N$ differentiates a laboratory stock obtained from the Nibert laboratory from a T3D clone obtained from L. W. Cashdollar (Medical College of Wisconsin), denoted $T3D^{CD}$. The $T3D^{CD}$ clone differs from the $T3D^N$ clone in viral factory morphology and in the nucleotide sequence of its M1 genome segment (28). Reovirus tsG453 is a temperature-sensitive mutant derived from T3D (34). At the restrictive temperature (39°C), tsG453 produces low levels of a mutated σ3 protein (amino acids N16K, P138S, M141I, and Q229D are mutated) that misfolds and cannot associate with μ1. Viruses were plaque-isolated and amplified in murine L929 cells in Joklik's modified minimal essential medium (Gibco) supplemented with 4% fetal bovine serum (HyClone), 2 mM glutamine (Cellgro), 100 U ml^{-1} penicillin, 100 μg ml^{-1} streptomycin, 250 ng ml^{-1} amphotericin B (antibiotic-antimycotic solution, Cellgro) and 50 μg ml^{-1} gentamycin (Cellgro).

Antibodies and reagents. Mouse monoclonal antibodies (mAbs) against μ1 (4A3, 8H6, 10F6) and σ3 (5C3), and rabbit polyclonal antisera against T1L virions,

μNS and σ3 have been described previously (3, 35, 36). Rat monoclonal antibody (mAb) against Hsc70 (1B5) (immunoglobulin G (IgG) isotype 2a (IgG_{2a})) was purchased from Stressgen (Victoria, BC, Canada) and rat mAB anti-HA (3F10) IgG_1 antibody was obtained from Roche Diagnostics (Mannheim, Germany). A rat mAb IgG_{2a} against Trichinella spiralis 18H1.1 (Tsp) and a mouse mAB IgG_{2b} against H5N1 (17A2.1.2) hemagglutinin were kind gifts from Dr. Judith Appleton. Secondary antibodies for immunofluorescence (IF) microscopy were goat anti-mouse immunoglobulin G (IgG), goat anti-rabbit IgG, and goat anti-rat IgG conjugated to Alexa 488, Alexa 594, or Alexa 647 (Invitrogen). Secondary antibodies for immunoblot detection were donkey anti-rabbit IgG and rabbit anti-rat IgG conjugated to horseradish peroxidase (HRP) (Jackson ImmunoResearch). Secondary antibodies used with the Odyssey Infrared Scanner (LI-COR) were IRDye 800CW goat anti-mouse IgG and IRDye 680 goat anti-rat IgG (LI-COR). All antibodies were titrated to optimize signal-to-noise ratios.

Oil Red O staining was used to visualize lipid droplets. After final antibody incubation slides were rinsed in 60% isopropanol and incubated in oil red O working solution (stock of 5 mg ml^{-1} Oil Red O in isopropanol diluted 3:2 in H_2O) for 2 min. Slides were rinsed in 60% isopropanol, then three times in PBS and once in H_2O.

Plasmid construction. The reovirus M2 and S4 genes from T1L were subcloned from plasmids pBKS-M2L and pcDNAI-S4L (7) into the mammalian expression vector pCI-neo (Promega) to produce pCI-M2(T1L) and pCI-S4(T1L), respectively. Plasmid pCI-M3(T1L) has been described previously (3).
The gene encoding Hsc70 was PCR-amplified using pEGFP-Hsc70 (courtesy of M. Ehrlich) as template. The PCR product was purified and cut with *XhoI* and *NheI* restriction enzymes (NEB Biolabs) then ligated into pCI-neo cut with the same enzymes. Dominant negative mutants K71M, D199S and T204V of Hsc70 were

cloned similarly from their pEGFP background into pCI-neo. Wild type and mutant Hsc70 were tagged at the C-terminus with an HA-tag by Phusion PCR. Cloning details and primers available upon request.

Infections and transfections. CV-1 cells (5×10^4) were seeded the day before transfection or infection in twelve-well plates containing 18-mm-diameter round glass cover slips. Infections were begun by adsorbing virus stocks to cells at an MOI of 5 PFU/cell or as indicated for 1 h at room temperature in phosphate-buffered saline (PBS)) (137 mM NaCl, 3 mM KCl, 8 mM Na_2HPO_4, 1 mM KH_2PO_4 [pH 7.5]). Cells were then overlaid with growth medium and incubated at 37°C for 24 h or as indicated. Cells infected with tsG453 were incubated at 32°C or 39°C as indicated. To infect 293F cells, cells were pelleted at 4°C at 500 × g for 5 min and resuspended in 2 ml media containing the virus inoculum. The suspension was incubated for 1 h at room temperature and then brought to a density of 1×10^6 cells per ml and incubated for 24 h at 37°C and shaking. For immunoprecipitation approximately 1.5×10^7 293F cells per IP sample were used. CV-1 cells were transfected using FuGene HD transfection reagent (Roche) according to the manufacturer's instructions. A 7:2 ratio of FuGene HD reagent to DNA was used. Transfected cells were incubated at 37°C for 24 h or as indicated. 293F cells were transfected using 293fectin (Invitrogen) according to the manufacturer's instructions. The day before transfection 293F cells were set up at a density of 5-7 × 10^5 cells per ml in 28 ml of antibiotic-free FreeStyle™ 293 Expression Medium. A 2:1 ratio of 293fectin to DNA was used.

siRNA treatment. For IF studies CV-1 cells (1.5×10^4) were seeded the day before transfection in twelve- well plates containing 18-mm-diameter round cover slips. Cells were transfected with 100 nM siRNA J-017609-08 (Dharmacon) using Dharmafect 1 transfection reagent (Dharmacon) according to the manufacturer's

instructions. The complexes were incubated for 20 min then added to cells and incubated at 37°C for the indicated amount of time.

To evaluate the knockdown efficiency, CV-1 cells (5×10^4) were seeded the day before transfection in six-well plates and transfected as above with either Hsc70 siRNA or non-specific control siRNA. Cells were harvested 48 h, 72 h and 96 h after transfection by trypsinization. Pellets were lysed in 30 µl of 10% SDS and 31.2 mM Tris-HCl pH 7.4 then sonicated with a microtip (power 2, duty cycle 20%, 2 × 10 times on ice). Total protein concentration of the lysates was determined (DC Protein Assay; BioRad) and equal amounts were analyzed by SDS-PAGE and immunoblotting. Simultaneous detection of Hsc70 and α-tubulin was performed with the Odyssey Infrared Scanner (LI-COR) utilizing primary antibodies rat anti-Hsc70 and mouse anti-α-tubulin followed by secondary antibodies IRDye 680 goat anti-rat IgG and IRDye 800CW goat anti-mouse IgG. The integrated intensity of the selected Hsc70 and α-tubulin bands was measured by the Odyssey program and the relative amount of Hsc70 was normalized to the amount of α-tubulin. Data from three independent experiments were collected and differences in the means were evaluated by a paired one-tailed Student's t-test.

Immunofluorescence (IF) microscopy. Cells on cover slips were fixed for 10 min at room temperature in 2% paraformaldehyde in PBS, washed 3 times in PBS, then permeabilized for 15 min in PBS containing 1% bovine serum albumin (BSA), 0.1% Triton X-100 and 0.05% sodium-azide (PBSA-T). All antibody incubations were carried out for 30 min at room temperature in PBSA-T. Cover slips were washed 3 times in PBS between primary and secondary antibody incubations. Cover slips were mounted on glass slides with ProLong + DAPI reagent (Molecular Probes). Fluorescence and phase images were obtained with a Nikon TE2000 inverted microscope equipped with fluorescence and phase optics through a 60 × 1.4 NA oil

objective with 1.5 × optical zoom. Images were collected digitally with a Coolsnap HQ CCD camera (Roper) and Openlab software (Improvision) then were prepared for publication using Photoshop and Illustrator software (Adobe Systems). Graphs were prepared using Kaleidagraph (Synergy Software).

Immunoprecipitation (IP) and Immunoblot. 293F cells were harvested by centrifugation (5 min at 500 × g, 4°C). Cells were washed twice with cold PBS and lysed in 1 ml lysis buffer (50 mM Tris-HCl pH 7.4, 150 mM NaCl, 1% Tween-20, 1 mM phenylmethylsulfonylfluoride) on ice for 30 min. Lysates were cleared by centrifuging for 15 min at 16,060 × g and 4°C. For each sample 5 μg of anti-Trichinella spiralis or anti-Hsc70 antibody was bound to 30 μl of protein G agarose (Invitrogen) by rotating for 1 h at room temperature in 500 μl PBS with 0.5 μl of 10% Triton X-100. Afterwards the antibody-bound agarose was washed 3 times in 1 ml of TBST (Tris buffered saline Tween-20) and incubated overnight at 4°C with the pre-cleared cell lysate while rocking. Anti-H5N1, anti-σ3 (5C3) and anti-μ1 (8H6 or 10F6) antibodies were incubated with cell lysate unbound as above and 30 μl of protein G agarose was added to each sample the next day and incubated for 1 h at 4°C while rocking. Samples were washed 4-6 × 5 min with 1 ml of wash buffer (50 mM Tris-HCl pH 7.4, 100 mM NaCl, 2% Tween-20) on ice. After a final wash with 1 ml PBS, 5 μl of 5 × sodium dodecyl sulfate (SDS) sample buffer were added to each sample and boiled for 5 min at 95°C. Bound proteins were separated by SDS polyacrylamide gel electrophoresis (PAGE). Proteins were transferred from gels to nitrocellulose membranes and blocked for 30 min at room temperature in 1 × PBS (pH 7.4) containing 0.1% Tween-20, 100 U ml^{-1} penicillin, 100 μg ml^{-1} streptomycin and 5% powdered milk. Precipitated proteins were detected with rabbit polyclonal antisera against T1L virions (to detect μ1) and σ3 and rat anti-Hsc70 antibody in blocking buffer for 1 h at RT or overnight at 4°C. Membranes were washed 3 × 5 min in 1 ×

TBST before incubation with secondary antibodies for 1 h at RT and final washes of 6 × 5 min in 1 × TBST. Secondary antibodies used were donkey anti-rabbit and rabbit anti-rat IgG conjugated to horseradish peroxidase (HRP) and were detected with SuperSignal West Pico Chemiluminescent Substrate (Pierce) and fluorography. For consecutive probing with different antibodies, immunoblots were stripped with 10% SDS, 6.25 mM Tris, 143 mM β-mercaptoethanol, heated to 65°C for 15 min at room temperature, followed by 3 × 5 min washes in 1 × TBST.

Results

Previous work in our lab addressed questions concerning the subcellular localization and trafficking of the outer capsid proteins μ1 and σ3. The findings have been published in Dr. Caroline Coffey's thesis (9) and will be partially recapitulated here in order to aid the understanding of my new data presented here. Coffey showed that the viral proteins μ1, σ3, and μNS exhibit distinct localization patterns when expressed individually in cells: μ1 localized predominantly to lipid droplets, the endoplasmic reticulum and mitochondria, σ3 localized to the nucleus and cytosol and μNS formed globular VFLs (Figure 3.1A). Co-expression experiments revealed the inability of μ1 to co-localize with μNS VFLs, while σ3 was able to co-localize with VFLs (Figure 3.1B). Further experiments with triply transfected cells (μ1, σ3 and μNS) showed that μ1 was only recruited to VFLs in the presence of σ3 (Figure 3.2A). This finding was corroborated using a temperature sensitive mutant of σ3. At the restrictive temperature the tsG453 strain does not produce viable σ3 protein and μ1 was no longer recruited to VFs (Figure 3.2B). Coffey also proposed a role for the cellular chaperone Hsc70 in outer capsid trafficking to VFs based on her finding that over-expression of Hsc70 increased the frequency of σ3 localization to VFLs in transfected cells (Figure 3.3).

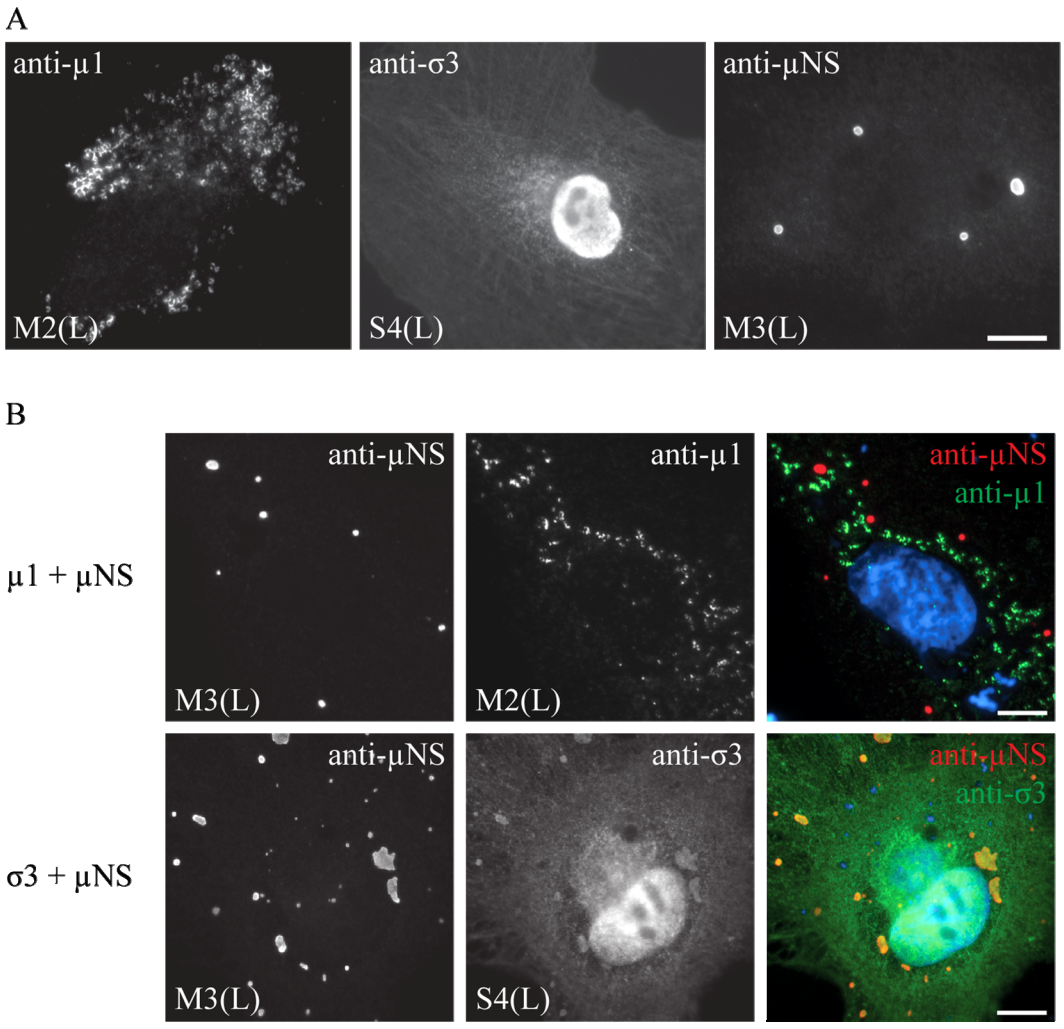

Figure 3.1: Subcellular distribution of μ1, σ3 and μNS expressed individually or in combination. The images were prepared by Caroline Coffey and reassembled into this figure (9). CV-1 cells were transfected with μ1, σ3 or μNS encoding plasmids A) individually or B) in combination as indicated. Cells were fixed 24 h post-transfection (hpt) and immunostained for μ1, σ3 and μNS. Scale bars, 10 μm.

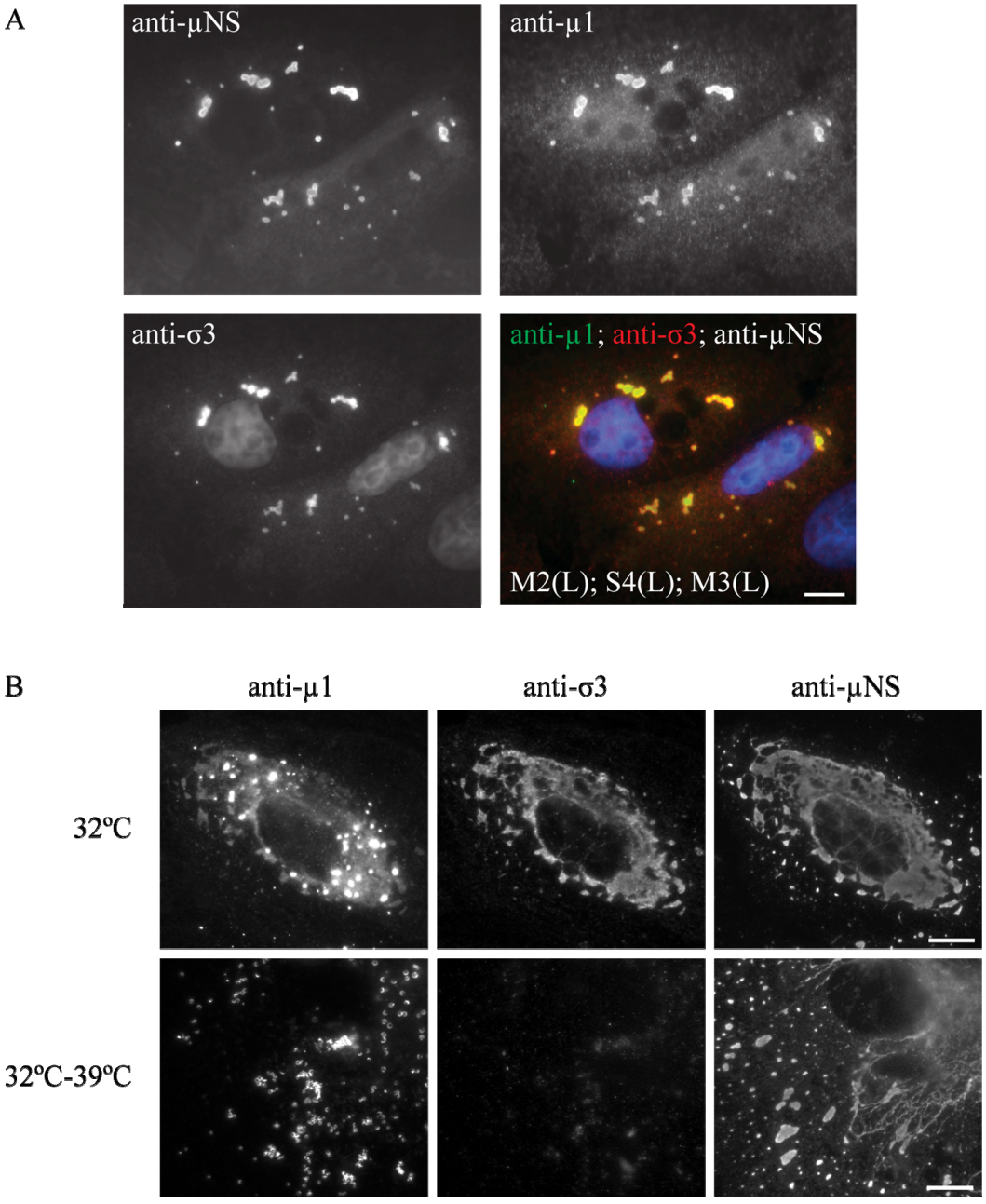

Figure 3.2: Dependence of μ1 on σ3 for recruitment to VFLs and VFs. The images in A were prepared by Caroline Coffey and reassembled into this figure (9). The images in B were reacquired by S. Kaufer. A) CV-1 cells were triply transfected with plasmids encoding μ1, σ3 and μNS. B) CV-1 cells were infected with reovirus tsG453 (MOI=5) and either incubated at 32°C for a total of 24 h or for 2 h at 32°C and then shifted to 39°C for an additional 18 h. Cells were fixed 24 h post-transfection or infection and immunostained for μ1, σ3 and μNS. Scale bars, 10 μm.

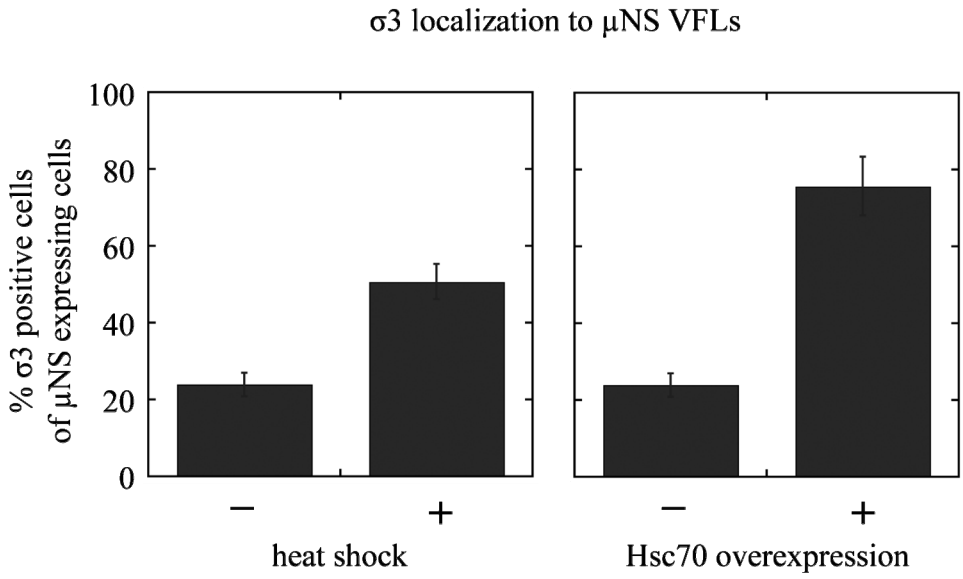

Figure 3.3: Heat shock or over-expression of Hsc70 increases the frequency of σ3 localization to VFLs. The data were collected by Caroline Coffey and reassembled into this figure (9). CV-1 cells were transfected with plasmids encoding σ3, μNS and Hsc70 (right graph). Heat shock was carried out by incubating cells at 42°C for 15 min at 18 h post-transfection and a following 6 h recovery period at 37°C. Cells were fixed 24 h post-transfection and immunostained for σ3 and μNS. Cells were analyzed for σ3 localization to μNS VFLs by immunofluorescence. The mean and SD of three experiments is shown.

Co-localization of Hsc70 and μ1 in transfected and infected cells. A corollary of the inability of μ1 to be recruited to VFs in the absence of σ3 is that assembly of the μ1:σ3 heterohexamer likely occurs outside of VFs. The assembly of large oligomeric complexes within the cytosol often requires cellular chaperones. Given the potential role of Hsc70 in σ3 recruitment to VFLs, I sought to investigate whether Hsc70 also had an influence on μ1. I transfected cells with a μ1 encoding plasmid and analyzed the subcellular distribution of endogenous Hsc70 in correlation to μ1. In mock transfected cells Hsc70 was diffusely distributed in the cytosol and the nucleus. As previously described, μ1 localized predominantly to lipid droplets which were visualized by staining for neutral lipids with Oil Red O (10). In cells expressing

μ1 I saw a concentration of Hsc70 around these lipid droplets which co-localized with μ1 staining (Figure 3.4). A similar localization pattern was observed in reovirus infected cells. Hsc70 was still diffusely distributed in the cytosol and the nucleus, but in addition showed pronounced recruitment to μ1-bound lipid droplets (Figure 3.4). This recruitment was consistent in different reovirus strains T1L, $T3D^{CD}$ and $T3D^{N}$ (data not shown for T1L and $T3D^{CD}$). Besides the co-localization with μ1, I also noted a recruitment of Hsc70 to VFs. This finding is discussed elsewhere (15).

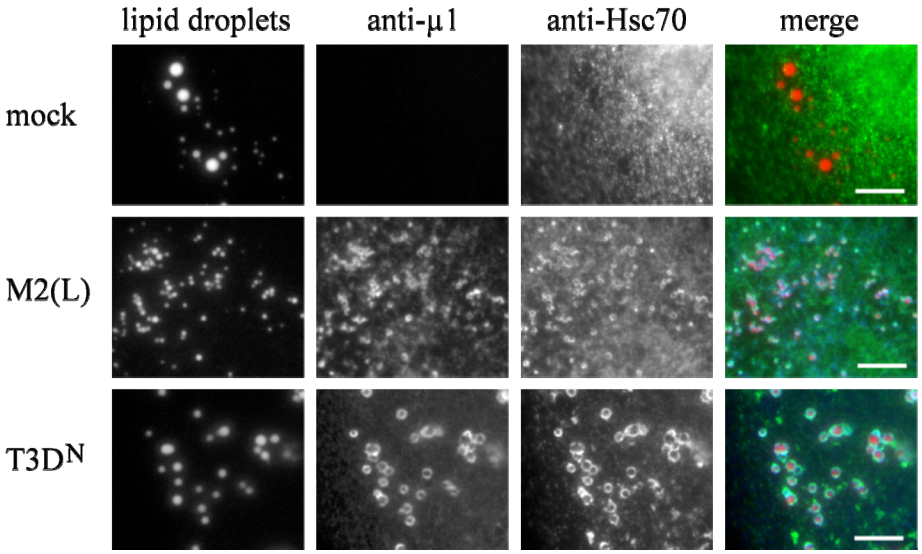

Figure 3.4: Co-localization of Hsc70 and μ1 on lipid droplets in transfected and infected cells. CV-1 cells were transfected with a mock vector or a μ1-encoding plasmid (M2(L)). CV-1 cells were also infected with reovirus $T3D^{N}$ (MOI=5). Cells were fixed 24 h post-transfection or infection and immunostained for μ1 and Hsc70. Lipid droplets were visualized by staining with Oil Red O. Scale bars, 10 μm.

Hsc70 interacts with μ1. As Hsc70 co-localized with μ1 on lipid droplets in infected and transfected cells, I used immunoprecipitation to further investigate the interaction between these two proteins. I transfected 293F cells with a μ1-encoding plasmid and then prepared lysates for co-immunoprecipitation assays using an anti-

Hsc70 antibody. Coffey et al previously showed that the normally low expression level of μ1 in transfected cells can be augmented by treating the cells with a broad-spectrum caspase inhibitor (10). Thus I treated the 293F cells with Q-VD-Oph in order to achieve higher μ1 protein levels. I was able to co-immunoprecipitate μ1 along with Hsc70 using an anti-Hsc70 antibody (Figure 3.5A). The control antibody (Tsp) did not immunoprecipitate Hsc70 or μ1. Similarly, in the reverse experiment Hsc70 co-immunoprecipitated with μ1 using an anti-μ1 antibody (10F6) (Figure 3.5B). Again, the control antibody anti-H5 hemagglutinin did not pull down Hsc70 or μ1. I conclude from these experiments that Hsc70 likely interacts directly with μ1.

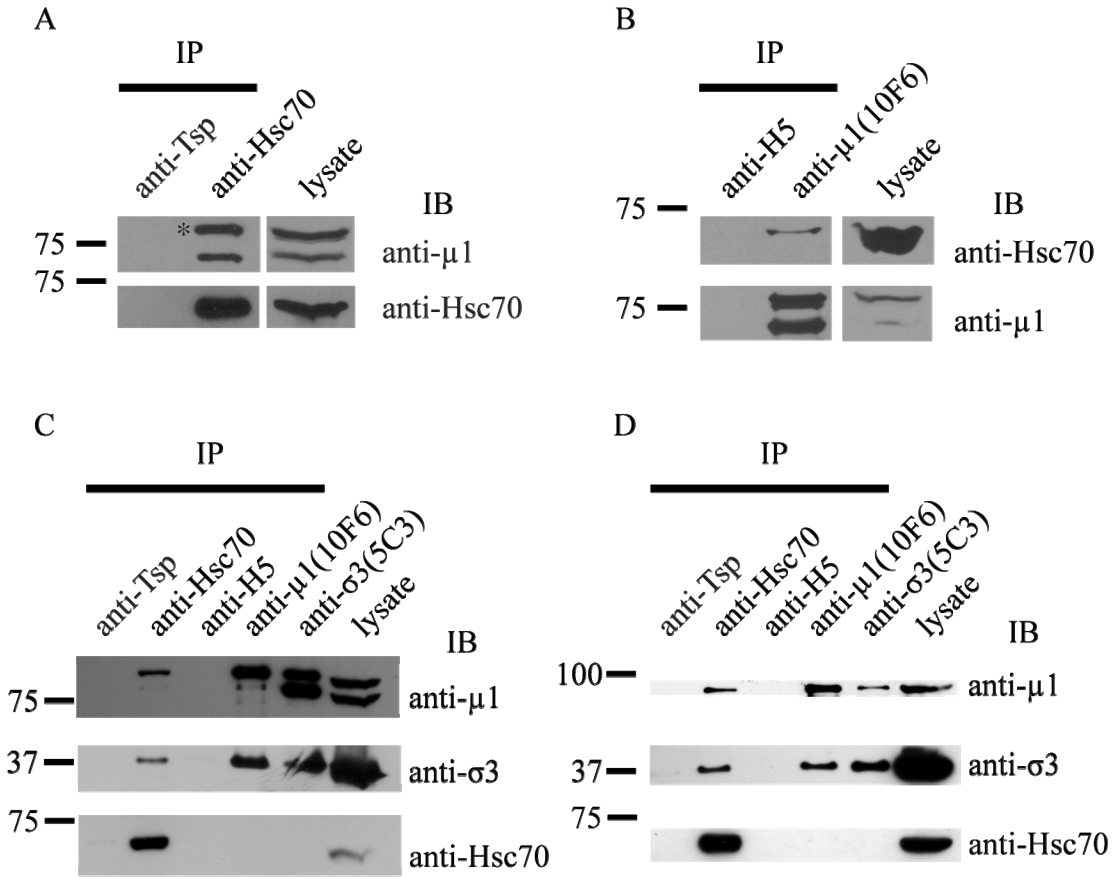

Figure 3.5: Immunoprecipitation of μ1 and the μ1:σ3 heterohexamer by Hsc70. A) and B) 293F cells were transfected with a μ1-encoding plasmid and treated with 10 μM Q-VD-Oph. 24 hpt cell lysates were prepared and A) μ1 was co-immunoprecipitated using anti-Hsc70 antibody or B) Hsc70 was co-immunoprecipitated using anti-μ1 10F6 antibody. Asteriks in A) denotes μ1 band. Isotype matched control antibodies were anti-Trichinella spiralis (Tsp) for anti-Hsc70 and anti-H5 hemagglutinin for anti-μ1 10F6. C) 293F cells were co-transfected with σ3, μ1 and Hsc70-EGFP encoding plasmids for 24 h. D) 293F cells were infected with reovirus T1L (MOI=5) for 24 h. C) and D) Cell lysates were prepared and proteins were immunoprecipitated using antibodies against Hsc70, μ1 (10F6) or σ3 (5C3). Isotype matched control antibodies were anti-Trichinella spiralis (Tsp) for anti-Hsc70 and anti-H5 hemagglutinin for anti-μ1 10F6 and anti-σ3 5C3. Immunoblots (IB) were probed with anti-Hsc70 antibody and antisera against T1L (anti-μ1) and σ3. Volume of lysate loaded corresponds to 5% of volume used in IP.

Hsc70 interacts with the μ1:σ3 heterohexamer. In order to test the hypothesis that Hsc70 could aid the formation of the μ1:σ3 heterohexamer, I wanted to investigate whether Hsc70 was associated with this complex. I co-transfected 293F cells with μ1- and σ3-encoding plasmids or infected 293F cells with reovirus strain T1L. In both cases, antibodies against Hsc70 co-immunoprecipitated μ1 and σ3 (Figure 3.5C and D). Given that Hsc70 interacts with μ1 alone, this result could indicate that Hsc70 interacts with both proteins only on an individual base. However, despite performing multiple experiments under different immunoprecipitation conditions, I was unable to show any association of Hsc70 with σ3 when they were co-expressed together (data not shown). Thus, I conclude that co-immunoprecipitation of μ1 and σ3 with Hsc70 indicates that Hsc70 associates with the assembled heterohexamer and not the individual proteins.

Although antibodies against μ1 (10F6) and σ3 (5C3) were able to co-immunoprecipitate the respective other protein, neither antibody was capable of co-immunoprecipitating Hsc70. This might be due to steric hindrance of Hsc70 versus antibody binding. Another possible explanation is that association of Hsc70 with the heterohexamer occurs transiently during assembly and thus by targeting the chaperone in immunoprecipitation, I could enrich the pull down for this specific intermediate. In order to stabilize the potentially transient interaction between Hsc70 and the μ1:σ3 heterohexamer, I co-transfected a dominant negative mutant of Hsc70, Hsc70-T204V-EGFP. This mutant is predominantly ADP-bound and thus releases its substrate at a slower rate (26). I hypothesized that co-expression of Hsc70-T204V-EGFP, which displays more stable substrate association, might enhance the co-immunoprecipitation of Hsc70 and the heterohexamer. I found that co-expression of this mutant facilitated the co-immunprecipitation of μ1 and σ3. However, further experiments revealed that this effect was not due to the enhanced substrate affinity of Hsc70. Over-expression of

wild type Hsc70-EGFP had a similar beneficial effect on the pull down of μ1 and σ3 by anti-Hsc70 antibody. This finding was unexpected and I can only provide a speculative explanation. I hypothesize that the enhancement of μ1 and σ3 pull down was due to the inherent dimerization properties of EGFP. Heterohexamer-bound Hsc70-EGFP might dimerize via the EGFP-tag and thus an anti-Hsc70 antibody could pull down multiple aggregates of μ1-σ3-Hsc70-EGFP. This hypothesis could be tested by using a differently tagged version of Hsc70. However, the co-immunoprecipitation of μ1 and σ3 with Hsc70 from infected cells was not influenced by exogenous Hsc70 or the presence of foreign protein tags and was achieved in two different virus strains, T1L and $T3D^{CD}$ (data not shown for $T3D^{CD}$). Thus, we conclude from our findings that Hsc70 interacts not only with μ1 alone, but also with the μ1:σ3 heterohexamer.

Dominant negative mutants of Hsc70 do not co-localize with μ1. Most proteins that interact with Hsc70 are chaperone substrates with exposed hydrophobic regions and depend on the chaperoning activity of Hsc70. Dominant negative forms of Hsc70 do not bind substrates (17). To investigate if μ1 behaves like a substrate of Hsc70, I expressed dominant negative mutants of Hsc70 with μ1 and examined their potential to co-localize with μ1. The dominant negative mutants of Hsc70 all have a mutation in their nucleotide binding site that affects the chaperone ATP-ADP-cycle (24). The ATPase rate of Hsc70-K71M is undetectable, while it is reduced 50-fold in Hsc70-D199S (25, 37). This means that these two mutants are predominantly ATP bound and that their substrate on-off rate is fast. Hsc70-T204V has a normal ATP hydrolysis activity together with a 100-fold reduced ATP binding activity (26). Thus, Hsc70-T204V is mainly ADP bound and binds and releases its substrate slowly. As the anti-Hsc70 antibody can not distinguish between endogenous wild type Hsc70 and mutant Hsc70, we HA-tagged the dominant negative mutants C-terminally.

Upon co-expression of μ1 and each of the dominant negative mutants of

Hsc70, I found that none of the mutants co-localized with μ1. All three mutants were diffusely distributed in the cytosol and nucleus. μ1 localized to lipid droplets (Figure 3.6). The loss of co-localization of the dominant negative mutants of Hsc70 with μ1 was not due to the HA-tagging of the mutants, as HA-tagged wild type Hsc70 was still recruited to lipid droplets in the presence of μ1. As another control we HA-tagged the VP1 capsid protein of feline calicivirus strain FCV5. There was no association between the VP1 protein and lipid droplets or Hsc70 (Figure 3.6 control). The result that dominant negative forms of Hsc70 no longer co-localized with μ1 indicates that Hsc70 requires wild type chaperoning function in order to co-localize with μ1.

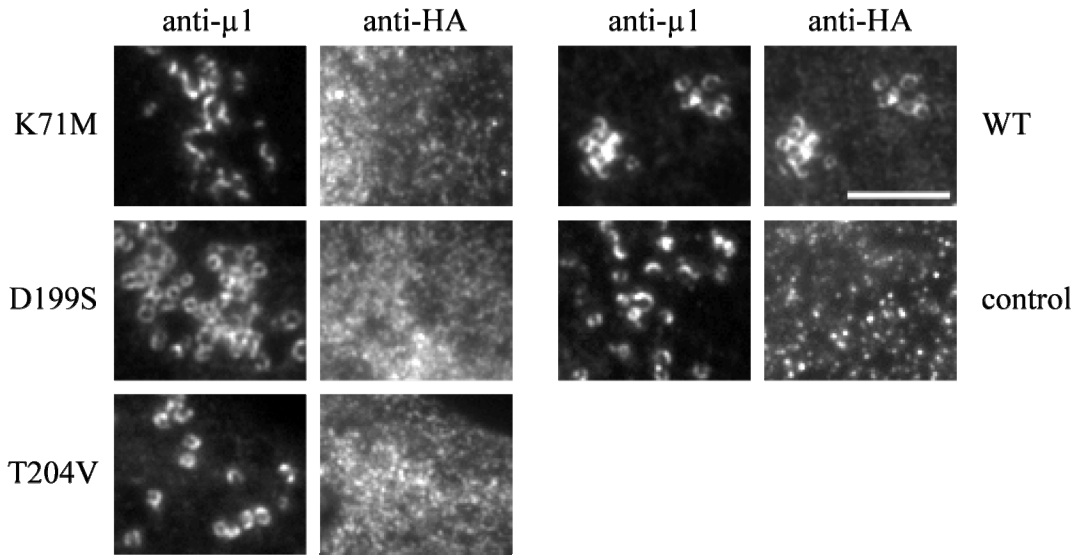

Figure 3.6: Hsc70 co-localization with μ1 depends on Hsc70s chaperone function. CV-1 cells were co-transfected with plasmids encoding μ1 and either wild type Hsc70 (WT) or a dominant negative mutant of Hsc70 (K71M, D199S, T204V). All Hsc70 proteins were HA-tagged. As a control the HA-tagged VP1 protein of calicivirus FCV5 was co-transfected (control). Cells were fixed 24 hpt and immunostained using anti-HA 3F10 and anti-μ1 4A3 antibodies. Scale bar, 10 μm.

Effect of Hsc70 knockdown on µ1 localization. To test the idea that Hsc70 might be important for µ1 localization to lipid droplets, I depleted Hsc70 from CV-1 cells using small interfering RNA (siRNA) and then transfected the cells with a plasmid encoding µ1. I measured the efficiency of depletion of Hsc70 by immunoblot and detection by infrared scanning and found that after treatment with Hsc70 siRNA 68%, 87%, and 96% of Hsc70 was depleted at 48 h, 72 h, and 96 h post-treatment, respectively (Figure 2.2). To evaluate the role of Hsc70 in µ1 localization to lipid droplets I treated cells with Hsc70 or control siRNA and transfected with a µ1-encoding plasmid 24 h post siRNA treatment. I could not detect any effect of the absence of Hsc70 on the recruitment of µ1 to lipid droplets. µ1 still localized predominantly to lipid droplets in Hsc70 or control siRNA treated cells (Figure 3.7).

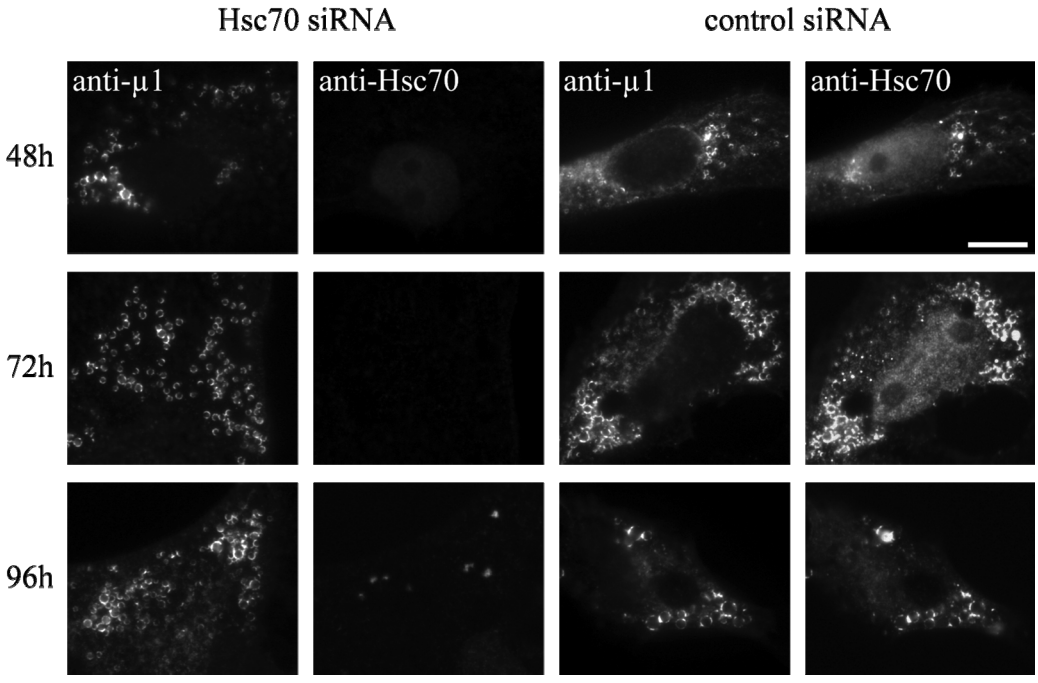

Figure 3.7: Knockdown of Hsc70 has no effect on µ1 recruitment to lipid droplets. CV-1 cells were transfected with control or Hsc70 siRNA. 24 h after siRNA treatment, cells were transfected with a µ1-encoding plasmid. Cells were fixed 48, 72 and 96 h post siRNA treatment and immunostained for Hsc70 and µ1. Scale bar, 10 µm.

Discussion

The process of reovirus assembly is not fully understood. Replication and assembly of new virions is thought to occur in viral factories (VFs) (29). The recruitment of the major outer capsid proteins μ1 and σ3 to viral factories has not been investigated extensively so far. σ3 has been observed to be recruited to VFs in infected cells, but it has not been determined if this association is dependent on other viral proteins. Coffey et al showed that μ1 is diffusely distributed in the cytosol at early time points and only localizes to VFs at later time points in infection (10). Coinciding with factory recruitment μ1 also targets membranous structures like the endoplasmic reticulum, mitochondria and lipid droplets (10). We found that σ3 was able to co-localize with μNS VFLs, but that μ1 was not recruited to VFLs if co-expressed with μNS. We detected μ1 at VFLs only in the presence of σ3, indicating a dependence of μ1 on σ3 for recruitment to VFLs. This finding was supported in infection experiments using a temperature sensitive mutant of σ3, tsG453. At the restrictive temperature this strain does not produce viable σ3 protein and we did not observe any association of μ1 with viral factories. These findings suggest that μ1 and σ3 are recruited to VFs together, most likely in the form of the heterohexamer which is the building block of the outer capsid. Although the possibility exists that σ3 and μ1 might be co-recruited in a different form and arrange into the heterohexamer within viral factories, it seems unlikely. The heterohexamer has been purified from insect cells co-expressing μ1 and σ3 showing that this complex can assemble independently of viral factories (18). The question remains why μ1 is not independently recruited to VFs. Maybe μ1 binding to Hsc70 prevents association with VFs until μ1 has assembled with σ3 into the heterohexamer. Uncomplexed μ1 could coat cores in a manner that would impair proper outer capsid formation and generate defective virions.

μ1 has been found to induce apoptosis in transfected as well as infected cells (10, 11). This occurs late in infection and is thought to be a viral strategy of egress and spread rather than a host defense mechanism (10, 30). It is unclear how the virus prevents apoptosis induction from happening too early as this would negatively impact progeny virion generation. The apoptotic capacity of μ1 is abrogated in the presence of σ3 most likely due to the assembly of the two proteins (10). Thus assembly could represent a means of regulating apoptosis induction by μ1. In the heterohexamer μ1 assumes a trimeric conformation, but it has not been investigated what conformational status μ1 has when it is not complexed with σ3. It seems likely that μ1, as monomer or trimer, has exposed hydrophobic regions which could lead to aggregation or misfolding. I have found that μ1 interacts with the cellular chaperone Hsc70 and that the two proteins co-localize on lipid droplets. This co-localization was dependent on the chaperoning function of Hsc70, but in the absence of Hsc70, μ1 was still targeted to lipid droplets. It is likely, though, that other chaperones mask a potential phenotype caused by Hsc70 depletion as I also detected Hsp70, the inducible form of Hsc70, on lipid droplets when μ1 was expressed (unpublished data). My findings suggest that μ1 is a substrate for Hsc70. I was also able to show an interaction of Hsc70 with the μ1:σ3 heterohexamer which is likely mediated by binding of Hsc70 to μ1 as I could not detect an association of σ3 and Hsc70. I speculate that heterohexamer formation might take place on lipid droplet membranes with the aid of Hsc70. Further experiments are necessary to substantiate this hypothesis. It has been reported that capsid proteins of Hepatitis C virus and dengue virus localize to lipid droplets and that these structures play a role in virus production (22, 31). Although μ1 localizes predominantly to lipid droplets, it also localizes to membranes of the endoplasmic reticulum (ER) and mitochondria and has been implicated in the penetration of these membranes (10). The ER and mitochondria membrane are both lipid bilayers, while

lipid droplets are composed of a single leaflet. The single leaflet membrane of lipid droplets might be immune to the membrane destabilizing effect of μ1 and thus pose a better place for the heterohexamer assembly than a bilayer membrane susceptible to penetration.

The fact that I was unable to find an association of σ3 and Hsc70 left me puzzled in light of data that showed an increase of the frequency of σ3 recruitment to VFLs after over-expression of Hsc70. I had hypothesized that Hsc70 would interact with σ3 and probably influence the conformation of σ3 allowing for a more efficient recruitment to VFLs. My findings do not support this hypothesis. Preliminary experiments suggest that σ3 localization to VFLs might not be a specific recruitment, but rather a non-specific entrapment. In related work I investigated the recruitment of Hsc70 to viral factories and found in immunoprecipitation assays that the substrate-binding domain was solely responsible for the interaction (15). However, in immunofluorescence experiments the ATPase domain localized to VFLs as well although it did not interact by immunoprecipitation. I discovered that this co-localization was an artifact caused by paraformaldehyde (PFA) fixation of cells and was overcome by using methanol. Similarly, I found that non-specific recruitment of GFP to VFLs was resolved by fixing cells with methanol. These findings lead me to speculate that small sized proteins might be able to diffuse into the μNS matrix and get trapped there by PFA fixation. σ3, like the ATPase domain of Hsc70 and GFP is only around 40 kDa and thus I hypothesized that σ3 localization to VFLs could likewise be a fixation artifact. Preliminary experiments using methanol fixation did indeed abolish the association of σ3 and μNS even after over-expression of Hsc70. Further experiments are necessary to conclusively determine if σ3 localization to μNS is real or artifactual.

However, previous findings in our lab indicated a role for Hsc70 in the recruitment of σ3 to VFLs. Given the fact that there seems to be no direct interaction between the two proteins, the question remains how Hsc70 promotes this recruitment? I recently investigated the localization of Hsc70 to viral factories. I found that although μNS is bound via the substrate-binding domain, it does not appear to be a substrate in the sense of a misfolded protein (15). The formation of viral factories was not impacted in the absence of Hsc70, and μNS also interacted with a dominant negative mutant of Hsc70 (15). I hypothesize that Hsc70 is involved in virus assembly. Additionally, Hsc70 might affect the μNS matrix of viral factories. It is thought that μNS forms small oligomers prior to assembling into larger multimeric complexes to create viral factories, but as an atomic resolution structure of μNS is unavailable, the nature of such an oligomer is unknown. Live cell microscopy has revealed that viral factories are dynamic and can fuse with other VFs in an infected cell (Parker, unpublished observation). These dynamic properties and the necessity for incorporation of larger viral proteins (140 kDa) into the viral factories require a certain flexibility of the μNS matrix. Hsc70 might regulate the accessibility of viral factories by rearranging μNS oligomers. Over-expression of Hsc70 would thus increase the permeability of the VFL matrix and more σ3 could gain access (Figure 3.8). Depending on the fixation method, σ3 would become fixed in place by PFA, while methanol leads to an extraction of small proteins of the size of σ3.

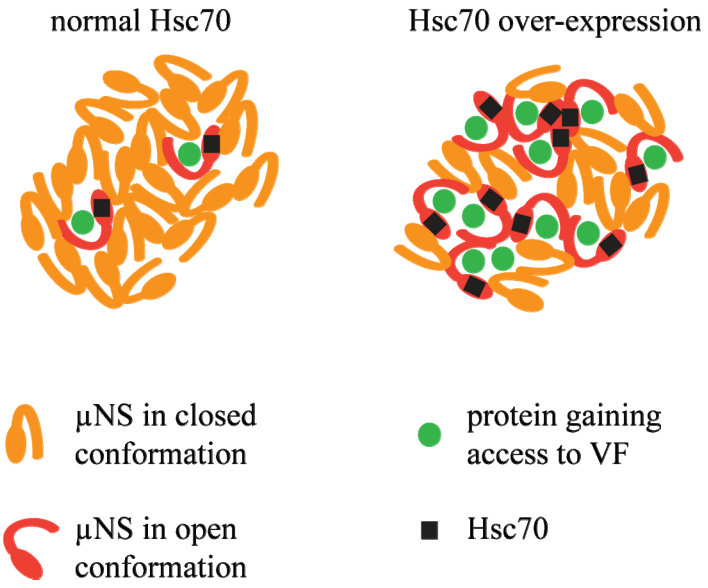

Figure 3.8: Model of Hsc70 influence on VF accessibility. Under normal Hsc70 expression conditions µNS is predominantly in a closed conformation allowing only moderate access of proteins. With Hsc70 over-expression more µNS changes to a open conformation which leads to an influx of proteins.

In summary, I have shown that µ1 and σ3 are most likely recruited to viral factories as a pre-assembled complex. Furthermore, I have demonstrated an interaction between µ1 and Hsc70 and between the µ1:σ3 heterohexamer and Hsc70. Future experiments will explore the role of Hsc70 in heterohexamer formation and virus assembly.

Acknoledgement

We thank Brian Ingel, Brenda Werner and Lynne Anguish for excellent technical support. We thank Drs. Judith Appleton and Sondra Schmid for the kind gift of reagents. This work was supported by a Burroughs Welcome Fund Investigators of Pathogenesis of Infectious Disease award (to J. S. L. P.) and by NIH grant R01 AI063036 (to J. S. L. P.), and T32 AI07618 (to C. M. C.).

Reference List

1. **Becker, M. M., T. R. Peters, and T. S. Dermody**. 2003. Reovirus σNS and μNS proteins form cytoplasmic inclusion structures in the absence of viral infection. J Virol **77**:5948-5963.

2. **Broering, T. J., J. Kim, C. L. Miller, C. D. Piggott, J. B. Dinoso, M. L. Nibert, and J. S. Parker**. 2004. Reovirus nonstructural protein μNS recruits viral core surface proteins and entering core particles to factory-like inclusions. J. Virol. **78**:1882-1892.

3. **Broering, T. J., A. M. McCutcheon, V. E. Centonze, and M. L. Nibert**. 2000. Reovirus nonstructural protein μNS binds to core particles but does not inhibit their transcription and capping activities. J Virol **74**:5516-5524.

4. **Broering, T. J., J. S. Parker, P. L. Joyce, J. Kim, and M. L. Nibert**. 2002. Mammalian reovirus nonstructural protein μNS forms large inclusions and colocalizes with reovirus microtubule-associated protein μ2 in transfected cells. J Virol **76**:8285-8297.

5. **Bukau, B., E. Deuerling, C. Pfund, and E. A. Craig**. 2000. Getting newly synthesized proteins into shape. Cell **101**:119-122.

6. **Cashdollar, L. W.** 1994. Characterization and structural localization of the reovirus λ3 protein. Res. Virol **145**:277-285.

7. **Chandran, K., S. B. Walker, Y. Chen, C. M. Contreras, L. A. Schiff, T. S. Baker, and M. L. Nibert**. 1999. In vitro recoating of reovirus cores with baculovirus-expressed outer-capsid proteins μ1 and σ3. J Virol **73**:3941-3950.

8. **Chandran, K., X. Zhang, N. H. Olson, S. B. Walker, J. D. Chappell, T. S. Dermody, T. S. Baker, and M. L. Nibert**. 2001. Complete in vitro assembly of the reovirus outer capsid produces highly infectious particles suitable for genetic studies of the receptor-binding protein. J Virol **75**:5335-5342.

9. **Coffey, C. M.** 2007. Studies on apoptosis induction by mammalian orthoreovirus outer caspid protein μ1 and regulation by outer capsid protein assembly and degradation. Thesis. Cornell University.

10. **Coffey, C. M., A. Sheh, I. S. Kim, K. Chandran, M. L. Nibert, and J. S. Parker**. 2006. Reovirus outer capsid protein μ1 induces apoptosis and associates with lipid droplets, endoplasmic reticulum, and mitochondria. J Virol **80**:8422-8438.

11. **Danthi, P., M. W. Hansberger, J. A. Campbell, J. C. Forrest, and T. S. Dermody**. 2006. JAM-A-independent, antibody-mediated uptake of reovirus into cells leads to apoptosis. J Virol **80**:1261-1270.

12. **Goral, M. I., M. Mochow-Grundy, and T. S. Dermody**. 1996. Sequence diversity within the reovirus S3 gene: reoviruses evolve independently of host species, geographic locale, and date of isolation. Virology **216**:265-271.

13. **Hartl, F. U.** 1996. Molecular chaperones in cellular protein folding. Nature **381**:571-580.

14. **Ivanovic, T., M. A. Agosto, K. Chandran, and M. L. Nibert**. 2007. A role for molecular chaperone Hsc70 in reovirus outer capsid disassembly. J. Biol. Chem. **282**:12210-12219.

15. **Kaufer, S., C. M. Coffey, and J. S. L. Parker**. The cellular chaperone Hsc70 is specifically recruited to reovirus viral factories independently of its chaperoning function.J Virol. In revision.

16. **Leone, G., M. C. Coffey, R. Gilmore, R. Duncan, L. Maybaum, and P. W. Lee**. 1996. C-terminal trimerization, but not N-terminal trimerization, of the reovirus cell attachment protein is a posttranslational and Hsp70/ATP-dependent process. J Biol. Chem. **271**:8466-8471.

17. **Li, L., L. A. Johnson, J. Q. Dai-Ju, and R. M. Sandri-Goldin**. 2008. Hsc70 focus formation at the periphery of HSV-1 transcription sites requires ICP27. PLoS. One. **3**:e1491.

18. **Liemann, S., K. Chandran, T. S. Baker, M. L. Nibert, and S. C. Harrison**. 2002. Structure of the reovirus membrane-penetration protein, μ1, in a complex with is protector protein, σ3. Cell **108**:283-295.

19. **Mbisa, J. L., M. M. Becker, S. Zou, T. S. Dermody, and E. G. Brown**. 2000. Reovirus μ2 protein determines strain-specific differences in the rate of viral inclusion formation in L929 cells. Virology **272**:16-26.

20. **Miller, C. L., M. M. Arnold, T. J. Broering, C. E. Hastings, and M. L. Nibert**. 2010. Localization of mammalian orthoreovirus proteins to cytoplasmic factory-like structures via nonoverlapping regions of μNS. J Virol **84**:867-882.

21. **Miller, C. L., T. J. Broering, J. S. Parker, M. M. Arnold, and M. L. Nibert**. 2003. Reovirus σNS protein localizes to inclusions through an association requiring the μNS amino terminus. J Virol **77**:4566-4576.

22. **Miyanari, Y., K. Atsuzawa, N. Usuda, K. Watashi, T. Hishiki, M. Zayas, R. Bartenschlager, T. Wakita, M. Hijikata, and K. Shimotohno**. 2007. The lipid droplet is an important organelle for hepatitis C virus production. Nat. Cell Biol. **9**:1089-1097.

23. **Morgan, E. M. and H. J. Zweerink**. 1974. Reovirus morphogenesis. Corelike particles in cells infected at 39 degrees with wild-type reovirus and temperature-sensitive mutants of groups B and G. Virology **59**:556-565.

24. **Newmyer, S. L. and S. L. Schmid**. 2001. Dominant-interfering Hsc70 mutants disrupt multiple stages of the clathrin-coated vesicle cycle in vivo. J Cell Biol. **152**:607-620.

25. **O'Brien, M. C., K. M. Flaherty, and D. B. McKay**. 1996. Lysine 71 of the chaperone protein Hsc70 Is essential for ATP hydrolysis. J Biol. Chem. **271**:15874-15878.

26. **O'Brien, M. C. and D. B. McKay**. 1993. Threonine 204 of the chaperone protein Hsc70 influences the structure of the active site, but is not essential for ATP hydrolysis. J Biol. Chem. **268**:24323-24329.

27. **Olland, A. M., J. Jane-Valbuena, L. A. Schiff, M. L. Nibert, and S. C. Harrison**. 2001. Structure of the reovirus outer capsid and dsRNA-binding protein σ3 at 1.8 Å resolution. EMBO J. **20**:979-989.

28. **Parker, J. S., T. J. Broering, J. Kim, D. E. Higgins, and M. L. Nibert**. 2002. Reovirus core protein μ2 determines the filamentous morphology of viral inclusion bodies by interacting with and stabilizing microtubules. J Virol **76**:4483-4496.

29. **Rhim, J. S., L. E. Jordan, and H. D. Mayor**. 1962. Cytochemical, fluorescent-antibody and electron microscopic studies on the growth of reovirus (ECHO 10) in tissue culture. Virology **17**:342-355.

30. **Richardson-Burns, S. M. and K. L. Tyler**. 2005. Minocycline delays disease onset and mortality in reovirus encephalitis. Exp. Neurol. **192**:331-339.

31. **Samsa, M. M., J. A. Mondotte, N. G. Iglesias, I. ssuncao-Miranda, G. Barbosa-Lima, A. T. Da Poian, P. T. Bozza, and A. V. Gamarnik**. 2009. Dengue virus capsid protein usurps lipid droplets for viral particle formation. PLoS. Pathog. **5**:e1000632.

32. **Schlieker, C., B. Bukau, and A. Mogk**. 2002. Prevention and reversion of protein aggregation by molecular chaperones in the E. coli cytosol: implications for their applicability in biotechnology. J Biotechnol. **96**:13-21.

33. **Schmechel, S., M. Chute, P. Skinner, R. Anderson, and L. Schiff**. 1997. Preferential translation of reovirus mRNA by a σ3-dependent mechanism. Virology **232**:62-73.

34. **Shing, M. and K. M. Coombs**. 1996. Assembly of the reovirus outer capsid requires μ1/σ3 interactions which are prevented by misfolded σ3 protein in temperature-sensitive mutant tsG453. Virus Res. **46**:19-29.

35. **Tyler, K. L., M. A. Mann, B. N. Fields, and H. W. Virgin**. 1993. Protective anti-reovirus monoclonal antibodies and their effects on viral pathogenesis. J Virol **67**:3446-3453.

36. **Virgin, H. W., M. A. Mann, B. N. Fields, and K. L. Tyler**. 1991. Monoclonal antibodies to reovirus reveal structure/function relationships between capsid proteins and genetics of susceptibility to antibody action. J Virol **65**:6772-6781.

37. **Wilbanks, S. M., C. Luca-Flaherty, and D. B. McKay**. 1994. Structural basis of the 70-kilodalton heat shock cognate protein ATP hydrolytic activity. I. Kinetic analyses of active site mutants. J Biol. Chem. **269**:12893-12898.

CHAPTER FOUR

Possible regulation of reovirus induced apoptosis by caspase cleavage and ubiquitination of outer capsid protein μ1

Abstract

Mammalian orthoreoviruses cause encephalitis and myocarditis in newborn mice secondary to virus-induced apoptosis. The primary determinant of reovirus-induced apoptosis is the outer capsid protein μ1. μ1 co-assembles with σ3 to form a heterohexameric complex and large amounts of μ1 are detected in infected cells. However, when expressed ectopically, the levels of detectable μ1 are low, suggesting that μ1 is unstable and degraded when expressed alone. Here we show that μ1 is ubiquitinated and upon induction of apoptosis is cleaved by cellular caspases. Mutation of a canonical caspase cleavage motif at position 487-490 increased the levels of ectopically expressed μ1. Although mutant forms of μ1 were expressed at higher levels, they induced similar levels of caspase 3/7 activation as the wild type protein; however, cell viability was increased. Ubiquitination of wild type μ1 was greatly increased after pan-caspase inhibition. In contrast, inhibition of caspase cleavage through mutation of the caspase cleavage site did not result in enhanced ubiquitination. A recombinant mutant virus bearing a mutation at the caspase cleavage site in μ1 had overall similar single cycle growth kinetics, but displayed a potential entry defect. In addition, this recombinant mutant virus had lower growth kinetics when infected at low moi. These findings suggest a possible regulation of cell death by caspase cleavage of μ1 and indicated a link between caspase cleavage and ubiquitination of μ1.

Introduction

Mammalian orthoreovirus (reovirus) consist of a double layered, non-enveloped capsid and contain a genome of ten double-stranded RNA (dsRNA) segments. Reovirus infections are asymptomatic in healthy adults, but cause pathology in newborn mice in the CNS, myocardium, hepatobiliary system, lungs and endocrine tissue (33). Myocarditis and encephalitis are the two most studied reovirus-induced diseases. The cytopathic effects seen in the CNS and heart co-localize with regions of reovirus replication and apoptosis induction (24, 28). Studies have shown that inhibition of apoptosis reduces tissue damage, curtails disease progression in the CNS and is protective in the heart (9, 10, 25, 26).

The outer capsid protein μ1 is responsible for reovirus-induced apoptosis in infection and also causes apoptosis in transfected cells (5, 7). μ1 is a 76 kDa protein and is a major component of the outer capsid layer where it occurs in a complex with the viral structural protein σ3 (21). During virus entry σ3 is proteolytically removed and μ1 itself undergoes proteolytic cleavage which gives rise to the intermediate subviral particle (ISVP) (11). Cleavage of μ1 results in the generation of three μ1 fragments. The N-terminal μ1N (4 kDa) and C-terminal Φ (13 kDa) fragments are released from the ISVP and have both been implicated in membrane penetration (6, 17, 19, 34). The central δ part is removed from the entering ISVP in the cytosol in a chaperone-aided process that generates the core particle (16). The region of μ1 necessary and sufficient for apoptosis induction *in vitro* has been identified as the Φ fragment (5). In infection the amount of μ1 protein is high compared to ectopic expression where μ1 levels are low. Coffey et al. showed that the detectability of μ1 is improved in the presence of pan-caspase inhibitors, suggesting that μ1 is a target for caspase-mediated cleavage (5).

Caspases constitute a family of cystein-dependent aspartate-directed proteases that are activated during apoptosis (12). They are expressed as inactive zymogens with an N-terminal prodomain followed by a large and a small subdomain. Caspase activation requires two cleavage events which remove the prodomain and separate the large and small subunit. The latter two remain associated and form a homo- or heterodimer together with two subdomains of another cleaved zymogen to generate an overall tetrameric, active caspase. Two subclasses of caspases can be distinguished in apoptosis, iniator and effector caspases. Initiator and effector caspases form a cascade where activated initiator caspases cleave and activate effector caspases, such as caspase 3, 6 and 7 which in turn cleave cellular proteins and thus induce apoptosis. The activation of initiator caspases such as caspase 2, 8, 9 and 10 occurs in association with a multimeric scaffold (12). These scaffolds form upon an external or internal stimulus and recruit inactive initiator caspases which due to the increased local concentration and/or a conformational change are able to cleave and activate each other. Such stimuli can be the binding of certain plasma membrane receptors (Fas, TNFR1, DR4, DR5) by their respective ligand (FasL, TNFα, TRAIL) or the release of proapoptotic proteins such as cytochrome c and smac/DIABLO from the intermembrane space of mitochondria into the cytosol.

It seems unlikely, however, that cleavage of μ1 by caspases is solely responsible for the low levels of μ1 in transfected cells. Coffey et al. found that the C-terminal Φ region of μ1 contains a PEST motif (5). PEST motifs are regions of twelve or more amino acids rich in proline (P), glutamate (E), serine (S) and threonine (T) flanked by lysine (K), arginine (R) or histidine (H) residues (27). Such sequences are often signals for phosphorylation and subsequent ubiquitination and degradation by the 26S proteasome. For example, the nuclear transcription factor NF-κB is retained in the cytosol by the binding of inhibitors of κB (IκB) which mask NF-κB's nuclear

localization signal. Given a certain stimulus IκB becomes phosphorylated within its PEST motif which in turn triggers ubiquitination of IκB and degradation by the 26S proteasome (18, 22, 23). It is unknown if μ1 is also phosphorylated, but preliminary data suggested that μ1 might be ubiquitinated (4). Ubiquitination is the process of covalent linkage of the 76 amino acid protein ubiquitin to a lysine residue in a target protein. This process involves at least three different proteins, an ubiquitin-activating enzyme (E1), an ubiquitin-conjugating or carrier enzyme (E2) and an ubiquitin ligase (E3) (14). E1 enzymes bind and thereby activate ubiquitin in an ATP-dependent manner. They then hand off the activated ubiquitin to the E2 enzyme which in conjunction with the E3 ligase transfers the ubiquitin onto the target protein. Modification of proteins with ubiquitin often occurs in the form of polyubiquitination, meaning that a chain of covalently bound ubiquitin monomers is linked to a target protein. A minimum of four ubiquitin moieties has been found to be necessary for interaction of an ubiquitin chain with the proteasome (29). The proteasome is a large multi-subunit complex which degrades proteins by hydrolyzing peptide bonds and thus cleaves proteins into small oligopeptides that in turn are further broken down into free amino acids that get recycled (13).

Here I investigated the relation between caspase inhibition and the increased steady state levels of μ1 and also the possible ubiquitination of μ1. These findings might be relevant for the understanding of the regulation of apoptosis induction by μ1.

Materials and Methods

Cells and viruses. CHO-S cells and 293F cells were maintained at 37ºC, 8% CO_2 in spinner culture (125 rpm) in CHO-S Serum Free Media II (Gibco) and FreeStyle™ 293 Expression Medium (Gibco), respectively, supplemented with 50 U ml^{-1} penicillin, 50 μg ml^{-1} streptomycin and 125 ng ml^{-1} amphotericin B (antibiotic-antimycotic solution, Cellgro). CV-1 cells were grown at 37°C in 5% CO_2 in Eagles Minimum Essential Medium (MEM) (CellGro) supplemented with 10% fetal bovine serum (HyClone), 100 U ml^{-1} of penicillin, 100 μg ml^{-1} streptomycin, 250 ng ml^{-1} amphotericin B (antibiotic-antimycotic solution, Cellgro), 50 μg ml^{-1} gentamycin, and non-essential amino acids (CellGro). HeLa cells (ATCC; CCL2) were maintained at 37ºC, 5% CO_2 in Dulbecco's Modified Eagle's Medium containing 10% fetal bovine serum (HyClone), 100 U ml^{-1} of penicillin, 100 μg ml^{-1} streptomycin, 250 ng ml^{-1} amphotericin B (antibiotic-antimycotic solution, Cellgro), 50 μg ml^{-1} gentamycin, and non-essential amino acids (CellGro). BHK-T7 cells were a kind gift from Dr. Ursula Buchholz and were maintained at 37ºC, 5% CO_2 in Glasgow MEM (Invitrogen) containing 5% fetal bovine serum (HyClone), 2 mM glutamine (Cellgro), 100 U ml^{-1} of penicillin, 100 μg ml^{-1} streptomycin, 250 ng ml^{-1} amphotericin B (antibiotic-antimycotic solution, Cellgro), 50 μg ml^{-1} gentamycin, non-essential amino acids (CellGro) and 1 mg ml^{-1} Geneticin (Mediatech). Reoviruses T1L and T3D were laboratory stocks of the isolates previously identified as T1/human/Ohio/Lang/1953 and T3/human/Ohio/Dearing/1955, respectively. The superscript N in $T3D^N$ differentiates a laboratory stock obtained from the Nibert laboratory from a T3D clone obtained from L. W. Cashdollar (Medical College of Wisconsin), denoted $T3D^{CD}$. The $T3D^{CD}$ clone differs from the $T3D^N$ clone in viral factory morphology and in the nucleotide sequence of its M1 genome segment. Viruses were plaque-isolated and amplified in murine L929 cells in Joklik's modified minimal essential medium (Gibco)

supplemented with 4% fetal bovine serum (HyClone), 2 mM glutamine (Cellgro), 100 U ml^{-1} penicillin, 100 μg ml^{-1} streptomycin, 250 ng ml^{-1} amphotericin B (antibiotic-antimycotic solution, Cellgro) and 50 μg ml^{-1} gentamycin (Cellgro).

Plasmids. pCI-M2(N), pCI-M2(N)-1-582 (μ1δ) were previously described (4). To create N- and C-terminal fusions of μ1, we subcloned the M2(N) gene into pEGFP-N and pEGFP-C (Clontech). The plasmids pMT107 (His-polyubiquitin) and pMT123 (His-c-jun) were kind gifts from Dr. Dirk Bohmann (30) and the reovirus genes encoding pT7 plasmids for the reverse genetics system were a kind gift from Dr. Terence Dermody (20). The caspase cleavage mutants D16N, D80N, D97E, D145E, D176N, D191A, D474N, D487N, D490E, D490N, D517N and D684K. The alanine scanning mutants Q485A, P486A, D487A, V488A, W489A, D490A, L492A, L493A, M494A and T495A were generated by standard mutagenesis technique. Primers and cloning strategies available upon request.

Antibodies and reagents. Rabbit polyclonal antisera against T3D reovirus was a gift from B. Sherry. Mouse monoclonal antibodies (mAbs) 4A3, 10H2, and 10F6 specific for μ1 and rabbit polyclonal antisera against T1L virion and σ3 have been described previously (31, 32). Mouse mAb anti-GFP was obtained from Clontech, mouse polyclonal antibody anti-6xHis was purchased from Novagen and mouse mAb anti-poly-ubiquitin (FK1) and FITC-conjugated goat anti-mouse IgM were obtained from Biomol. Secondary antibodies for immunofluorescence (IF) microscopy were goat anti-mouse immunoglobulin G (IgG and IgG_{2b}), goat anti-rabbit IgG conjugated to Alexa 488 or Alexa 594 (Invitrogen). Secondary antibodies for immunoblot detection were donkey anti-rabbit IgG, donkey anti-mouse IgG and goat anti-chicken IgY conjugated to horseradish peroxidase (HRP) (Jackson ImmunoResearch). Secondary antibodies used with the Odyssey Infrared Scanner (LI-COR) were IRDye 800CW goat anti-mouse IgG and IRDye 680 goat anti-rat IgG (LI-

COR). Antibodies were titrated to optimize signal-to-noise ratios. To determine cell viability we used the Live/Dead Cell Viability Kit (Molecular Probes, Invitrogen). Pan-caspase inhibitor q-VD-Oph was purchased from Kamiya Biomedical Company.

Caspase 3/7 activation. Caspase 3/7 activity was determined with a FLICA caspase 3/7 kit (Immunochemistry Technologies, LLC). Briefly, cells were pelleted at 500 × g, 5 min, 4ºC and washed in 1 ml PBS. Cells were resuspended in 300 µl PBS containing 5 µl FLICA reagent and incubated for 1 h in the dark. Cells were washed twice in PBS and fixed in 3.7% formaldehyde in PBS for 15 min in the dark. Cells were washed three more times in PBS and analyzed by flow cytometry.

Transfections and infections. CHO-S cells were transfected with FreeStyle MAX reagent (Invitrogen, Grand Island, NY) according to the manufacturer's instructions. The plasmid-FreeStyle MAX mixture was inoculated in 2 ml single cell suspension (1.0-1.2 × 10^6 cells per ml) of CHO-S cells and incubated for 24 h in antibiotic-free medium. Caspase inhibitor (q-VD-Oph, final concentration 10 µM) was supplemented during transfection. CV-1 cells were seeded the day before transfection or infection at a density of 5 × 10^4 cells per well in twelve-well plates containing 18-mm-diameter round glass cover slips. CV-1 cells were transfected using FuGene HD transfection reagent (Roche) according to the manufacturer's instructions. A 7:2 ratio of FuGene HD reagent to DNA was used. 293F cells were transfected using 293fectin (Invitrogen) according to the manufacturer's instructions. The day before transfection 293F cells were set up at a density of 5-7 × 10^5 cells per ml in 28 ml of antibiotic-free FreeStyle™ 293 Expression Medium. A 2:1 ratio of 293fectin to DNA was used. HeLa cells were seeded the day before transfection or infection at a density of 1 × 10^5 cells per well in twelve-well plates containing 18-mm-diameter round glass cover slips. HeLa were transfected with FuGene 6 transfection reagent (Roche) according to the manufacturer's instructions. A ratio of 3:2 of FuGene 6 to DNA was used. BHK-

T7 cells were transfected using TransIT-LT1 (Mirus) as described in (20).

Immunofluorescence (IF) microscopy. Cells on cover slips were fixed for 10 min at room temperature in 2% paraformaldehyde in PBS, washed 3 times in PBS, then permeabilized for 15 min in PBS containing 1% bovine serum albumin (BSA), 0.1% Triton X-100 and 0.05% sodium-azide (PBSA-T). All antibody incubations were carried out for 30 min at room temperature in PBSA-T. Cover slips were washed 3 times in PBS between primary and secondary antibody incubations. Cover slips were mounted on glass slides with ProLong + DAPI reagent (Molecular Probes). Fluorescence and phase images were obtained with a Nikon TE2000 inverted microscope equipped with fluorescence and phase optics through a 60 × 1.4 NA oil objective with 1.5 × optical zoom. Images were collected digitally with a Coolsnap HQ CCD camera (Roper) and Openlab software (Improvision) then were prepared for publication using Photoshop and Illustrator software (Adobe Systems). Graphs were prepared using Kaleidagraph (Synergy Software).

Ni-NTA pulldown of His-polyubiquitin-tagged conjugates. Method was adapted from (1). 293F cells were transfected with wild type or mutant pCI-M2(L) and either pMT107 (His-polyubiquitin) or pMT123 (His-c-jun). 24 h post-transfection cells were harvested by centrifugation (5 min at 500 × g, 4°C) and washed twice in cold PBS. The cell pellet was resuspended in 1 ml of PBS and 60 µl of the PBS-cell suspension were retained and lysed by sonication (2 × 30 sec, duty cycle 20-30%, power 2-3). This small aliquot of lysate was used for quantification of total protein levels (Biorad DC protein assay) and as source for the total cell lysate in immunoblotting. The remaining cell suspension was pelleted and lysed in 1 ml of Buffer A (6 M guanidine-HCl, 0.1 M Na_2HPO_4/NaH_2PO_4, 10 mM imidazole, pH 8). The cell lysate was sonicated 2 × 30 sec at duty cycle 50% and power 5. 150 µl of unsettled 50% Ni-NTA agarose slurry (QIAGEN) was washed 3 times in 1 ml of

Buffer A. Equal amounts of protein were incubated with the Ni-NTA agarose for 3 h at room temperature while turning. After incubation the protein-bound agarose was washed twice in 1 ml of Buffer A, then twice in 1 ml of Buffer A/TI (1:3 v/v) and once in 1 ml of Buffer TI (25 mM Tris-HCl, 20 mM imidazole, pH 6.8). Residual buffer was sucked out with a 27 gauge needle. Purified proteins were eluted by boiling the agarose for 7 min at 95°C in 50 µl of 5× SDS sample buffer and 10 µl of 10 M imidazole and analyzed by SDS-PAGE and immunoblotting.

Immunoblotting. Proteins separated by SDS polyacrylamide gel electrophoresis (PAGE), were transferred to nitrocellulose membranes and blocked for 30 min at room temperature in 1 × PBS (pH 7.4) containing 0.1% Tween-20, 100 U ml^{-1} penicillin, 100 µg ml^{-1} streptomycin and 5% powdered milk. Proteins were detected with primary antibodies in blocking buffer for 1 h at RT or overnight at 4°C. Membranes were washed 3 × 5 min in 1 × TBST before incubation with secondary antibodies for 1 h at RT and final washes of 6 × 5 min in 1 × TBST. Secondary antibodies were detected with SuperSignal West Pico Chemiluminescent Substrate (Pierce) and fluorography. For consecutive probing with different antibodies, immunoblots were stripped with 10% SDS, 6.25 mM Tris, 143 mM β-mercaptoethanol, heated to 65°C for 15 min at room temperature, followed by 3 × 5 min washes in 1 × TBST.

Flow cytometry analysis. Transfected cells were harvested by centrifugation (500 × g, 5 min, 4°C) and fixed for 15 min at room temperature with 1% paraformaldehyde in PBS. Cells were washed twice in 1 ml PBS and resuspended in 1 ml permeabilization buffer (0.15% Triton X-100, 2% bovine serum albumin, 5% fetal bovine serum in PBS) for 30 min at room temperature. Primary antibodies were incubated in 1 ml of 1% bovine serum albumin and 0.1% Triton X-100 in PBS for 1 h. Secondary antibodies were incubated in 1 ml of 0.1% Triton X-100 in PBS for 30 min

in the dark. Between antibody incubations, cells were washed twice in 1 ml of PBS. After the secondary antibody incubation cells were washed twice in 1 ml of PBS and resuspended in a final volume of 500 µl. Samples were measured using a FACSCalibur (BD Biosciences) and analyzed with CellQuest software (BD Biosciences) and FlowJo software (Tree Star, Ashland, OR).

Statistical analysis. Prism (GraphPad Software) statistical analysis software was used for statistical analyses. Data shown represent a minimum of three independent experiments. Mean and standard deviations are shown unless otherwise noted.

Results

Treatment of cells with pan-caspase inhibitors increases the steady-state levels of µ1 in transfected CHO-S cells. Ectopic expression of reovirus outer capsid protein µ1 induces apoptosis in ~30% of transfected CHO cells, and the Φ region of µ1 is both necessary and sufficient for this activity (5) (see Figure 4.1A for diagram of µ1 fragments). The steady-state levels of µ1 in transfected cells are low as detected by immunoblotting with rabbit anti-reovirus virion serum compared to levels in infected cells (5). However, when transfected cells were treated with the pan-caspase inhibitor q-VD-Oph at the time of transfection, the levels of full-length µ1 increased approximately 4-fold (Figure 4.1B). In addition to a prominent band of ~ 76 kDa representing full-length µ1, I detected several additional immunoreactive bands of lower molecular weight in lysates from transfected cells treated with q-VD-Oph (Figure 4.1B). These bands were absent or of much lower intensity in lysates from vehicle-only treated µ1-transfected cells. In contrast, ectopic expression levels of the µ1δ fragment, which does not induce apoptosis in transfected cells, were unaffected by q-VD-Oph (Figure 4.1B). Based on these findings, I hypothesized that µ1 was being cleaved by activated caspases and that epitopes recognized by the anti-reovirus serum were being destroyed.

To further explore this possibility, I examined the forward and side scatter characteristics of CHO-S cells transiently expressing µ1 by flow cytometry. I noted two subpopulations of cells with distinctive forward and side scatter characteristics, which were absent in the vector-only-transfected and µ1δ-expressing cells (Figure 4.1C, vector only not shown). One subpopulation of cells that represented 23.6% of the total had relatively low forward scatter and increased side scatter, characteristics that are often seen in cells undergoing early apoptosis (8). However, when the total population was gated for expression of µ1, only 8.9% of the low forward scatter and

increased side scatter subpopulation were μ1 positive (Figure 4.1C, top left panels). When cells expressing μ1 were treated with the pan-caspase inhibitor q-VD-Oph the subpopulation with low forward and high side scatter disappeared or diminished suggesting that these cells were indeed apoptotic (Figure 4.1C, top right panels). In addition, treatment of cells transfected with μ1 with pan-caspase inhibitor significantly increased the numbers of cells expressing μ1 (Figure 4.1D left panel). I considered two possible explanations for these findings: (i) μ1 was inducing apoptosis directly in cells, but its levels were subsequently decreased below the levels of detection by proteolytic cleavage of the epitopes being recognized or (ii) cells expressing μ1 caused bystander apoptosis in surrounding cells. Bystander apoptosis has been reported during reovirus infection of HeLa cells (3). To directly address the possibility that cells expressing μ1 released factors that induced bystander apoptosis, I collected media from μ1- or μ1δ-expressing cells at 24 h post-transfection and incubated this media with fresh untransfected cells. I found that media collected from μ1-transfected cells had no effect on untransfected cells (data not shown). Taken together these results suggest that μ1 induces apoptosis and is then itself degraded by activated caspases leading to a small population of apoptotic cells that are μ1-negative.

Figure 4.1: Effect of a pan-caspase inhibitor on the expression levels of μ1 and light scatter characteristics of cells expressing μ1. A) Diagram of μ1 cleavage fragments; B) Immunoblot of lysates from 293F cells expressing μ1 or μ1δ and treated with DMSO or q-VD-Oph. 293F cells were transfected with plasmids encoding μ1 or μ1δ and then treated with 10 μM q-VD-Oph or an equal volume of DMSO. Cells were harvested 24 h post-transfection and lysates were prepared and immunobloted. μ1 or μ1δ were detected with rabbit anti-reovirus serum followed by IRDye 680 conjugated goat anti-rabbit IgG. Fluorescence emission from bound fluorescent antibody was detected using an infrared gel scanner (Odyssey, LI-COR). Bracket indicates high molecular weight banding. Circles denote immunoreactive bands of lower molecular weight than full-length μ1. C) Effect of q-VD-Oph on the forward and side scatter characteristics of cells expressing μ1 or μ1δ. CHO-S cells were transfected with the indicated plasmids. At 24 h post-transfection, cells were harvested, fixed, immunostained for μ1 and analyzed by flow cytometry. Cells positive for μ1 or μ1δ were gated (10,000 events) and their side and forward scatter characteristics compared to those of the total cell population. The percentage of μ1-positive cells present within the outlined regions is indicated. D) Histogram of μ1 or μ1δ expressing CHO-S cells with DMSO or q-VD-Oph treatment. Cells were transfected with the indicated plasmids and then treated with 10 μM q-VD-Oph (black line) or an equal volume of DMSO (grey line). At 24 h post-transfection, cells were harvested, fixed, immunostained for μ1 and analyzed by flow cytometry.

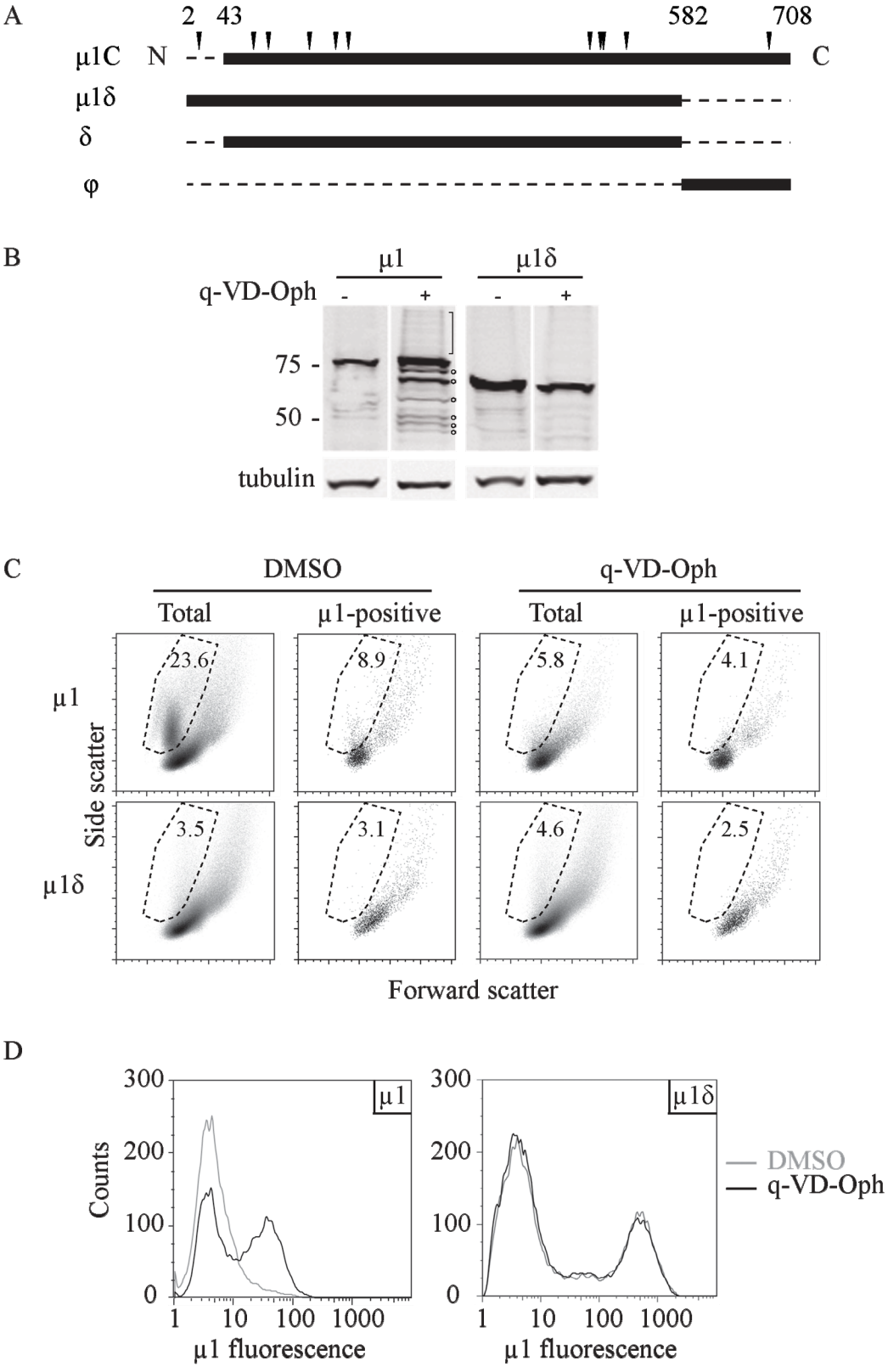
A
2
43
582
708
μ1C
N
C
μ1δ
δ
φ
B
μ1
μ1δ
q-VD-Oph
-
+
-
+
75 -
50 -
tubulin
C
DMSO
q-VD-Oph
Total
μ1-positive
Total
μ1-positive
μ1
μ1δ
Side scatter
23.6
8.9
5.8
4.1
3.5
3.1
4.6
2.5
Forward scatter
D
300
200
100
0
Counts
μ1
μ1δ
1
10
100
1000
μ1 fluorescence
DMSO
q-VD-Oph

My results thus far indicated that the low levels of immunoreactive μ1 might be explained by loss of the epitope recognized by anti-reovirus serum following proteolytic cleavage by caspases. Monoclonal antibodies raised against virions that recognize μ1 recognize the δ region of μ1 (32). To test this hypothesis, I examined the steady state expression levels of μ1 fusion proteins in which EGFP was fused to the C- or N-terminus (fused to residue 2) of μ1 (using pEGFP-N-M2(N) and pEGFP-C-M2(N) vectors, respectively) in transfected 293F cells (Figure 4.2A). The subcellular distribution of EGFP-μ1 and μ1-EGFP were similar to that of wild type μ1 when expressed in cells and both fusion proteins were recognized by mAb anti-μ1 10H2 (Figure 4.2B), suggesting that the fusion had not substantially altered the folding of μ1. Similar to wild type μ1, the levels of full-length μ1-EGFP and EGFP-μ1 when detected with an anti-reovirus serum or an anti-GFP antibody increased upon treatment with q-VD-Oph (Figure 4.2A). However, when the fusion proteins were detected with anti-GFP antibodies, bands of lower molecular weight than the full-length fusion protein, but larger than EGFP alone were detected, particularly in the μ1-EGFP lysates (Figure 4.2A). Although additional faint lower molecular weight bands were detected in the EGFP-μ1 lysates probed with anti-GFP, there were at least six additional lower molecular weight bands of greater intensity present in μ1-EGFP lysates. These findings supported my hypothesis that μ1 was being proteolytically cleaved and that fragments of lower molecular weight were no longer recognized by the anti-reovirus serum, but were recognized by the anti-GFP serum. In addition, when I compared the banding pattern of μ1-EGFP in immunoblots probed with anti-GFP antibodies in the presence or absence of q-VD-Oph it was clear that some lower molecular weight bands became more intense in the presence of q-VD-Oph and at least one lower molecular weight band present in lysates from cells without q-VD-Oph became less intense in lysates from cells treated with q-VD-Oph. Taken together these

findings confirm that µ1 was being cleaved by q-VD-Oph-inhibitable proteases, most likely caspases, and suggest that this cleavage was occurring predominantly towards the C-terminal region of µ1.

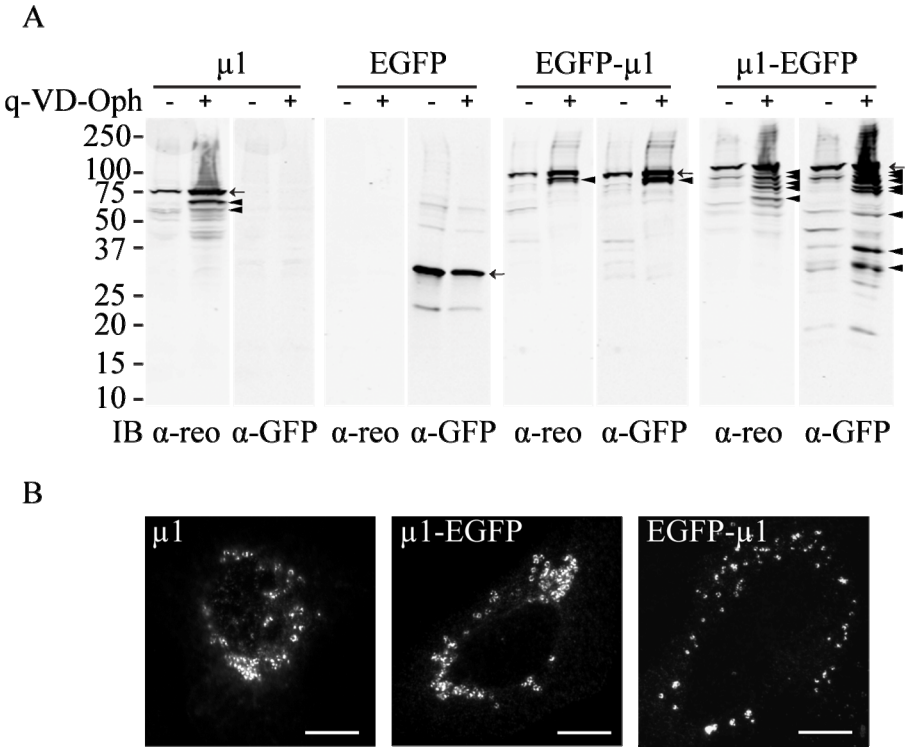

Figure 4.2: Comparison of the expression levels of µ1, µ1-EGFP and EGFP-µ1 in 293F cells treated with DMSO or q-VD-Oph. A) Immunoblots of 293F cells expressing µ1, EGFP, EGFP-µ1, and µ1-EGFP. 293F cells were transfected with plasmids for the indicated proteins and treated with 10 µM q-VD-Oph or an equal volume of DMSO. At 24 h post-transfection, lysates were prepared, immunoblotted and probed with rabbit anti-reovirus serum and mouse anti-GFP followed by IRDye 680 goat anti-rabbit IgG and IRDye 800CW goat anti-mouse IgG. Fluorescence emission from bound fluorescent antibodies was detected using an infrared gel scanner (Odyssey, LI-COR). Arrows indicate full length proteins (µ1 o EGFP), arrowheads indicate cleavage fragments. B) Immunofluorescence images of the subcellular distribution of µ1, EGFP-µ1, and µ1-EGFP in transfected CV-1 cells. CV-1 cells on glass cover slips were transfected with plasmids for the indicated proteins. At 24 h post-transfection the cells were fixed and immunostained for µ1 or the intrinsic fluorescence of EGFP was detected. Scale bars, 10 µm.

µ1 expressed in transfected cells is ubiquitinated. In addition to low molecular weight bands, I also noted the appearance of a high molecular weight smear if µ1-expressing cells were treated with the pan-caspase inhibitor q-VD-Oph. The presence of these high molecular weight bands in the µ1-transfected cell lysates suggested that µ1 was ubiquitinated. Therefore, I co-expressed full-length µ1 with a his-tagged polyubiquitin-encoding plasmid and precipitated his-polyubiquitin-tagged proteins from the lysates with Ni-NTA agarose. Immunoblots of co-precipitated proteins probed with anti-reovirus serum revealed that µ1 was pulled down along with his-polyubiquitin (Figure 4.3A). As controls I expressed µ1 or the his-polyubiquitin plasmid with empty vector or co-expressed µ1 with his-tagged c-jun protein. µ1 was not precipitated if expressed alone, indicating µ1 did not interact with the Ni-NTA resin non-specifically. Co-expression with c-jun-his did also not result in µ1 precipitation ensuring that the his-tag was not responsible for the interaction seen between µ1 and his-polyubiquitin. The amount of detectable µ1 in the precipitation was low, as seen before in transfected cells. Therefore, I treated cells at the time of transfection with q-VD-Oph and repeated the precipitation assay. I saw a dramatic increase in the level of ubiquitinated µ1 under conditions of caspase inhibition (Figure 4.3B, note 15 min vs. 1 min exposure). This increase of ubiquitinated µ1 did not reflect an overall augmentation of ubiquitination, as treatment of his-polyubiquitin expressing cells with q-VD-Oph did not alter the amount of ubiquitinated protein that was precipitated (Figure 4.3C). I conclude from these results that µ1 is polyubiquitinated and likely targeted for proteasome-mediated degradation. In support of these findings, I found that polyubiquitin co-localized with µ1 in transfected and infected cells on ring-like structures in the cytosol of cells (Figure 4.4). It has been shown previously that these ring-like structures are lipid droplets (5).

Figure 4.3: μ1 is ubiquitinated. 293F cells were transfected with plasmids expressing the indicated proteins and then treated with A) DMSO or B) 10 μM q-VD-Oph at the time of transfection. Cell lysates were prepared and his-ubiquitin-tagged conjugates were isolated from equal amounts of protein by Ni-NTA chromatography as described in Materials and Methods. The isolated conjugates were separated on SDS-polyacrylamide gels and immunoblotted for μ1 and the polyhistidine epitope tag using the indicated antibodies. Lysate only lane (Lys) shows expression of μ1. High molecular weight bands indicative of polyubiquitination are bracketed. Asterisks indicate non-specific immunoreactive bands. C) q-VD-Oph treatment does not increase the levels of polyubiquitination. 293F cells were transfected with a His-polyubiquitin expressing plasmid and treated with DMSO or 10 μM q-VD-Oph at the time of transfection. His-polyubiquitinated proteins were precipited using Ni-NTA agarose, immunoblotted and probed with anti-6xHis antibody. Note that blots in A) and B) have different exposure times, A) 15 min B) 1 min.

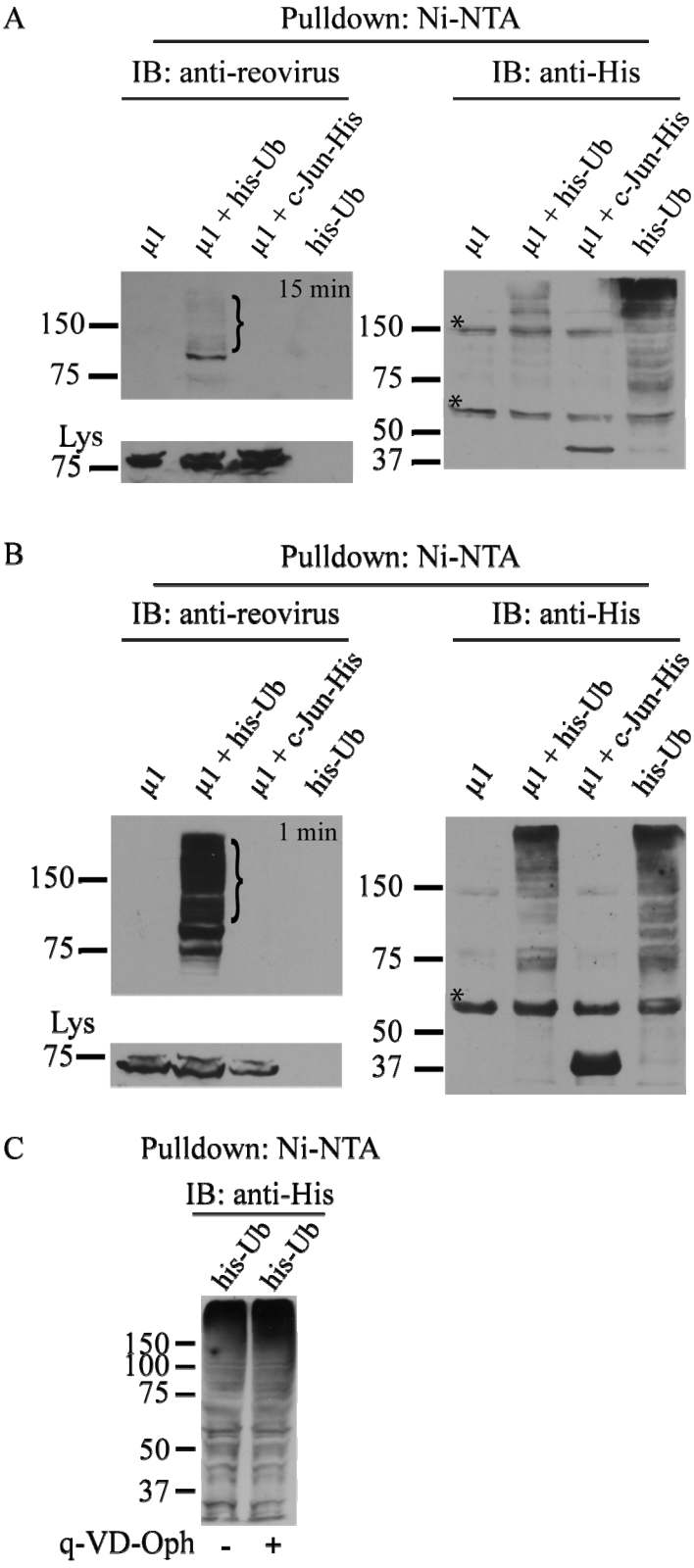
A
Pulldown: Ni-NTA
IB: anti-reovirus
IB: anti-His
μ1
μ1 + his-Ub
μ1 + c-Jun-His
his-Ub
15 min
150
75
Lys
75
150
75
50
37
*
*
B
Pulldown: Ni-NTA
IB: anti-reovirus
IB: anti-His
μ1
μ1 + his-Ub
μ1 + c-Jun-His
his-Ub
1 min
150
75
Lys
75
150
75
50
37
*
C
Pulldown: Ni-NTA
IB: anti-His
his-Ub
his-Ub
150
100
75
50
37
q-VD-Oph - +

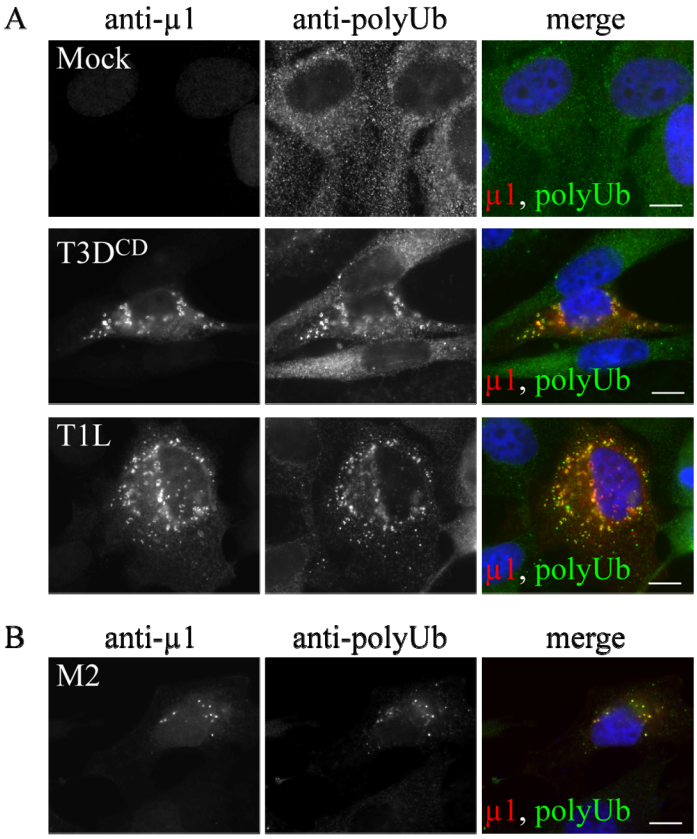

Figure 4.4: Co-localization of μ1 and polyubiquitin. A) Immunofluorescent images of mock, $T3D^{CD}$, and T1L-infected HeLa cells. B) Immunofluorescent images of M2-transfected HeLa cell. Cells on cover slips were infected (MOI = 5) or transfected as indicated, then fixed and immunostained with anti-μ1 mAb 4A3 (isotype IgG2b) and mAb FK1 (isotype IgM). Primary antibodies were detected with Alexa-594 conjugated goat anti-mouse IgG2b and FITC-conjugated goat anti-mouse IgM, respectively. Scale bars, 10 μm.

Mutations at predicted caspase cleavage sites at residues 487 and 490 of μ1 stabilize protein levels in transfected cells. Based on my findings, I hypothesized that μ1 was a target for caspases and thus contained caspase cleavage sites. To test this hypothesis, I analyzed the μ1 amino acid sequence for potential caspase cleavage sites using three prediction algorithms. The predicted cleavage sites were not randomly distributed throughout the protein, but were clustered within the δ region and no predicted sites were present between residues 582-611, the minimal region of Φ

required for μ1-induced apoptosis (5). Using this information, I prepared twelve point mutations in which the predicted P1 aspartate residue was mutated to either an alanine, asparagine, glutamate or lysine. All of the mutants were expressed and had a subcellular distribution similar to that of wild type μ1 (data not shown). I screened the expression levels of these mutants in CHO-S cells by flow cytometry (Figure 4.5A and B) and found that three mutants, D487N, D490E, and D490N had significantly higher expression levels than wild type μ1 when assessed as fold-change in geometric mean fluorescence (Figure 4.5A) and also in the percentage of cells expressing detectable μ1 (Figure 4.5B). These results correlated with immunoblot results from transfected 293F cells (a subset of mutants is shown in Figure 4.5C). In the presence of q-VD-Oph, I noted a significant eight-fold increase in the percentage of cells expressing wild type μ1. In contrast, although there was a 1.5 to 3-fold increase in expression of mutants D487N, D490E, and D490N in the presence of q-VD-Oph, this was significantly less than the increase seen for wild type and the null mutants D191A (see Figure 4.5C) and D97E (Figure 4.6A and B). This result suggested that amino acids 487-490 was a caspase cleavage site, as mutation of this motif diminished the responsiveness of μ1 to the pan-caspase inhibitor q-VD-Oph.

Figure 4.5: Expression of μ1 and mutants in CHO-S and 293F cells treated with DMSO or q-VD-Oph. A) Normalized change in mean fluorescence index of CHO-S cells expressing WT and mutant forms of μ1. B) Percentage of cells expressing μ1. CHO-S cells were transfected with plasmids expressing the indicated WT and mutant forms of μ1 and treated with 10 μM q-VD-Oph or an equal volume of DMSO. At 24 h post-transfection the cells were fixed, immunostained for μ1 and analyzed by flow cytometry. C) Immunoblots of μ1 and indicated mutants expressed in 293F cells treated with DMSO or 10 μM q-VD-Oph at the time of transfection. Blots were probed with rabbit anti-reovirus serum and mouse mAb anti-tubulin. * $p < 0.05$; ** $p < 0.001$.

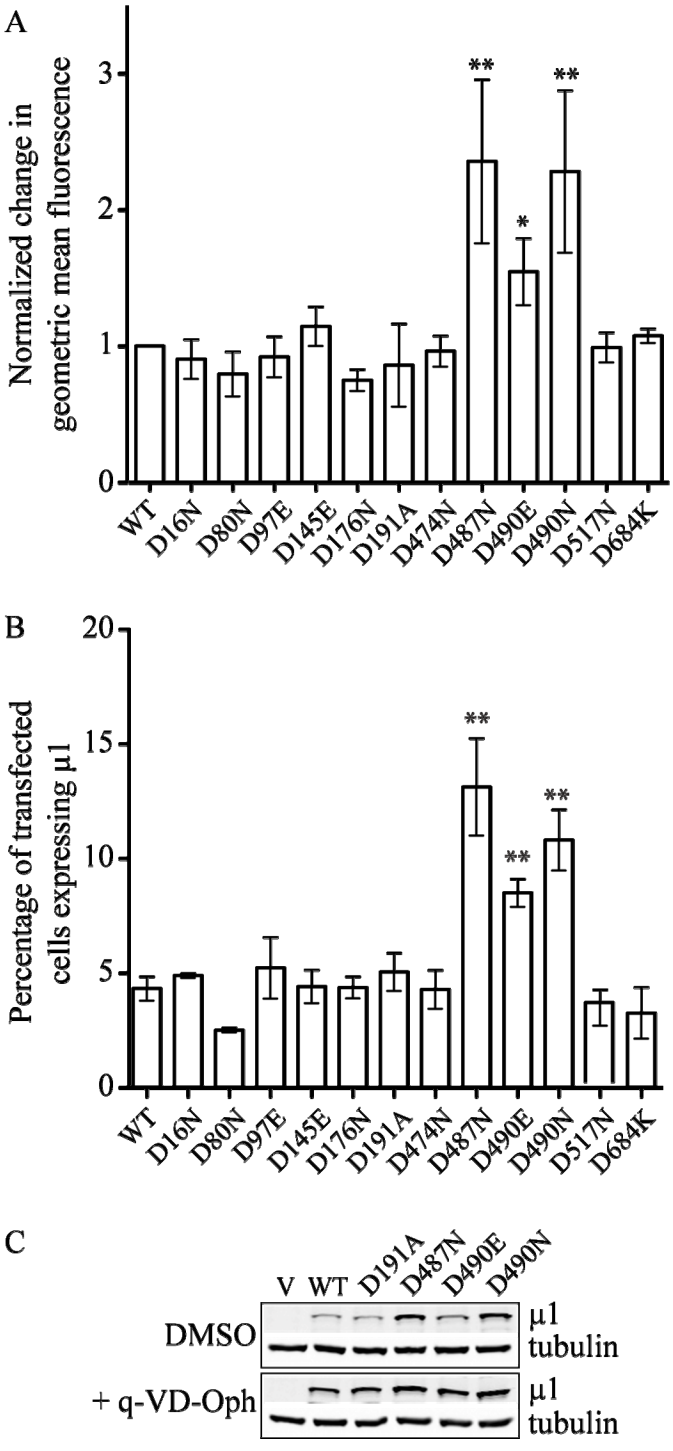
A
Normalized change in geometric mean fluorescence
0
1
2
3
**
*
**
WT
D16N
D80N
D97E
D145E
D176N
D191A
D474N
D487N
D490E
D490N
D517N
D684K
B
Percentage of transfected cells expressing µ1
0
5
10
15
20
**
**
**
WT
D16N
D80N
D97E
D145E
D176N
D191A
D474N
D487N
D490E
D490N
D517N
D684K
C
V
WT
D191A
D487N
D490E
D490N
DMSO
µ1
tubulin
+ q-VD-Oph
µ1
tubulin

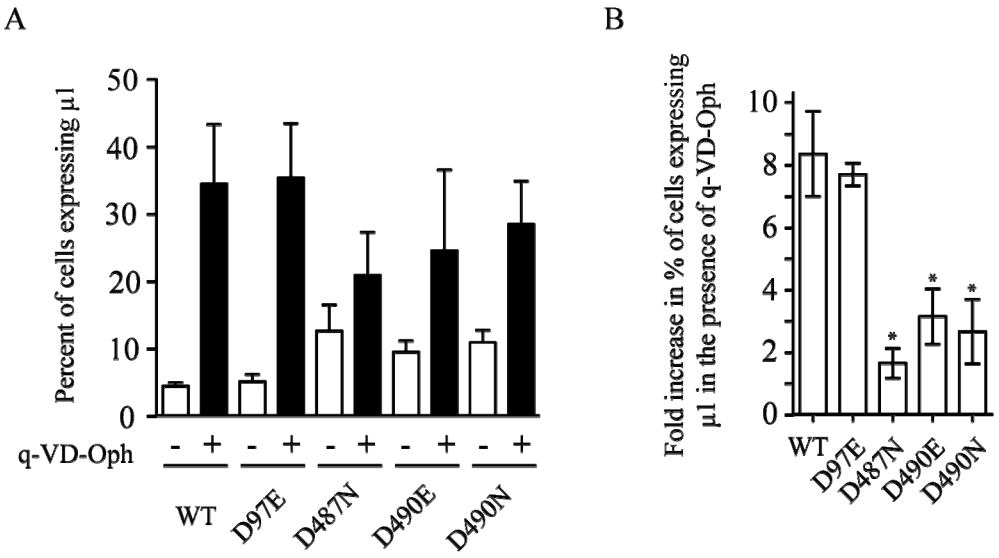

Figure 4.6: A) Effect of q-VD-Oph on the percentage of WT or mutant-transfected cells expressing µ1. B) Data in A) expressed as fold increase in percentage of cells expressing µ1 in the presence of q-VD-Oph. Data shown are the means and standard deviations of a minimum of three independent experiments. * $p < 0.05$.

Given these findings I predicted that the cleavage pattern of µ1 would differ in the mutants D487N, D490E and D490N. To test this hypothesis I prepared constructs in which EGFP was fused to the C-terminus of these mutants and examined their cleavage pattern in transfected 293F cells in the presence or absence of q-VD-Oph (Figure 4.7). I found that, in contrast to wild type µ1, the immunodetectable levels of µ1 did not change as markedly in the presence of q-VD-Oph. For all mutants and the wild type, a number of small molecular weight bands were detected by immunoblot both with and without caspase inhibitor, suggesting µ1 had been cleaved by other proteases. Both the wild type and mutant D191A exhibited a slightly different pattern of low molecular weight bands upon q-VD-Oph addition, while the fragment banding pattern for mutants D487N, D490E and D490N remained the same. This finding supported my conclusion about amino acid 490 being a caspase cleavage site.

Figure 4.7: Cleavage patterns and expression levels of μ1-EGFP and mutants in the absence or presence of a pan-caspase inhibitor. A) anti-reovirus immunoblot B) anti-GFP immunoblot C) two-color fluorescent immunoblot (red = anti-reovirus; green = anti-GFP) D) comparison of banding pattern for μ1-EGFP lysates immunostained for μ1 and GFP [data derived from panels A) and B)]. The indicated plasmids were transfected into 293F cells that were treated with 10 μM q-VD-Oph or an equal volume of DMSO. 24 h post-transfection cell lysates were prepared, immunoblotted and probed with rabbit anti-reovirus (T3D) serum and mouse mAb anti-GFP followed by IRDye 680 goat anti-rabbit IgG and IRDye 800CW goat anti-mouse IgG. Fluorescence emission from bound fluorescent antibodies was detected using an infrared gel scanner (Odyssey LI-COR). Brackets in panels A) and B) indicate high molecular weight banding. The filled arrowheads in B) indicate EGFP and the empty arrowhead indicates ~ 37 kDa band. In panel D) arrows indicate bands not detected with both antibodies.

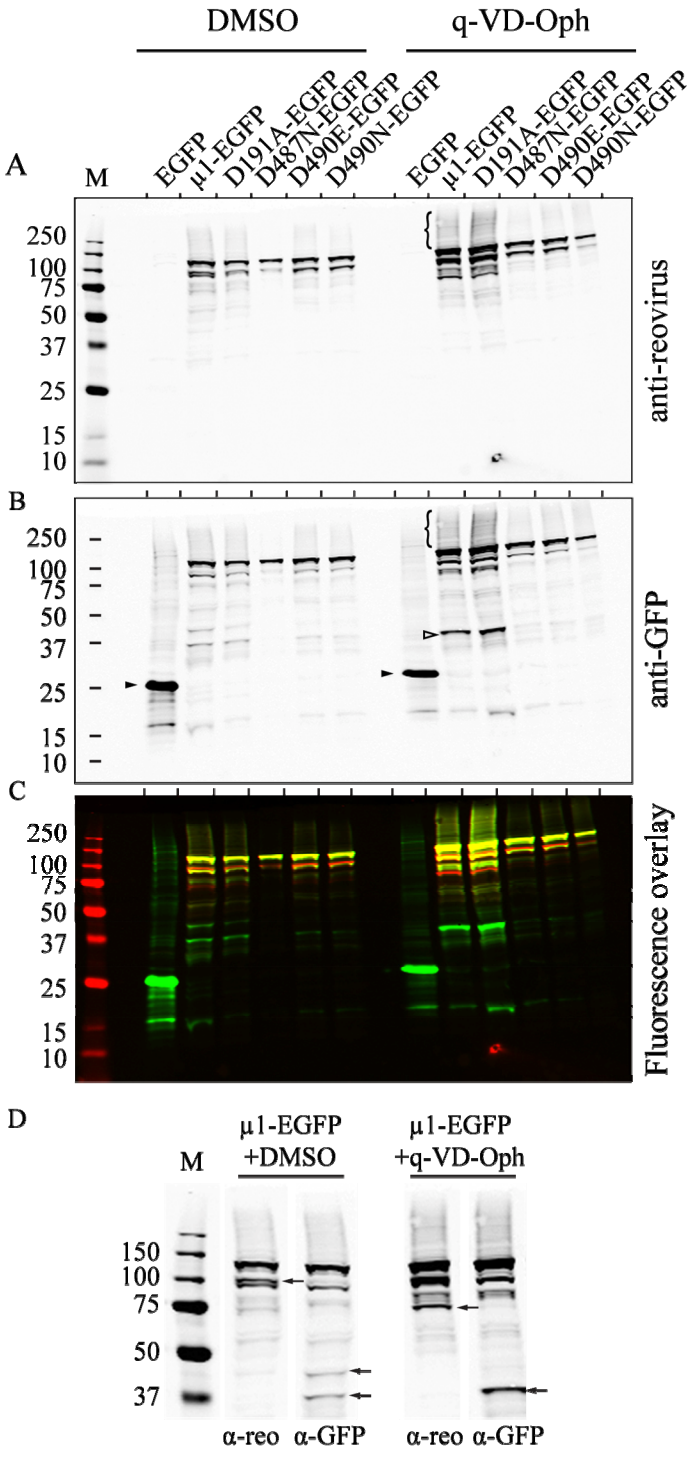
DMSO
q-VD-Oph
EGFP
μ1-EGFP
D191A-EGFP
D487N-EGFP
D490E-EGFP
D490N-EGFP
A
M
250
100
75
50
37
25
15
10
anti-reovirus
B
anti-GFP
C
Fluorescence overlay
D
μ1-EGFP
+DMSO
μ1-EGFP
+q-VD-Oph
150
100
75
50
37
α-reo
α-GFP
α-reo
α-GFP

Capacity of wild type and mutant forms of µ1 to induce apoptosis in transfected cells. The µ1 mutants D487N, D490E and D490N were expressed at higher steady-state levels than wild type µ1 in transfected cells. Therefore, I examined the possibility that these mutants would induce greater levels of apoptosis in transfected CHO-S cells. I found that mutants D97E, D490E and D490N induced similar levels of caspase 3/7 activity in CHO-S cells as wild type µ1 (Figure 4.8A). However, mutant D487N induced significantly lower mean levels of apoptosis than wild type µ1 (38.6 vs 23.8 %). When I analyzed cells that were caspase 3/7 positive, I found that mutants D487N, D490E, and D490N had a higher percentage of cells that were µ1 positive and a lower percentage of cells that were µ1 negative in comparison to cells transfected with wild type µ1 or mutant D97E (Figure 4.8B), indicating that more µ1 was detectable in cells expressing mutants D487N, D490E, and D490N. This observation was concurrent with the results in wild type µ1 where treatment with the pan-caspase inhibitor q-VD-Oph increased the number of cells with detectable levels of µ1 (Figure 4.1D).

Mutant forms of µ1 cause less cytotoxicity than wild type µ1. When I investigated the overall number of dead cells in wild type compared to mutant µ1 expressing CHO-S cells, I found that there was a significant difference. Caspase cleavage mutants D487N, D490E and D490N showed a reduction in the number of dead cells while the null mutant D97E caused cell death to an extent similar to wild type µ1 (Figure 4.8C). This was a surprising result given my finding that the caspase cleavage mutants (except D487) were as effective in inducing caspase 3/7 activation as wild type µ1. I hypothesize that wild type µ1 causes cell death not only by inducing apoptosis, but might also have other cytotoxic effects which are no longer available to the caspase cleavage mutants.

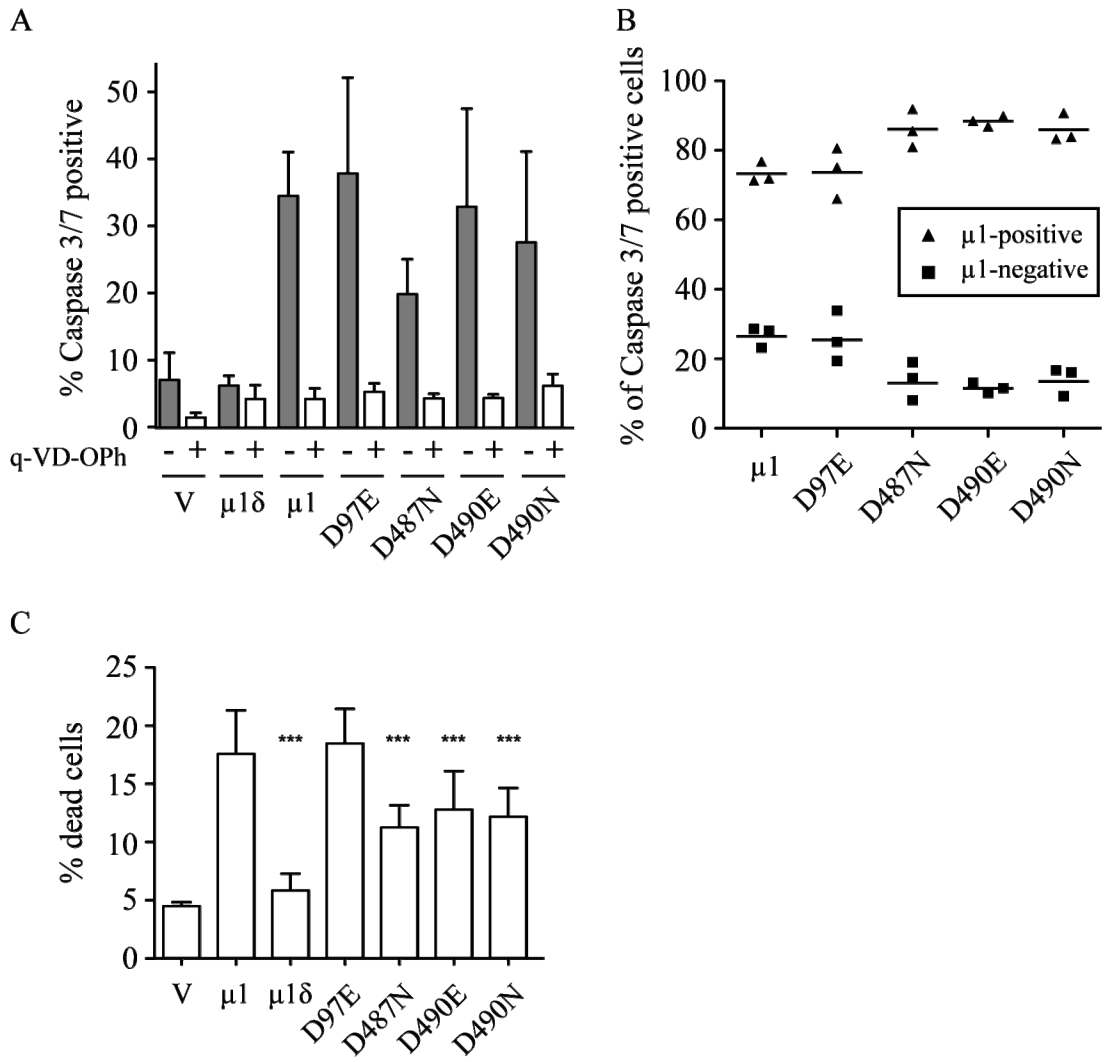

Figure 4.8: µ1 mutants deficient for cleavage at residue 490 activate caspase 3/7 as efficiently as wild type, but induce less cytotoxicity. A) Percent cells with active caspase 3/7 expressing the indicated plasmids with or without caspase inhibitor, V denotes empty vector. B) Distribution of active caspase 3/7 positive cells according to the detectability of wild type or mutant µ1 expression. Caspase 3/7 activation was analyzed with FLICA caspase3/7 kit. C) Percent cytotoxicity in cells expressing the indicated plasmids, V denotes empty vector. Cell viability was analyzed with Live/Dead Cell Viability Kit. CHO-S cells were transfected with plasmids expressing the indicated wild type and mutant forms of µ1 or µ1δ and treated with 10 µM q-VD-Oph or an equal volume of DMSO. At 24 h post-transfection the cells were fixed, immunostained for µ1 and analyzed by flow cytometry.

Mutant forms of μ1 have an ubiquitination defect. I showed before that μ1 was ubiquitinated and that ubiquitination increased substantially after treatment with the pan-caspase inhibitor q-VD-Oph. Thus, I investigated if the caspase cleavage mutants responded similarly. I co-expressed the caspase cleavage mutants with His-polyubiquitin and purified His-polyubiquitin-tagged proteins through Ni-NTA chromatography. I found that the D487A mutant showed increased ubiquitination in the absence of q-VD-Oph compared to wild type μ1 (Figure 4.9A left panel). After treatment with q-VD-Oph, however, the extent of ubiquitination of the D487 mutant did not increase further as seen for wild type μ1 (Figure 4.9A right panel). The seemingly different level of ubiquitination in D487N versus D487A μ1 in Figure 4.9A could be explained by the different exposure time of the two immunoblots. Although prevention of caspase cleavage through mutation of amino acid D487 did lead to similarly increased ubiquitination of μ1 as caspase inhibition had, the mutation of aa D490 led to a different phenotype. This mutation, although targeting the same caspase cleavage site as the mutation of aa D487, did not show increased ubiquitination in the absence of q-VD-Oph (Figure 4.9A left panel). This phenotypic incongruence prompted me to consider that the D487 mutant might be misfolding and thus was ubiquitinated more strongly than wild type μ1. In support of this hypothesis, I found that the mutants D487N and D487A had severe defects in μ1:σ3 co-immunoprecipitation assays, indicating that a mutation at residue 487 abolished the capacity of μ1 to assemble with σ3 (data not shown). Mutation of residue 490 did not only not increase ubiquitination of μ1, but also abrogated the ubiquitination-enhancing effect of q-VD-Oph treatment seen in wild type μ1 (Figure 4.9A). These findings suggested that prevention of caspase cleavage by a chemical inhibitor and by mutation of the cleavage site caused two different phenotypes, inhibiting the enzyme increased ubiquitination while mutation of the target reduced ubiquitination.

Nonetheless, both scenarios implied a link between caspase activity and ubiquitination. In order to test whether the reduction in ubiquitination was confined to mutation of the caspase cleavage site, I constructed several alanine substitution mutants (aa 485-495) targeting residues up- and downstream of the D490 cleavage site. The amino acid 491 is already an alanine and was thus not mutated. The alanine mutants were co-expressed with His-polyubiquitin and analyzed for their ubiquitination status with or without q-VD-Oph treatment. Figure 4.9B shows that mutant D487A was again highly ubiquitinated in comparison to wild type µ1, but also that mutation of the preceding residues, Q485 and P486 caused more ubiquitination than wild type µ1 in the absence of the caspase inhibitor. This could indicate that this region does not tolerate mutations and that substitutions lead to misfolding and ubiquitination. The mutation of residues 488 to 495 did not enhance ubiquitination in the absence of q-VD-Oph (Figure 4.9B) which suggested that these mutants were not misfolding. The mutants L492A and T494A seemed to be even less ubiquitinated then wild type µ1, which might have been due to lower expression levels (lysate Figure 4.9B). In the presence of q-VD-Oph the mutants V488A and M495A behaved like wild type µ1 and showed a strong increase in ubiquitination (Figure 4.9C). Mutation of residues 493 and 494 led to a moderate reduction in ubiquitination while the mutations closest to aa 490 (W489A, L492A) caused a severe reduction in ubiquitination (Figure 4.9C). This result suggested that the effect of decreased ubiquitination was tightly linked to the mutation of the D490 caspase cleavage site. I also noted that all mutants that exhibited a defect in ubiquitination lacked a lower molecular weight fragment of µ1 seen in the lysate, with the exception of the D487A mutant which was highly ubiquitinated as a consequence of misfolding (lysate Figure 4.9C). The concurrence of µ1 cleavage inhibition and ubiquitination reduction further supported my hypothesis that caspase activity and ubiquitination are connected.

Figure 4.9: Caspase cleavage mutants exhibit an ubiquitination defect. 293F cells were transfected with the indicated plasmids and a His-polyubiquitin-expressing plasmid and treated with A) right and C) 10 μM q-VD-Oph or A) left and B) an equal volume of DMSO. 24 h post-transfection lysates were prepared and His-polyubiquitinated proteins were precipitated, immunoblotted and probed with anti-reovirus serum. Equal amounts of protein were used in precipitations. Note that blots have different exposure times, 15 min without q-VD-Oph and 1 min with q-VD-Oph. Mutants were alanine, asparagine or glutamate substitutions of amino acids in the caspase cleavage site (aa 487 and 490) or alanine substitutions of the surrounding residues.

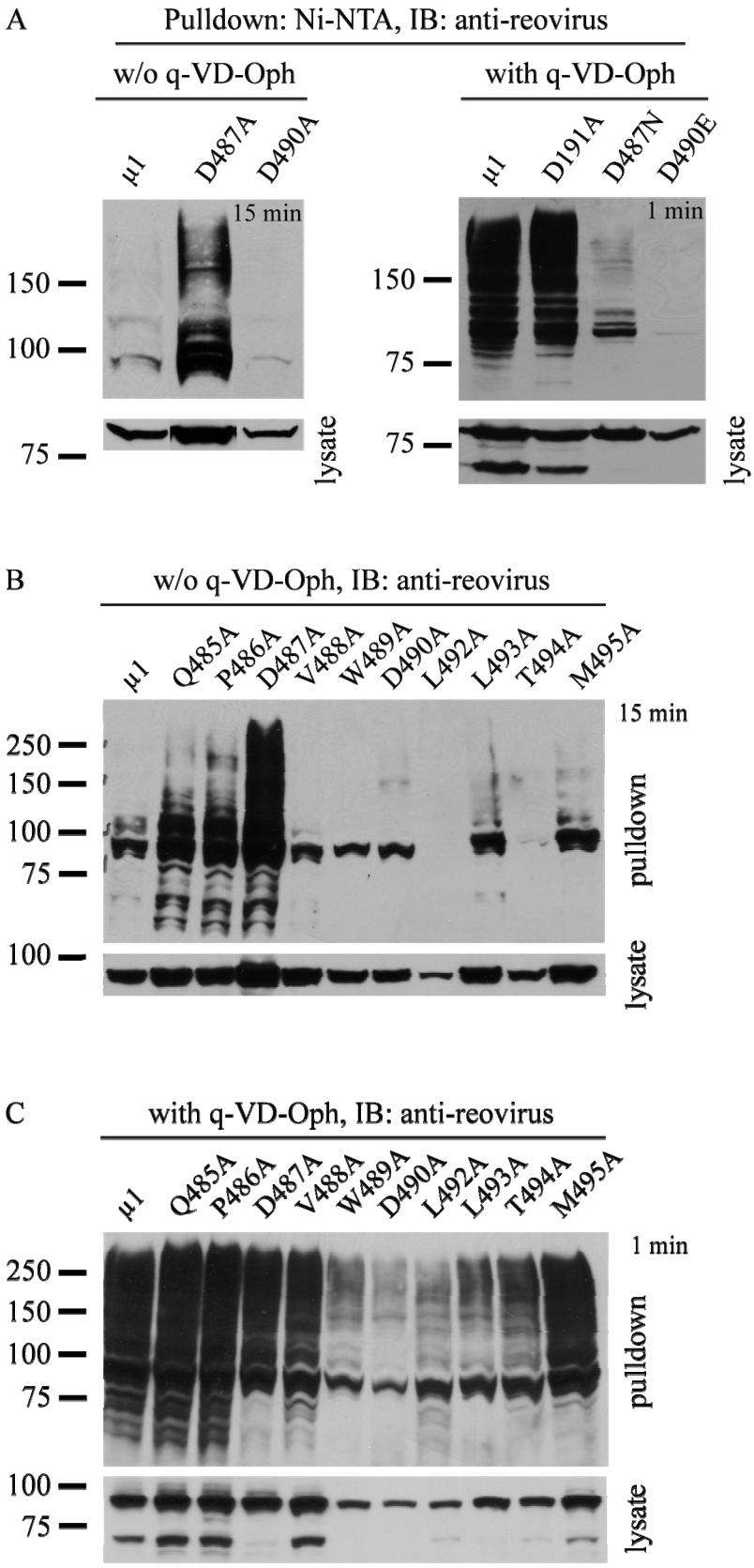
A
Pulldown: Ni-NTA, IB: anti-reovirus
w/o q-VD-Oph
with q-VD-Oph
μ1
D487A
D490A
μ1
D191A
D487N
D490E
15 min
1 min
150
100
75
150
75
75
lysate
lysate
B
w/o q-VD-Oph, IB: anti-reovirus
μ1
Q485A
P486A
D487A
V488A
W489A
D490A
L492A
L493A
T494A
M495A
15 min
250
150
100
75
100
pulldown
lysate
C
with q-VD-Oph, IB: anti-reovirus
μ1
Q485A
P486A
D487A
V488A
W489A
D490A
L492A
L493A
T494A
M495A
1 min
250
150
100
75
100
75
pulldown
lysate

Generation and initial characterization of a µ1-D490E mutant virus. In order to investigate the biological significance of the caspase cleavage site mutation, I used reverse genetics to generate a virus that carries the D490E mutation in its M2 gene segment (20). I was not able to recover virus with the other mutations, D191A, D487N and D490N. As a first step to characterize the D490E mutant virus I performed single and multiple cycle growth kinetics. Overall there seemed to be no difference between the amount of virus produced in a single cycle of replication of wild type and mutant virus (Figure 4.10C). I harvested the supernatant in the single cycle growth kinetics separately from the cells in order to distinguish between released and cell-associated virus. I found that at early times after infection, there was more virus released in the mutant than the wild type virus (Figure 4.10B). This release however occurred so early at 3 h post-infection that this virus likely constitutes input virus and not newly generated virions. I hypothesize that the D490E mutant virus was initially bound to cells, but did not become internalized and ultimately detached from the cell into the supernatant. If the D490E mutation causes an entry defect will be investigated using a hemolysis assay. The amount of cell-associated mutant virus was reduced by approximately half a log which may be due to the proposed entry defect of the mutant (Figure 4.10A). In addition, there seemed to be a slight delay in virus release from the D490E-infected cells; see right shift of D490E curve in Figure 4.10A. The analysis of the multiple cycle growth kinetic revealed that the D490E mutant virus grew to significantly lower titers when compared to wild type virus (Figure 4.10D). If the D490E mutation causes an entry defect this reduction in titer could be a cumulative effect.

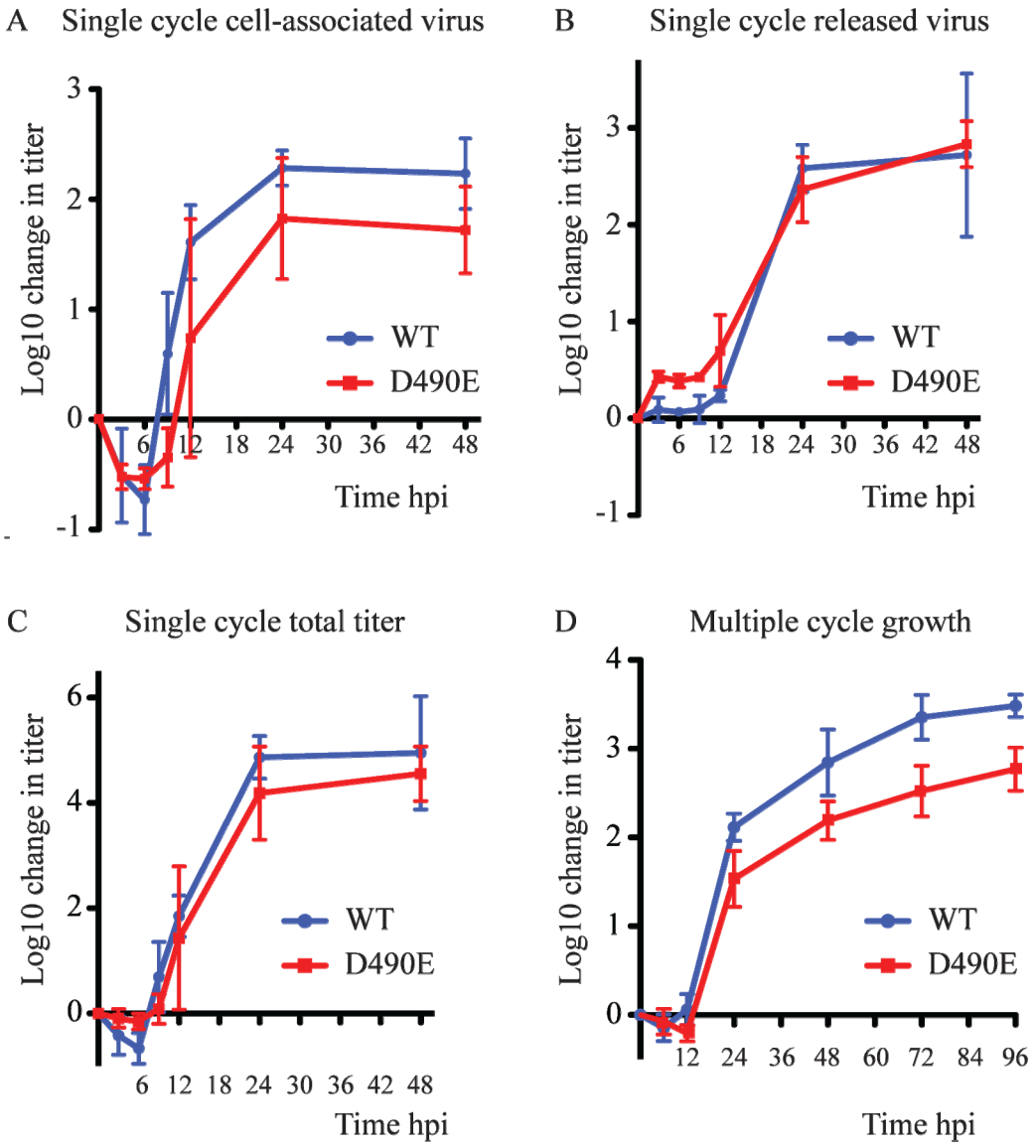

Figure 4.10: Single and multiple cycle growth kinetics of µ1-D490E mutant virus in comparison to recombinant wild type virus. A-C) Single cycle growth kinetics. L929 cells were infected with recombinant wild type (WT) or D490E mutant virus at MOI=5. Supernatant and cells were harvested separately 3, 6, 9, 12, 24 and 48 h post-infection. D) Multiple cycle growth kinetics. L929 cells were infected with recombinant wild type (WT) or D490E mutant virus at MOI=0.1. Cells with supernatant were harvested 6, 12, 24, 48, 72 and 96 h post-infection. Titers were analyzed with standard plaque assay. Graphs show mean and standard deviation of change in log10 titer in comparison to 0 h time point from at least four independent experiments.

Discussion

Apoptosis in reovirus infection is not a host defense mechanism, but is induced by the virus. It is thought that apoptosis induction aids viral spread (26). In order for the virus to benefit from apoptosis, the induced cell death has to be regulated so that it does not occur too early before replication and assembly are completed. Coffey et al. showed that the reovirus outer capsid protein μ1 induces apoptosis if expressed ectopically in cells (5). It has also been demonstrated that μ1 is responsible for apoptosis induction in virus infection (7). I previously noted that the μ1 protein levels are substantially greater in infected cells than in cells ectopically expressing μ1. I speculated that μ1 might be unstable and degraded in transfected cells. Here I investigated possible mechanisms for μ1 degradation and found that μ1 is a target for cleavage by caspases and ubiquitination. Treatment of μ1 expressing cells with the pan-caspase inhibitor q-VD-Oph caused a 4-fold increase in the detectable levels of μ1. In addition I observed the appearance of a number of small molecular weight fragments and also a high molecular weight smear. Analysis of the primary amino acid sequence of μ1 revealed a dozen potential caspase cleavage sites, but mutational analysis confirmed only one site at amino acids 487-490. The fact that mutation of amino acids D487 and D490 led to a different cleavage pattern of the mutant μ1 protein signified that this site was a functional caspase cleavage site. The high molecular weight smear seen in immunoblotting after treatment of μ1-expressing cells with pan-caspase inhibitor could be identified as ubiquitination of μ1. The extent of μ1 ubiquitination after caspase inhibition was dramatically increased. Given the fact that caspase inhibition did not increase the total amount of protein ubiquitination, I speculate that not only the amount of μ1 protein increased with caspase inhibition, but that ubiquitination was somehow facilitated as well. How caspase inhibition might augment ubiquitination remains to be elucidated. An example where caspase cleavage

and ubiquitination are linked has been demonstrated in the oncoprotein MDM2 and its substrate p53. MDM2 is an E3 ubiquitin ligase which ubiquitinates p53 and thus targets it for degradation (15). In apoptotic cells MDM2 is cleaved by caspase 3 into two subdomains, the N-terminal fragment which can still bind p53 and inhibit its function and the C-terminal fragment which contains the ubiquitin ligase activity (2). This region is no longer able to interact with p53 and thus, inhibition of caspase 3 should prevent MDM2 cleavage and maintain its ubiquitination activity. So far no ubiquitin ligase has been identified that interacts or co-localizes with μ1.

But it seems that the situation in the case of μ1 is more complicated. After identifying a caspase cleavage site at amino acid 490 I expected to see a similar increase in ubiquitination in a mutant of this cleavage site as I had for wild type μ1 under conditions of caspase inhibition. Surprisingly, I found that D490 mutants did not show enhanced ubiquitination. Thus it appears that prevention of caspase cleavage by different means, chemical inhibition of the enzyme or mutation of the recognition site in the substrate, has different phenotypic outcomes. In contrast, the D487 mutant did exhibit strong ubiquitination when compared to wild type μ1 under conditions of active caspases. However, when I examined the caspase cleavage site mutants for their ability to interact with σ3, I found that the D487N mutant had a severe defect (data not shown). Thus, I hypothesize that this mutant might be misfolded, triggering ubiquitination. In order to explain the results seen for caspase cleavage inhibition by inhibitor or mutation I hypothesize that caspases function in two separate ways. The increase in ubiquitination of wild type μ1 after treatment with a pan-caspase inhibitor could suggest that caspases cleave and destroy an enzyme of the ubiquitination machinery responsible for ubiquitination of μ1. Simultaneously, caspase cleavage of μ1 seems necessary for ubiquitination as the mutation of the caspase cleavage site reduces ubiquitination. This would imply though that it is a cleavage fragment of μ1

that becomes ubiquitinated. Immunoblots of ubiquitinated μ1, however, do not show any small fragments, only bands that are larger than full length μ1. Taking into account that cleavage of μ1 seems to destroy immunoreactive epitopes, the lack of smaller ubiquitinated fragments of μ1 could be explained by their indetectability. Preliminary experiments with simultaneously N- and C-terminally tagged μ1 did indeed reveal the presence of ubiquitinated μ1 fragments of around 50 kDa.

The caspase cleavage mutants at residue D487 and D490 did show an increased μ1 steady state levels in transfected cells. Surprisingly, although they activated caspases 3 and 7 to a similar extent as wild type μ1, they caused significantly less cytotoxicity. Coffey et al found that the C-terminal Φ fragment (amino acids 582-708) of μ1 is necessary and sufficient for apoptosis induction (5). They also showed that this fragment alone exhibits a slightly different subcellular localization. Full length μ1 localized predominantly to lipid droplets and to a lesser extent to mitochondria and the endoplasmic reticulum (ER). Φ, however, demonstrated a preferential localization to mitochondria and less to lipid droplets and the ER (5). It seems possible that while full length μ1 is capable of activating caspases 3 and 7, cleavage of μ1 into a fragment that contains Φ enables this fragment to target additional membranes, thus causing increased cytotoxicity. It would be interesting to investigate the subcellular distribution of the different cleavage fragments of μ1 using a simultaneously N- and C-terminally tagged version of μ1.

I was unable to recover recombinant viruses harboring the mutations D191A, D487N, D490E and D490N in their M2 gene segment. I was only able to recover the mutant virus D490E. The D191 residue is located in an α-helical region in the basal part of the μ1 trimer and is likely buried (21). A mutation might interfere with the proper folding and/or assembly of μ1. The amino aids D487 and D490 are in the head part of the μ1 trimer where the three jelly-roll β barrels arrange around a central

channel of approximately 5 Å diameter (21). Residue D490 appears to face into this channel while D487 does not seem to be exposed. The D487N mutation most likely causes problems in the association of the three μ1 head domains. If this was the case, this mutant would certainly be defective in its ability to assemble with σ3, which is exactly what I found in μ1-D487N:σ3 co-immunoprecipitation assays (data not shown). It was surprising that I could recover the D490E mutant virus, but not the D490N variant. The μ1 head domain is thought to undergo a conformational change during virus entry which results in a more open conformation of this domain (21). It is possible that a glutamate at position 490 is more conducive to such a conformational change or the maintenance of either the closed or open status than an asparagine. Indeed, the D490E mutant virus did show a possible entry defect in single cycle growth kinetics, but these findings need to be addressed more specifically.

In summary, I have provided evidence that μ1 is a target for caspase cleavage and ubiquitination and that both processes are somehow linked. Cleavage of μ1 also seems to regulate cytotoxicity. The exact mechanism and interconnectivity of these occurrences remains to be elucidated.

Acknowledgements

Experiments for figures 4.1B, 4.2A and B, 4.5C and 4.7 were performed by Brenda Werner. Experiments for figures 4.5A and B, 4.6 and 4.8 were performed by Dr. Jae-Won Kim. Experiments for figures 4.1C and D were performed by Dr. Meagan Wisniewski. Experiments for figure 4.4 were performed by Dr. John S. L. Parker. Experiments for figures 4.3, 4.9 and 4.10 were performed by Susanne Kaufer. The caspase cleavage point mutants and the recombinant mutant virus were generated by Susanne Kaufer. We thank Brian Ingel, Brenda Werner and Lynne Anguish for excellent technical support. We thank Drs. Terence Dermody, Ursula Buchholz and Dirk Bohmann for the kind gift of reagents. We thank Drs. Terence Dermody, Karl Boehme and Mine Ikizler for technical assistance. This work was supported by a Burroughs Welcome Fund Investigators of Pathogenesis of Infectious Disease award (to J. S. L. P.) and by NIH grant R01 AI063036 (to J. S. L. P.).

Reference List

1. **Campanero, M. R. and E. K. Flemington**. 1997. Regulation of E2F through ubiquitin-proteasome-dependent degradation: stabilization by the pRB tumor suppressor protein. Proc. Natl. Acad. Sci. U. S. A **94**:2221-2226.

2. **Chen, L., V. Marechal, J. Moreau, A. J. Levine, and J. Chen**. 1997. Proteolytic cleavage of the mdm2 oncoprotein during apoptosis. J Biol. Chem. **272**:22966-22973.

3. **Clarke, P., S. M. Meintzer, S. Gibson, C. Widmann, T. P. Garrington, G. L. Johnson, and K. L. Tyler**. 2000. Reovirus-induced apoptosis is mediated by TRAIL. J. Virol. **74**:8135-8139.

4. **Coffey, C. M.** 2007. Studies on apoptosis induction by mammalian orthoreovirus outer caspid protein μ1 and regulation by outer capsid protein assembly and degradation. Thesis. Cornell University.

5. **Coffey, C. M., A. Sheh, I. S. Kim, K. Chandran, M. L. Nibert, and J. S. Parker**. 2006. Reovirus outer capsid protein μ1 induces apoptosis and associates with lipid droplets, endoplasmic reticulum, and mitochondria. J Virol **80**:8422-8438.

6. **Danthi, P., C. M. Coffey, J. S. Parker, T. W. Abel, and T. S. Dermody**. 2008. Independent regulation of reovirus membrane penetration and apoptosis by the μ1 Φ domain. PLoS. Pathog. **4**:e1000248.

7. **Danthi, P., M. W. Hansberger, J. A. Campbell, J. C. Forrest, and T. S. Dermody**. 2006. JAM-A-independent, antibody-mediated uptake of reovirus into cells leads to apoptosis. J Virol **80**:1261-1270.

8. **Darzynkiewicz, Z., S. Bruno, B. G. Del, W. Gorczyca, M. A. Hotz, P. Lassota, and F. Traganos**. 1992. Features of apoptotic cells measured by flow cytometry. Cytometry **13**:795-808.

9. **Debiasi, R. L., C. L. Edelstein, B. Sherry, and K. L. Tyler**. 2001. Calpain inhibition protects against virus-induced apoptotic myocardial injury. J Virol **75**:351-361.

10. **Debiasi, R. L., B. A. Robinson, B. Sherry, R. Bouchard, R. D. Brown, M. Rizeq, C. Long, and K. L. Tyler**. 2004. Caspase inhibition protects against reovirus-induced myocardial injury in vitro and in vivo. J Virol **78**:11040-11050.

11. **Dryden, K. A., G. Wang, M. Yeager, M. L. Nibert, K. M. Coombs, D. B. Furlong, B. N. Fields, and T. S. Baker**. 1993. Early steps in reovirus infection are associated with dramatic changes in supramolecular structure and protein conformation: analysis of virions and subviral particles by cryoelectron microscopy and image reconstruction. J Cell Biol. **122**:1023-1041.

12. **Earnshaw, W. C., L. M. Martins, and S. H. Kaufmann**. 1999. Mammalian caspases: structure, activation, substrates, and functions during apoptosis. Annu. Rev. Biochem. **68**:383-424.

13. **Hanna, J. and D. Finley**. 2007. A proteasome for all occasions. FEBS Lett. **581**:2854-2861.

14. **Hershko, A. and A. Ciechanover**. 1998. The ubiquitin system. Annu. Rev. Biochem. **67**:425-479.

15. **Honda, R., H. Tanaka, and H. Yasuda**. 1997. Oncoprotein MDM2 is a ubiquitin ligase E3 for tumor suppressor p53. FEBS Lett. **420**:25-27.

16. **Ivanovic, T., M. A. Agosto, K. Chandran, and M. L. Nibert**. 2007. A role for molecular chaperone Hsc70 in reovirus outer capsid disassembly. J. Biol. Chem. **282**:12210-12219.

17. **Ivanovic, T., M. A. Agosto, L. Zhang, K. Chandran, S. C. Harrison, and M. L. Nibert**. 2008. Peptides released from reovirus outer capsid form membrane pores that recruit virus particles. EMBO J **27**:1289-1298.

18. **Karin, M. and Y. Ben-Neriah**. 2000. Phosphorylation meets ubiquitination: the control of NF-κB activity. Annu. Rev. Immunol. **18**:621-663.

19. **Kim, J. W., S. M. Lyi, C. R. Parrish, and J. S. Parker**. 2011. A proapoptotic peptide derived from reovirus outer-capsid protein μ1 has membrane-destabilizing activity. J Virol **85**:1507-1516.

20. **Kobayashi, T., A. A. Antar, K. W. Boehme, P. Danthi, E. A. Eby, K. M. Guglielmi, G. H. Holm, E. M. Johnson, M. S. Maginnis, S. Naik, W. B. Skelton, J. D. Wetzel, G. J. Wilson, J. D. Chappell, and T. S. Dermody**. 2007. A plasmid-based reverse genetics system for animal double-stranded RNA viruses. Cell Host. Microbe **1**:147-157.

21. **Liemann, S., K. Chandran, T. S. Baker, M. L. Nibert, and S. C. Harrison**. 2002. Structure of the reovirus membrane-penetration protein, μ1, in a complex with is protector protein, σ3. Cell **108**:283-295.

22. **Lin, R., P. Beauparlant, C. Makris, S. Meloche, and J. Hiscott**. 1996. Phosphorylation of IκBα in the C-terminal PEST domain by casein kinase II affects intrinsic protein stability. Mol. Cell Biol. **16**:1401-1409.

23. **McKinsey, T. A., Z. L. Chu, and D. W. Ballard**. 1997. Phosphorylation of the PEST domain of IκBβ regulates the function of NF-κB/IκBβ complexes. J Biol. Chem. **272**:22377-22380.

24. **Oberhaus, S. M., R. L. Smith, G. H. Clayton, T. S. Dermody, and K. L. Tyler**. 1997. Reovirus infection and tissue injury in the mouse central nervous system are associated with apoptosis. J Virol **71**:2100-2106.

25. **Richardson-Burns, S. M., D. J. Kominsky, and K. L. Tyler**. 2002. Reovirus-induced neuronal apoptosis is mediated by caspase 3 and is associated with the

activation of death receptors. J Neurovirol. **8**:365-380.

26. **Richardson-Burns, S. M. and K. L. Tyler**. 2005. Minocycline delays disease onset and mortality in reovirus encephalitis. Exp. Neurol. **192**:331-339.

27. **Rogers, S., R. Wells, and M. Rechsteiner**. 1986. Amino acid sequences common to rapidly degraded proteins: the PEST hypothesis. Science **234**:364-368.

28. **Sherry, B.** 1998. Pathogenesis of reovirus myocarditis. Curr. Top. Microbiol. Immunol. **233**:51-66.

29. **Thrower, J. S., L. Hoffman, M. Rechsteiner, and C. M. Pickart**. 2000. Recognition of the polyubiquitin proteolytic signal. EMBO J **19**:94-102.

30. **Treier, M., L. M. Staszewski, and D. Bohmann**. 1994. Ubiquitin-dependent c-Jun degradation in vivo is mediated by the delta domain. Cell **78**:787-798.

31. **Tyler, K. L., M. A. Mann, B. N. Fields, and H. W. Virgin**. 1993. Protective anti-reovirus monoclonal antibodies and their effects on viral pathogenesis. J Virol **67**:3446-3453.

32. **Virgin, H. W., M. A. Mann, B. N. Fields, and K. L. Tyler**. 1991. Monoclonal antibodies to reovirus reveal structure/function relationships between capsid proteins and genetics of susceptibility to antibody action. J Virol **65**:6772-6781.

33. **Virgin, H. W., K. L. Tyler, and T. S. Dermody**. 1997. Reovirus, p. 669-699. *In* N. Nathanson (ed.), Viral Pathogenesis. Lippincott-Raven, Philadelphia, Pa.

34. **Zhang, L., M. A. Agosto, T. Ivanovic, D. S. King, M. L. Nibert, and S. C. Harrison**. 2009. Requirements for the formation of membrane pores by the reovirus myristoylated μ1N peptide. J Virol **83**:7004-7014.

CHAPTER FIVE

Summary and Future Directions

μNS-Hsc70 interaction

The involvement of chaperones in the reovirus life cycle has not been studied extensively. Although the cellular chaperones Hsp70 and Hsp90 have been found necessary for proper folding of the σ1 attachment protein, no further studies have looked at chaperones in other assembly or replicative processes (10). In chapter 2, I presented evidence that the constitutively expressed cellular chaperone heat shock cognate protein 70 (Hsc70) interacted with the viral factory (VF) matrix protein μNS. I showed that Hsc70 co-localized with viral factories in reovirus infected cells and also with viral factory-like structures (VFLs) formed by ectopic expression of μNS. A direct interaction between Hsc70 and μNS was confirmed using co-immunoprecipitation. The interaction and co-localization of Hsc70 with μNS was independent of chaperone function. This indicated that although the minimal interaction domain in Hsc70 was mapped to the substrate binding site, μNS was not bound as a substrate for the chaperone. In general, chaperones recognize exposed unfolded hydrophobic regions present in proteins during synthesis or exposed in protein complex subunits prior to assembly into the full complex (7, 8).

μNS is thought to form the matrix of VFs by oligomerization. But as an atomic structure of μNS is not available, the nature of such oligomers remains elusive. Therefore, it seems possible that Hsc70 is recruited to VFs in order to aid in the oligomerization of individual μNS proteins. I have found, however, that knockdown of Hsc70 had no detectable effect on viral factory formation or maintenance. The K71M dominant negative mutant of Hsc70 does not interact with substrates (11). My

hypothesis that μNS is not a substrate for Hsc70 is supported by my finding that this and other dominant negative mutants of Hsc70 co-localized and interacted with μNS. I mapped the minimal interaction domain in μNS to lie between amino acids 222-271. However, point mutants within this region in context of the full length protein or deletion of the region did not abrogate μNS interaction with Hsc70. The deletion of the middle part of the μNS protein might very well have led to misfolding of the protein and thus interaction with Hsc70. But given the fact that this truncation mutant also interacted with a dominant negative mutant of Hsc70, I believe that the association was not due to μNS misfolding. Based on this finding I hypothesize that there is a second Hsc70 binding domain in μNS. I suspect this second interaction domain lies between amino acids 272-470, as amino acids 1-221 and 471-721 did not interact with μNS. To investigate this hypothesis I have generated a plasmid encoding amino acids 272-470 in order to assess its capacity to interact with Hsc70. If this fragment associated with Hsc70, this would also explain why point mutants in the amino acid region 222-271 did not show an effect in context of the full length protein.

Almost all experiments in Chapter 2 were performed with ectopically expressed proteins. Although we demonstrated a co-localization of Hsc70 and viral factories and co-immunoprecipitated Hsc70 and μNS from infected cells, the biological significance of the interaction of Hsc70 with μNS has not been addressed. One possibility to investigate the role of Hsc70 μNS interaction in infection would be to transfect cells with dominant negative mutants of Hsc70 or siRNA against Hsc70 and evaluate changes in viral titer. However, such experiments might not show any difference in viral output. Given the fact that the inducible form of Hsc70, heat shock protein 70 (Hsp70) also co-localizes with viral factories (data not shown) it seems possible that Hsp70 could compensate for the loss of Hsc70 and mask a potential phenotype. On the other hand if knockdown of Hsc70 with subsequent infection does

exhibit a change in viral production, it would be impossible to attribute this result to the interruption of the μNS Hsc70 interaction.

As discussed in chapter 3, Hsc70 also interacts with the outer capsid protein μ1 and the μ1:σ3 heterohexamer and also impacts the recruitment of σ3 to VFLs. Furthermore, Hsc70 aids in the final steps of μ1 removal from infecting virions (9). Thus knockdown of Hsc70 during infection would very likely affect more than only μNS-associated tasks of Hsc70, but might also interfere with heterohexamer assembly and possibly recruitment to viral factories. In order to specifically investigate the purpose of Hsc70 at viral factories, we would have to target the μNS protein and find mutants that no longer recruit Hsc70 and generate recombinant virus. Single point mutants in the so far identified interaction domain of μNS still bound Hsc70, but multiple mutations might be able to abrogate the association. Although the prior mutants of μNS still associated with Hsc70 *in vitro*, it is possible that these mutants would affect the function of μNS in the context of infection. Also, if region 272-470 harbored a second interaction domain, additional mutations in this region could complement point mutants within amino acids 222-271 and abolish Hsc70 interaction. However, if Hsc70 serves a vital role at viral factories, the complete abrogation of association might prevent the recovery of recombinant virus. On the other hand, if such a defective virus could be rescued by expression of wild type μNS *in trans*, it might give insights into early assembly processes of reovirus as μNS has been found early in infection in complexes containing viral mRNA, σ3 and σNS (1).

μ1-Hsc70 interaction and Hsc70 influence on σ3 trafficking

The processes during assembly of the outer capsid proteins μ1 and σ3 and their recruitment to viral factories are largely unknown. Coffey et al have showed that μ1 depends on σ3 for its recruitment to viral factories (3). They further described a role

for Hsc70 in recruitment of σ3 to viral factory-like structures (3). In chapter 3, I expanded on these findings and showed that Hsc70 interacted with the outer capsid protein μ1 alone and with μ1 in complex with σ3. I was able to co-immunoprecipitate μ1 using an anti-Hsc70 antibody and likewise Hsc70 using an anti-μ1 antibody. Given the fact that Hsc70 over-expression increased the frequency of σ3 co-localization with μNS VFLs, I expected to find an interaction between σ3 and Hsc70 (3). However, I could not detect any association of these two proteins by immunoprecipitation. I was able to co-immunoprecipitate σ3 with Hsc70 in the presence of μ1. Both μ1 and σ3 were pulled down from infected as well as transfected cells using an anti-Hsc70 antibody. These findings indicated that Hsc70 interacts with the μ1:σ3 heterohexamer via association with μ1. I also demonstrated that Hsc70 co-localized with μ1 on lipid droplets. This co-localization was dependent on chaperone function as dominant negative mutants of Hsc70 did not localize with μ1 on lipid droplets. I investigated if μ1 localization to lipid droplets was dependent on Hsc70, but found that siRNA-mediated knockdown of Hsc70 or over-expression of dominant negative mutants of Hsc70 did not abrogate μ1 association with lipid droplets.

Further investigations will aim to unravel the role of Hsc70 in μ1:σ3 heterohexamer assembly and recruitment to viral factories. Hsc70 localization to μ1 on lipid droplets suggests that these membranous structures could be the location of chaperone-aided heterohexamer assembly. In order to test this hypothesis I plan on using *in vitro* transcription and translation of μ1 and σ3 to assess their capacity to associate in the absence or presence of membranes. Preliminary experiments revealed that μ1 and σ3 form a complex and can be co-immunoprecipitated from reticulocyte lysates in the absence of membranes. Next, I will investigate if the addition of membranes in the form of microsomes changes the efficiency of μ1-σ3 co-immunoprecipitation. In a similar fashion I would like to address the hypothesis that

Hsc70 is necessary for μ1:σ3 heterohexamer formation. One possibility is to assess the efficiency of μ1:σ3 co-immunoprecipitation in transfected cells after siRNA-mediated knockdown of Hsc70. If Hsc70 was necessary for μ1:σ3 assembly, then co-immunoprecipitation of the two proteins should be reduced while immunoprecipitation of the individual proteins would be unaffected. However, as the transfection efficiency after siRNA treatment is diminished, μ1 and σ3 expression might be too low to detect μ1 and σ3 after immunoprecipitation. Another approach could be the triple transfection of μ1, σ3 and a dominant negative mutant of Hsc70 in order to prevent endogenous wild type Hsc70 from aiding in the heterohexamer formation. As there is no guarantee though that all μ1/σ3-expressing cells will also express dominant negative Hsc70, the result could be skewed by the presence of a population of cells in which μ1:σ3 complex formation can occur under normal Hsc70 conditions. Alternatively, reticulocyte lysate could be immunodepleted of chaperones and used for simultaneous *in vitro* transcription/translation of μ1 and σ3 followed by co-immunoprecipitation of μ1 and σ3. Immunodepletion would ensure a uniform, chaperone-free environment for μ1:σ3 interaction. In addition, by also immunodepleting Hsp70, I could rule out possible substitution effects of Hsp70 for Hsc70.

An interesting topic for further exploration is the relationship between Hsc70 and σ3. There is no obvious co-localization between σ3 and Hsc70 as they are both distributed diffusely in the cytosol and nucleus. There also seems to be no physical interaction connecting these two proteins. Still, Coffey et al showed that Hsc70 over-expression impacts σ3 localization to viral factory-like structures (3). My preliminary data indicate that the co-localization of σ3 and VFLs is an artifact of the fixation of cells with paraformaldehyde. In cells fixed with methanol the association of σ3 with VFLs is abolished even with over-expression of Hsc70. Nevertheless, the increase in

localization of σ3 to VFLs with Hsc70 over-expression in cells fixed with paraformaldehyde was a reproducible finding. Given that Hsc70 does not seem to interact with σ3, this suggests that the association of Hsc70 with the VFLs influences the frequency of σ3-VFL co-localization. In chapter 2, I showed that Hsc70 interacts with μNS and is recruited to VFLs and VFs. Thus it seems possible that the effect of Hsc70 on σ3 recruitment to VFLs actually reflects a role of Hsc70 in viral factory dynamics. The idea is that Hsc70 modulates the permeability of the viral factory μNS matrix in order to facilitate the admittance of viral proteins. A mutant of μNS that no longer associated with Hsc70 could provide information about this hypothesis. Alternatively, if such a mutant remains elusive, I could investigate if over-expression of Hsc70 has a similar enhancing effect on the recruitment of other proteins to VFLs. I found in chapter 2 that the ATPase domain of Hsc70 co-localizes to VFLs in an artifactual manner akin to σ3. Both proteins exhibit co-localization with VFLs after paraformaldehyde but not methanol fixation. If the Hsc70 ATPase domain co-localized more frequently with VFLs after over-expression of Hsc70, this would support my hypothesis that Hsc70 increases the permeability of VFLs.

μ1 caspase cleavage and ubiquitination

Many studies focused on the different pathways contributing to reovirus induced apoptosis, but less attention has been directed towards the regulation of apoptosis. Apoptosis is induced late in infection and μ1 has been found to be the determining factor of reovirus induced cell death (4, 5). In chapter 4, I presented evidence that μ1 was a target for caspases and was also ubiquitinated. I showed that expression levels of μ1 increased after treatment of μ1-expressing cells with a pan-caspase inhibitor. I had also found a discrepancy between the number of apoptotic cells after μ1 expression and the number of cells actually being positive for μ1. A

subpopulation of apoptotic cells did not register positive for μ1 expression. My hypothesis was that activated caspases during apoptosis cleave μ1 and destroy the immunoreactive epitope. EGFP-labeling of μ1 at either the N- or C-terminus revealed that there were indeed μ1 fragments generated during apoptosis that were only detected with an anti-GFP antibody, but not by an anti-reovirus serum. Mutation of several potential caspase cleavage sites in μ1 revealed one site, amino acids 487-490, that upon mutation caused a similar increase in detectable μ1 protein levels. Additionally, point mutants at position 487 or 490 exhibited a different banding pattern than wild type μ1 indicating that mutation of this site abolished cleavage of μ1. Mutants of this caspase cleavage site induced similar levels of caspase 3/7 activation, but caused significantly less cytotoxicity. I also showed that μ1 was ubiquitinated and that ubiquitination increased dramatically after treatment of μ1-expressing cells with a pan-caspase inhibitor. However, ubiquitination of the caspase cleavage mutant D490 was not increased in the absence or presence of caspase inhibitor compared to wild type μ1. The lack of ubiquitination enhancement after caspase inhibition was correlated to the abrogation of μ1 cleavage at residue 490. Alanine substitution mutants surrounding amino acid D490 that were no longer cleaved also showed a defect in ubiquitination. The generation and initial characterization of a recombinant reovirus carrying the μ1-D490E mutation revealed a possible entry defect of this virus. Very soon after infection, too early to constitute newly generated virions, more virus was found in the supernatant of D490E than wild type virus infected cells. I hypothesize that this virus was initially bound to the cell surface, but was unable to infect the cell and ultimately detached into the supernatant. The mutant virus also grew to lower titers in multiple cycle growth kinetics which might be a due to the suspected entry defect.

Many questions about the role of caspase cleavage and ubiquitination of μ1 remain. How are the two phenotypes related? The inhibition of caspase cleavage by pan-caspase inhibitor increased μ1 ubiquitination which indicated that active caspases have a negative effect on μ1 ubiquitination. However, mutation of the caspase cleavage site did not increase μ1 ubiquitination which suggests that μ1 needs to be cleaved to be efficiently ubiquitinated. So far it is also unclear which ubiquitin ligase and which caspase μ1 is targeted by. Tandem-affinity purification studies on μ1 did not identify any known ubiquitin ligase (Amaro and Parker unpublished data). In order to determine which caspase cleaves μ1, I intend to immunoprecipitate μ1 and then incubate the protein with different, active, recombinant caspases and evaluate possible fragments by immunoblotting.

It would also be interesting to investigate the subcellular distribution and ubiquitination status of the individual μ1 caspase cleavage fragments, namely amino acids 1-490 and 491-708. The latter fragment contains the Φ domain which has been found to be necessary and sufficient for apoptosis induction (4). Ubiquitination and subsequent degradation of this Φ containing fragment might be a mechanism to regulate apoptosis induction by μ1. σ3 has been established as the protector protein of μ1, as μ1 no longer induces apoptosis when it is co-expressed with σ3 (3). Similarly, μ1 association with σ3 might prevent caspase cleavage and ubiquitination, if we assume that these modifications are only targeted towards free μ1. Although pan-caspase inhibitor led to an increase in the detectable levels of μ1, there were still fragments of μ1 present. These fragments might be caused by cleavage due to residual caspase activity considering that the caspase inhibitor was added at the time of transfection and might have lost some of its potency over the 24 h time course of the experiment. This could be explored by adding caspase inhibitor repeatedly throughout the 24 h time period of the experiment to achieve a constant level of caspase

inhibition. Alternatively, μ1 could be cleaved by other proteases, possibly calpains which have been shown to be activated upon reovirus infection (6). It is unknown though if μ1 alone can also activate calpains. A surprising finding was that although the caspase cleavage mutants caused equal levels of activated caspase 3/7 compared to wild type μ1, they caused less cytotoxicity. It seems possible that μ1 causes cell death not only by inducing apoptosis, but has an additional cytotoxic potential and that the caspase cleavage mutants are less cytotoxic while preserving their apoptotic capacity.

In order to establish a biological role for μ1 caspase cleavage and ubiquitination, it is necessary to fully characterize the μ1-D490E recombinant virus. Initial experiments revealed a possible entry defect of this mutant. This finding needs to be revisited with more specific experiments such as a hemolysis assay. Previous data generated in transfected cells have to be repeated in infected cells in order to address whether D490E-μ1 behaves similar in the context of infection. Such experiments include the extent of caspase 3/7 activation and cytotoxicity and the subcellular distribution, ubiquitination and fragmentation of mutant μ1. It would also be interesting to investigate the D490E mutant virus in animal infections and assess this virus for its capacity to spread, replicate and cause apoptosis and tissue damage in different organs. It is possible that the D490E mutation in μ1 has different effects in an *in vitro* versus an *in vivo* infection, similarly to a mutant virus which does not produce the non-structural protein σ1s. This σ1s-null virus shows no defect in replication in tissue culture, but is deficient in the dissemination from the intestine to the bloodstream and secondary replication sites (2, 12).

Reference List

1. **Antczak, J. B. and W. K. Joklik**. 1992. Reovirus genome segment assortment into progeny genomes studied by the use of monoclonal antibodies directed against reovirus proteins. Virology **187**:760-776.

2. **Boehme, K. W., K. M. Guglielmi, and T. S. Dermody**. 2009. Reovirus nonstructural protein σ1s is required for establishment of viremia and systemic dissemination. Proc. Natl. Acad. Sci. U. S. A **106**:19986-19991.

3. **Coffey, C. M.** 2007. Studies on apoptosis induction by mammalian orthoreovirus outer caspid protein μ1 and regulation by outer capsid protein assembly and degradation. Thesis. Cornell University.

4. **Coffey, C. M., A. Sheh, I. S. Kim, K. Chandran, M. L. Nibert, and J. S. Parker**. 2006. Reovirus outer capsid protein μ1 induces apoptosis and associates with lipid droplets, endoplasmic reticulum, and mitochondria. J Virol **80**:8422-8438.

5. **Danthi, P., M. W. Hansberger, J. A. Campbell, J. C. Forrest, and T. S. Dermody**. 2006. JAM-A-independent, antibody-mediated uptake of reovirus into cells leads to apoptosis. J Virol **80**:1261-1270.

6. **Debiasi, R. L., M. K. Squier, B. Pike, M. Wynes, T. S. Dermody, J. J. Cohen, and K. L. Tyler**. 1999. Reovirus-induced apoptosis is preceded by increased cellular calpain activity and is blocked by calpain inhibitors. J. Virol. **73**:695-701.

7. **Frydman, J., E. Nimmesgern, K. Ohtsuka, and F. U. Hartl**. 1994. Folding of nascent polypeptide chains in a high molecular mass assembly with molecular chaperones. Nature **370**:111-117.

8. **Hartl, F. U. and M. Hayer-Hartl**. 2002. Molecular chaperones in the cytosol: from nascent chain to folded protein. Science **295**:1852-1858.

9. **Ivanovic, T., M. A. Agosto, K. Chandran, and M. L. Nibert**. 2007. A role for molecular chaperone Hsc70 in reovirus outer capsid disassembly. J. Biol. Chem. **282**:12210-12219.

10. **Leone, G., M. C. Coffey, R. Gilmore, R. Duncan, L. Maybaum, and P. W. Lee**. 1996. C-terminal trimerization, but not N-terminal trimerization, of the reovirus cell attachment protein is a posttranslational and Hsp70/ATP-dependent process. J Biol. Chem. **271**:8466-8471.

11. **Li, L., L. A. Johnson, J. Q. Dai-Ju, and R. M. Sandri-Goldin**. 2008. Hsc70 focus formation at the periphery of HSV-1 transcription sites requires ICP27. PLoS. One. **3**:e1491.

12. **Rodgers, S. E., J. L. Connolly, J. D. Chappell, and T. S. Dermody**. 1998. Reovirus growth in cell culture does not require the full complement of viral proteins: identification of a σ1s-null mutant. J Virol **72**:8597-8604.